LUND UNIVERSITY

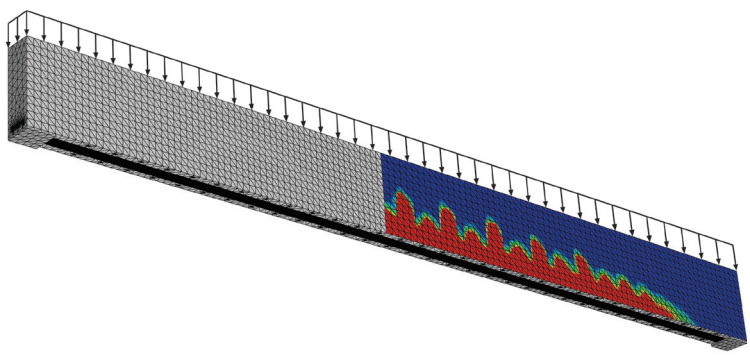

STRUCTURAL RETROFITTING OF CONCRETE BEAMS USING FRP - Debonding Issues

YASMEEN TALEB OBAIDAT

Structural Mechanics

Doctoral Thesis

Department of Construction Sciences
Structural Mechanics

ISRN LUTVDG/TVSM--11/1023--SE (1-163)
ISBN 978-91-7473-194-1 ISSN 0281-6679

STRUCTURAL RETROFITTING OF CONCRETE BEAMS USING FRP - Debonding Issues

Doctoral Thesis by

YASMEEN TALEB OBAIDAT

Printed by Media-Tryck LU, Lund, Sweden, October 2011 *(PI)*.

For information, address:
Division of Structural Mechanics, LTH, Lund University, Box 118, SE-221 00 Lund, Sweden.
Homepage: http://www.byggmek.lth.se

To my parents, my brothers, my sisters, my nephews and my nieces
for their love, endless support
and encouragement....

"The important thing in science is not so much to obtain new facts as to discover new ways of thinking about them."

Sir William Bragg

Acknowledgments

First, I would like to thank my supervisor, Professor Ola Dahlblom for his support and guidance throughout this research project. He has been a constant presence throughout my study in Sweden and was able to keep me motivated, challenged and productive at all time.

I also feel so lucky and blessed to have Dr. Susanne Heyden as my co-advisor. Her comments and suggestions have contributed to clarify certain aspects and strengthen the work. Her patience, leadership, and encouragement gave me the confidence to focus and proceed. She could not even realize how much I have learned from her.

I would also like to acknowledge my fellow graduate students and staff who I have known during my time here at Structural Mechanics at Lund University.

I wish to acknowledge the financial support provided by the Erasmus Mundus External Cooperation Window Lot 3 and Lund University.

Friendship is a precious gift and fine friends are very few, I express my immense thanks to my friends and all those friends who have directly or indirectly supported me throughout my study.

I would like to thank my parents, brothers, sisters, and lovely nephews and nieces for their prayers, their love, their belief in my potential and encouragement throughout my entire life. Thank you for giving me the freedom and opportunity to pursue my own interests.

Yasmeen Taleb Obaidat
Lund in October 2011

Abstract

A 3D nonlinear finite element analysis modelling framework was developed for simulating the behaviour of beams retrofitted with fibre reinforced polymer (FRP). The ABAQUS program was used for this purpose. Concrete was modelled using a plastic damage model. Steel bars were modelled as an elastic perfectly plastic material, with perfect bond between concrete and steel. A cohesive model was used for modelling the FRP-concrete interface. Bond properties needed as input to the cohesive model, such as initial stiffness, shear strength and fracture energy were proposed based on fitting FEM results to experimental results from literature. Initial stiffness was related to the adhesive properties. Shear strength and fracture energy were expressed as functions of tensile strength of concrete and of adhesive properties.

Experimental tests were performed to investigate the behaviour of retrofitted beams. The model was verified through comparison with the experimental data regarding failure mode and load-displacement behaviour.

The influence of several parameters such as length and width of FRP and properties of the adhesive were investigated. The result showed that when the length of FRP increases, the load capacity of the beam increases for both shear and flexural strengthening. The result also showed that the FRP to concrete width ratio and the stiffness of FRP affect the failure mode of retrofitted beams. The maximum load increases with increased width ratio. Increased FRP stiffness increases the maximum load only up to a certain value of the stiffness, and thereafter the maximum load decreases. The maximum load also increases when the stiffness of adhesive decreases.

An improvement of the calculation of interfacial shear stress at plate end in a design rule for simply supported beams bonded with FRP was proposed. The proposed design rule was applied to an existing defective beam and the result was verified using the FEM model.

Popular abstract

Concrete is one of our most common building materials and is used both for buildings, bridges and other heavy structures. Typically, concrete structures are very durable, but sometimes they need to be strengthened. The reason may be cracking due to environmental effects, that a bridge is to be used for heavier traffic, new building codes, or damage resulting from earthquakes.

Concrete is a material that can withstand compressive loads very well but is sensitive to tensile forces. Therefore, concrete structures are typically reinforced by casting in steel bars in areas where tension can arise. This cannot be done afterwards, and one strengthening method, is therefore to glue reinforcement on the exterior of the structure in the areas exposed to tension.

Fibre composite can be used in reinforcing concrete structures externally. Fibre composite materials have low density, can be easily installed and are easy to cut to length on site. Therefore, fibre composite as external reinforcement for concrete structures has become very attractive and popular around the world.

It is important to understand the behaviour of a strengthened structure well and realize what parameters affect the failure mode and load-bearing capacity. The aim of this thesis is therefore to investigate and improve the understanding of the behaviour of reinforced concrete beams strengthened with fibre composite.

These structures have a critical problem implying that they may fail in a sudden manner. This failure involves separation between composite and concrete. Special attention is paid to this phenomenon, which is called debonding.

One scope of this study was to develop computer modelling framework. Therefore, three dimensional computations were conducted considering the nonlinear behaviour of the materials. A new model for the concrete-fibre composite interface was included.

The computations were verified against experiments. The results confirmed the ability of the computations to recreate the load-deflection behaviour, the crack distribution, and the failure modes. Simulations and experiments showed that application of fibre composite can increase the load capacity and the stiffness of the beams.

The influence of several parameters such as length and width of fibre composite and properties of adhesive were investigated. Large width and length of fibre composite and soft adhesive would yield to reduce tendency of debonding and increase thus of the utilization of fibre composite and increase load capacity.

The findings from this study yield a proposal for a modification of design code rules.

Contents

Part I

Introduction and Overview

1 Introduction

1.1 Background

Reinforced concrete structures often have to face modification and improvement of their performance during their service life. The main contributing factors are change in their use, new design standards, deterioration due to corrosion in the steel caused by exposure to an aggressive environment and accident events such as earthquakes. In such circumstances there are two possible solutions: replacement or retrofitting. Full structure replacement might have determinate disadvantages such as high costs for material and labour, a stronger environmental impact and inconvenience due to interruption of the function of the structure, e.g. traffic problems. When possible, it is often better to repair or upgrade the structure by retrofitting.

Figures 1-3 illustrate structures in need of repair or upgrading, a bridge in Al Zarqa–Jordan with spalled concrete cover, a beam that has inadequate strength and need upgrading in Om Katheer school-Jordan and a crack in a wall in Om Katheer school-Jordan.

Figure 1: Bridge in the Al Zarqa-Jordan.

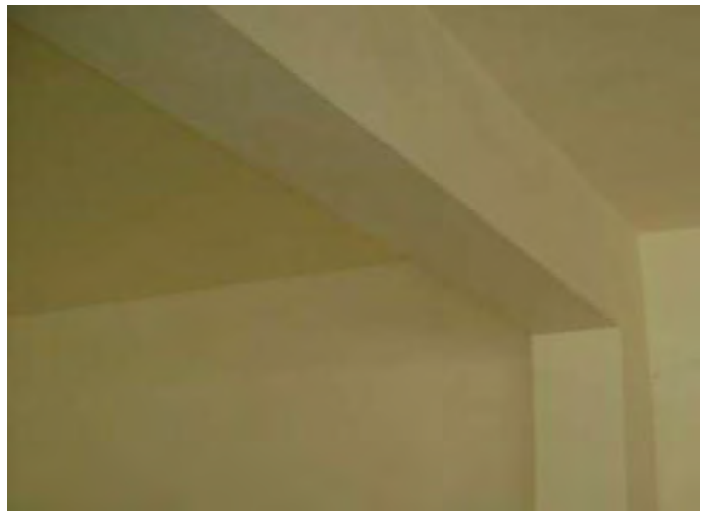

Figure 2: Reinforced concrete beam in Om Katheer school-Jordan.

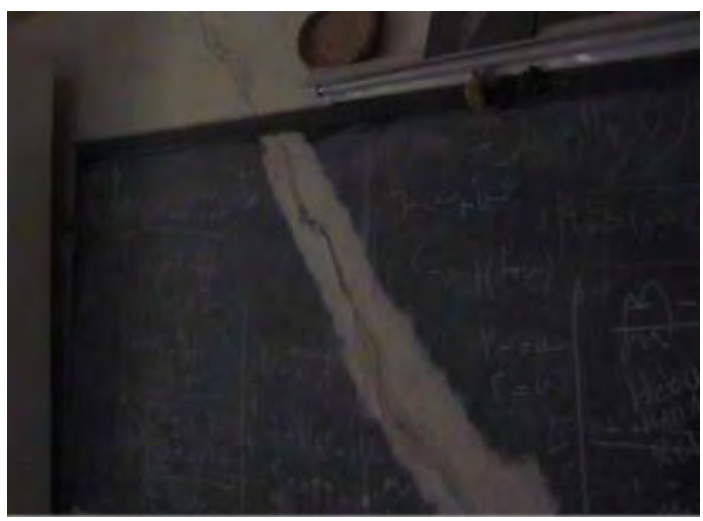

Figure 3: Crack in a wall in Om Katheer school-Jordan.

In the last decade, the development of strong epoxy glue has led to a technique which has great potential in the field of upgrading structures. Basically the technique involves gluing steel plates or fibre reinforced polymer (FRP) plates to the surface of the concrete. The plates then act compositely with the concrete and help to carry the loads.

Each material has its specific advantages and disadvantages. Steel plates have been used for many years and are very effective to use as bonding reinforcement. However, they are heavy to transport and install, prone to corrosion and delivery length of plates are limited.

FRP can therefore be convenient compared to steel. These materials have higher ultimate strength and lower density than steel. The installation is easier and temporary support until the adhesive gains its strength is not required due to the low weight. They can be formed on site into complicated shapes and can also be easily cut to length on site.

Debonding is a major problem in structures retrofitted with FRP. Debonding implies complete loss of composite action between concrete and FRP. This prevents full utilization of the FRP-concrete system and may lead to failure before the design load is reached. Debonding due to a stress concentration may initiate either at the plate end or around cracks.

This work is a study of the behaviour of concrete beams retrofitted with FRP, using experiments and finite element modelling. One main focus is the debonding issues, that limit the composite system from achieving the desired load capacity.

1.2 Aim and scope

The overall aim of the present study is to investigate and improve the understanding of the behaviour of reinforced concrete beams retrofitted with FRP. The scope is to develop a modelling of framework consisting of suitable constitutive models and a FEM methodology. The modelling framework will then be used as a tool for investigating the behaviour of retrofitted beams.

1.3 Limitations

This research is limited to investigate the application of FRP material as external reinforcement. Only simply supported reinforced concrete beams retrofitted with unidirectional FRP were studied. Only static load is included in this study. Long term behaviour and environmental effects as well as pre-stressed FRP and concrete are not treated.

1.4 Outline of the present work

There are many ways to describe a research work. The way chosen in Figures 4-6 is to position the different parts of the work in a plane defined by the axes ‘‘Structural unit’’ and ‘‘Representation’’.

The ‘‘Structural unit’’ axis refers to that several structural levels may be of interest when the behaviour of a structure is investigated. Constitutive models are formulated on the material point level, simple specimens are often used for measurements providing data for a certain material model and the behaviour of a structural element is what we are often actually interested in in a practical application.

The axis "Representation" refers to different ways of handling, or relating to, reality. We could perform measurements to observe reality. Based on the results from the measurements and theoretical reasoning we could propose a physical model that describes reality. To be able to use the physical model we most often need a numerical implementation. The knowledge obtained from using the numerical model can be used for formulating design rules that could be used by engineers. These design rules often provide a simplified description of reality, but require less time and expertise compared to a more fundamental modelling approach.

In the first part of the study, Paper A, measurements were performed on structural elements, see Figure 4. The elements were retrofitted beams, which had insufficient flexural or shear strength prior to retrofitting. The load-displacement relationship was measured and the fracture mode was observed. All these beams failed through debonding.

In papers B and C, Figure 4, the development of a modelling framework was initiated. Different constitutive models and FEM strategies from literature were evaluated and the result was simulations that were able to reproduce the behaviour of the beams tested experimentally in paper A. The simulations were 3D, and used a plastic damage model for describing the concrete and a cohesive model for the FRP-concrete bond.

The modelling framework was used for parameter studies presented in Paper D, Figure 4. The parameter study focused on the influence of FRP stiffness and FRP to concrete width ratio on the fracture mode and ultimate load.

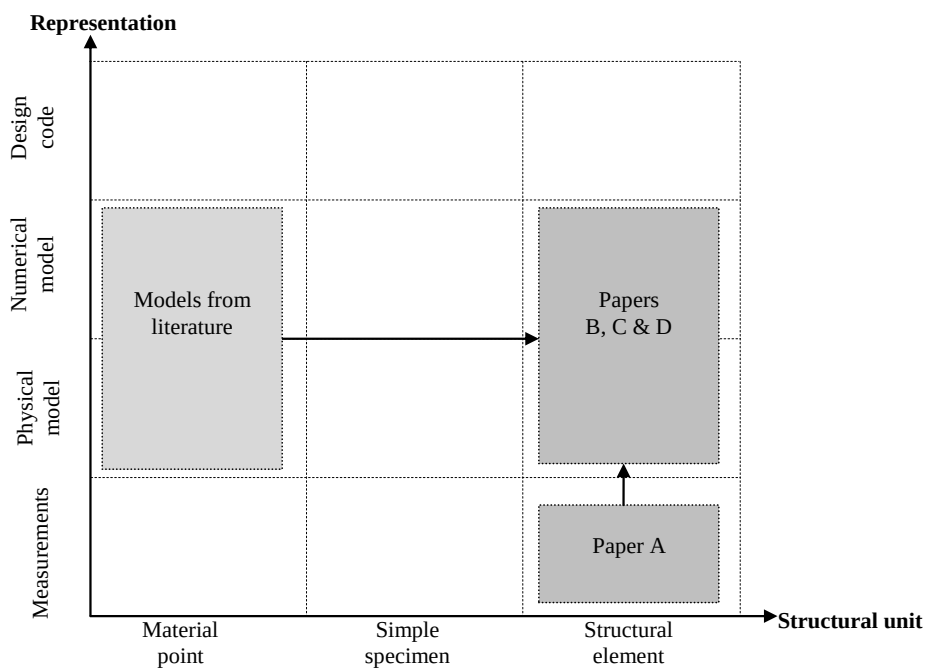

Figure 4: Outline of papers A, B, C and D.

Conclusions from the work with papers A-D included that debonding is a central issue, and that the properties of the FRP-concrete bond are very important in this context. The description of the FRP-concrete interface was identified as a weak point in the modelling framework and further improvements were needed.

Thus, the next step in the work was to find a better constitutive model for the bond, that is, a physical model at the material point level, see Figure 5. Since it is difficult to measure on the material point level, measurements on simple specimens were used for developing a better model. A series of tests from literature were chosen for this purpose. The idea of a cohesive model was maintained and focus was on finding a suitable shape of the bond-slip relation and to relate the parameters of this model (initial stiffness, shear strength and fracture energy) to the properties of the adhesive and the concrete. FEM simulations of the specimens used in the tests were performed and through fitting of the parameters mentioned above, an improved constitutive model for the bond was proposed, Figure 5.

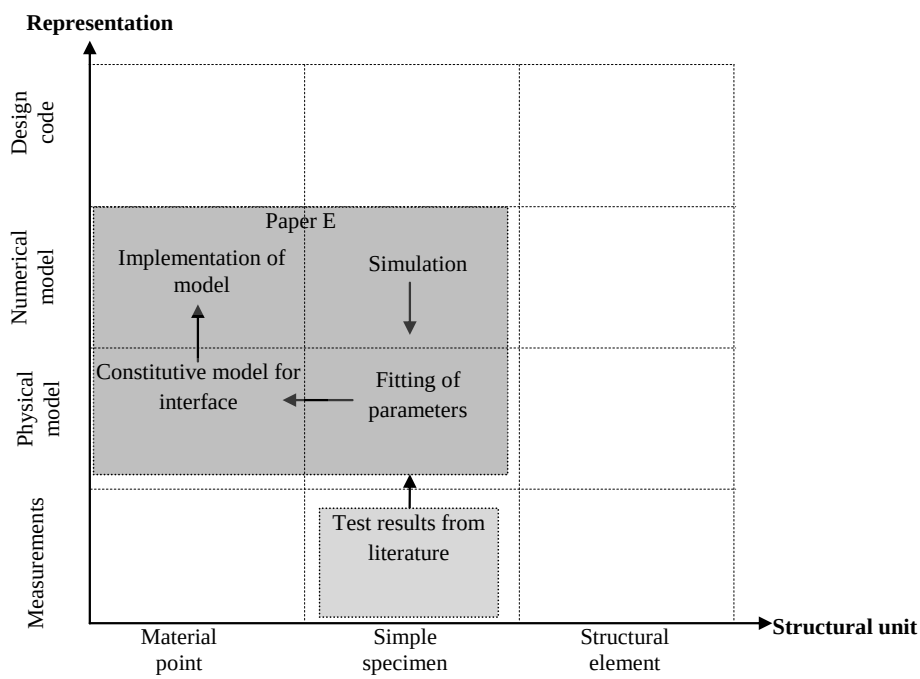

Figure 5: Outline of paper E.

The improved modelling framework made it possible to suggest improvements in design codes and focus was again on the structural element level, Figure 6. Since a main focus of the work is debonding, the design criteria for plate end debonding in fib Bulletin 14 [1] was evaluated, Paper F. The present equation for calculating shear stress at the plate end in the design code does not include the FRP to concrete width ratio. Simulations showed that this is

an important parameter and a correction factor including the width ratio was proposed. This modification was shown to give better agreement between shear stress predictions from equation and simulation, respectively.

In paper G, a case study was performed. A defective beam in a school that was in need of strengthening was analysed according to fib Bulletin 14 [1] and by FEM simulations. Comparison of the results showed that in some cases the design code did not result in a safe structure. If the modified equation for shear stress suggested in paper F was used, and the plate end debonding was checked in the ultimate limit state, instead of in the serviceability limit state, the problem was eliminated.

The performed work thus covers a substantial part of the plane used in Figures 4-6, but the main focus is on modelling at the structural element level.

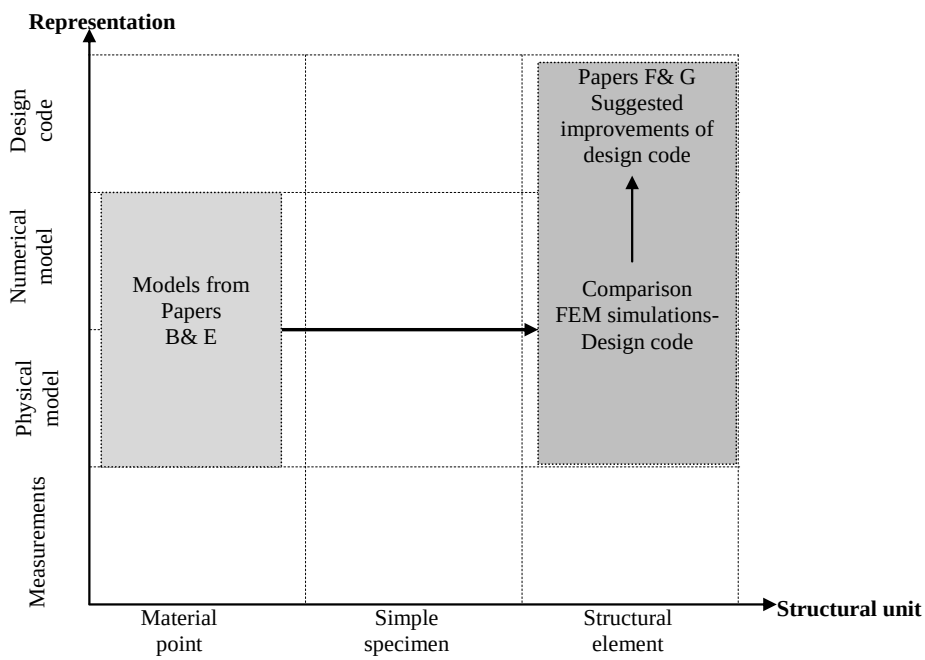

Figure 6: Outline of papers F and G.

1.5 Summary of the Papers

Paper A Obaidat, Y.T., Heyden, S., Dahlblom, O., Abu-Farsakh, G., and Abdel-Jawad, Y.: Retrofitting of reinforced concrete beams using composite laminates. Published in *Construction & Building Materials*, 2011; 25: 591-597.

This paper presents the results of an experimental study to investigate the behaviour of structurally damaged full-scale reinforced concrete beams retrofitted with CFRP laminates in shear or in flexure. The main variables considered were the internal reinforcement ratio, position of retrofitting and the length of CFRP. The experimental results, generally, indicate that beams retrofitted in shear and flexure by using CFRP laminates are structurally efficient and are restored to stiffness and strength values nearly equal to or greater than those of the control beams. It was found that the efficiency of the strengthening technique by CFRP in flexure varied depending on the length. The main failure mode in the experimental work was plate debonding in retrofitted beams.

Paper B Obaidat,Y.T., Heyden, S. and Dahlblom, O.: The Effect of CFRP and CFRP/ Concrete Interface Models when Modelling Retrofitted RC Beams with FEM. Published in *Composite Structures*, 2010; 92: 1391–1398.

This paper presents a finite element analysis which is validated against laboratory tests of eight beams. All beams had the same rectangular cross-section geometry and were loaded under four point bending, but differed in the length of the carbon fibre reinforced plastic (CFRP) plate. The commercial numerical analysis tool Abaqus was used, and different material models were evaluated with respect to their ability to describe the behaviour of the beams. Linear elastic isotropic and orthotropic models were used for the CFRP and a perfect bond model and a cohesive bond model was used for the concrete–CFRP interface. A plastic damage model was used for the concrete. The analyses results show good agreement with the experimental data regarding load–displacement response, crack pattern and debonding failure mode when the cohesive bond model is used. The perfect bond model failed to capture the softening behaviour of the beams. There is no significant difference between the elastic isotropic and orthotropic models for the CFRP.

Paper C Obaidat,Y.T., Dahlblom, O. and Heyden, S.: Nonlinear FE modelling of shear behaviour in RC beam retrofitted with CFRP. Published in proceedings of *Computational Modelling of Concrete Structures (EURO-C 2010)*, 2010, 671–677.

A nonlinear 3-D numerical model has been developed using the ABAQUS finite element program, and it was used to examine the shear behaviour of beams retrofitted by CFRP. Two models were used to represent the interface between CFRP and concrete, a perfect bond model and a cohesive model. Validation of the model was performed using data obtained from an experimental study. The results showed that the cohesive model is able to simulate the composite behaviour of reinforced concrete beams retrofitted by CFRP in shear correctly. The model is then used to examine the influence of length and orientation of CFRP. It is shown that the length of CFRP and the orientation strongly influence on the behaviour of the retrofitted beams.

Paper D Obaidat,Y.T., Heyden, S. and Dahlblom, O.: FEM Study on the Effect of CFRP Stiffness and Width on Retrofitted Reinforced Concrete Beam Behaviour. Submitted for publication.

The finite element program ABAQUS was used to study the effect of different parameters on the behaviour of an RC beam retrofitted with carbon fibre reinforced polymer (CFRP). These parameters were the stiffness and width of the CFRP. A linear elastic isotropic model was used for the CFRP and a cohesive bond model was used for the concrete–CFRP interface. A plastic damage model was used for the concrete. The material models were validated against experimental work and the results showed good agreement between experimental data and numerical results. Observations indicate that the CFRP width to beam width ratio and CFRP stiffness influence the type of failure mode of a beam retrofitted with CFRP. For small width and for large value of stiffness debonding will occur before steel yielding due to stress concentration at the end of the plate. For small values of stiffness, rupture of CFRP will occur. It was found that when the stiffness of CFRP increases the maximum load increases until a certain value of stiffness, then the maximum load decreases again. Simulations also show that the external load at steel yielding and the maximum load increase with the CFRP width.

Paper E Obaidat,Y.T., Heyden, S. and Dahlblom, O.: Bond action between FRP and concrete – A new model. Submitted for publication.

In this study, based on fitting a non-linear finite element model to experimental results from literature, a new model of the behaviour of the interface between concrete and fibre reinforced polymer (FRP) was proposed. An initial interface stiffness model was proposed based on the adhesive properties, to predict the strain distribution at low load. Comparison between the proposed model, test results and a previous model was performed to demonstrate the accuracy of the proposed model in predicting strain distribution at low load. The proposed model showed better agreement with test results of strain at low load than the previous model. In addition, shear strength and fracture energy models based on tensile strength of concrete and the adhesive shear modulus were proposed. According to the analysis the models provide a good estimation of ultimate load and strain distribution in FRP compared to test results. Finally, bilinear, trilinear and exponential bond-slip curves were compared. The results showed that the bond-slip curve shape has a minor effect on the behaviour of the concrete-FRP specimen.

Paper F Obaidat,Y.T., Heyden, S. and Dahlblom, O.: Plate End Debonding: A Modified Approach to Predict Stress in FRP – Concrete Bond. Submitted for publication.

An important failure mode of RC beams retrofitted with FRP plates is plate end debonding. Design codes provide equations for estimating shear stress at the plate end, but none of these equations include the FRP to concrete width ratio. This paper suggests an improved equation for calculating shear stress that includes the width ratio. The new equation was obtained by fitting 3D nonlinear FEM results to a proposed relation and provided a clearly improved prediction of the shear stress. The simulations also showed that a large width ratio and an adhesive of low stiffness decrease the risk of debonding.

Paper G Obaidat,Y.T., Heyden, S. and Dahlblom, O.: Evaluation of debonding criteria in fib Bulliten 14 – A case study. Submitted for publication.

In this case study, a defective beam in Om Katheer School in Jordan was studied. One aim was to propose a suitable method for strengthening the beam by application of fibre reinforced polymer. Another aim was to evaluate the design criteria in fib Bulletin 14 by comparing with FEM analysis results. Three CFRP widths and three different adhesives of different stiffness were evaluated. The results indicate that brittle failure can develop at a load much

lower than expected when CFRP of too small width or length and too stiff adhesive are used. The results showed that modification of the criterion used for checking plate end debonding is needed. The suggested modification implies when calculation shear stress at the plate end considering the width ratio between concrete and CFRP.

2 Related research and design codes

2.1 Retrofitted beam behaviour

2.1.1 General

FRP retrofit technology has been introduced in the civil engineering area in the recent decades. For structural applications, FRP is mainly used in two areas. The first area involves the use of FRP bars instead of steel reinforcing bars or pre-stressing strands in concrete structures. The other application, which is the focus of this thesis, is to retrofit structurally deficient structural members with external application of FRP.

FRP can be bonded to reinforced concrete structural elements using various techniques such as external bonding, wrapping and near surface mounting. FRP plates or sheets may be glued to the tension side of a structural member to provide flexural strength or glued to the web side of a beam to provide shear strength. FRP sheets can also be wrapped around a beam to provide shear strength and be wrapped around a column to provide confinement and thus increase the strength and ductility. Near surface mounting consists of sawing a longitudinal groove in a concrete member, applying a bonding material in the groove and inserting an FRP bar or strip.

2.1.2 Flexural strengthening of beams

Recently, FRP has started to be used to increase the flexural strength of members. To increase flexural capacity, the FRP should be glued to the member in the way that fibres are parallel to the direction of the principal stress.

FRP plates have been proved to increase the stiffness of the member and the load capacity, and reduce the cracking, Lacasse et al. [2]. The deflection of a retrofitted beam is considerably smaller than that of an un-retrofitted. This is due to the fact that stiffness is added to the member by the FRP plate or sheet, David et al. [3]. Moreover, the number of FRP sheet layers has considerable effect on the ultimate load and stiffness of a beam. The load carrying capacity was shown to increase with an increased number of layers of carbon fibre sheets for up to six sheets, by Toutanji et al. [4], Shahaway et al. [5] and Shehata et al. [6].

The initial load at the time of strengthening is also an important factor that affects the ultimate strength of RC beams strengthened with FRP. A beam strengthened at a higher level of load will produce a lower ultimate strength than a beam strengthened at a lower level of load, Wenwei and Guo [7]. It is also possible to apply FRP on continuous beams, either in the negative moment or positive moment zone, Grace et al. [8] and Aiello et al. [9]. The use of FRP laminates to strengthen continuous beams is effective for reducing deflections and for

increasing their load carrying capacity. A practical example in this field is a highway RC bridge slab in China retrofitted using FRP as shown in Figure 7.

Figure 7: Flexural strengthening of a highway RC bridge slab in China, [10].

2.1.3 Shear strengthening of beams

In the past decade, beams retrofitted for increased shear strength has attracted scientific attention; e.g Khalifa et al. [11], Daiaud and Chang [12] and Sundarraja and Rajamohan [13]. Shear strengthening is usually provided by bonding external FRP reinforcement on the sides of the beam with the fibre direction perpendicular to the beam axis or with an angle corresponding to the principal stress direction.

The modes of failure and gain in the ultimate strength depend on the orientation of the FRP, Norris et al. [14]. Using inclined FRP strips can result in increased shear strength and stiffness with substantial reduction in the shear cracking, Sundarraja and Rajamohan [13].

U-wrap, with FRP also in the flexural region, is the most effective configuration with respect to load capacity. Using U-wrap with FRP in the flexural region, both the shear and the flexural capacity increase and this may also prevent brittle failure, Sundarraja and Rajamohan [13] and Khalifa and Nanni [15].

The shear capacity is also dependent upon steel stirrup spacing and amount and distribution of FRP, Khalifa and Nanni [15].

2.1.4 Failure modes

There are three main categories of failure in concrete structures retrofitted with FRP that have been observed experimentally, Esfahani et al. [16], Ashour et al. [17], Garden and Hollaway [18], Smith and Teng [19]. The first and second type consist of failure modes where the composite action between concrete and FRP is maintained. Typically, in the first failure mode, the steel reinforcement yields, followed by rupture of FRP as shown in Figure 8(a). In the second type there is failure in the concrete. This type occurs either due to crushing of concrete before or after yielding of tensile steel without any damage to the FRP laminate, Figure 8(b), or due to an inclined shear crack at the end of the plate, Figure 8(c). In the third type, the failure modes involving loss of composite action are included. The most recognized failure modes within this group are debonding modes. In such a case, the external reinforcement plates no longer contribute to the beam strength, leading to a brittle failure if no stress redistribution from the laminate to the interior steel reinforcement occurs. Figures 8(d)-(g) show failure modes of the third type for RC beams retrofitted with FRP. In Figure 8(d), the failure starts at the end of the plate due to the stress concentration and ends up with debonding propagation inwards. Stresses at this location are essentially shear stress but due to small but non-zero bending stiffness of the laminate, normal stress can arise. For the case in Figure 8(e) the entire concrete cover is separated. This failure mode usually results from the formation of a crack at or near the end of the plate, due to the interfacial shear and normal stress concentrations. Once a crack occurs in the concrete near the plate end, the crack will propagate to the level of tensile reinforcement and extend horizontally along the bottom of the tension steel reinforcement. With increasing external load, the horizontal crack may propagate to cause the concrete cover to separate with the FRP plate. In Figures 8(f) and (g) the failure is caused by crack propagation in the concrete parallel to the bonded plate and adjacent to the adhesive to concrete interface, starting from the critically stressed portions towards one of the ends of the plate. It is believed to be the result of high interfacial shear and normal stresses concentrated at a crack along the beam. Also mid span debonding may take concrete cover with it.

One method to reduce the stress concentration at the plate end and retard or avoid brittle failure is taper end FRP design, Gao et al. [20]. Taper end FRP design means length difference between the adjacent FRP layers at the end.

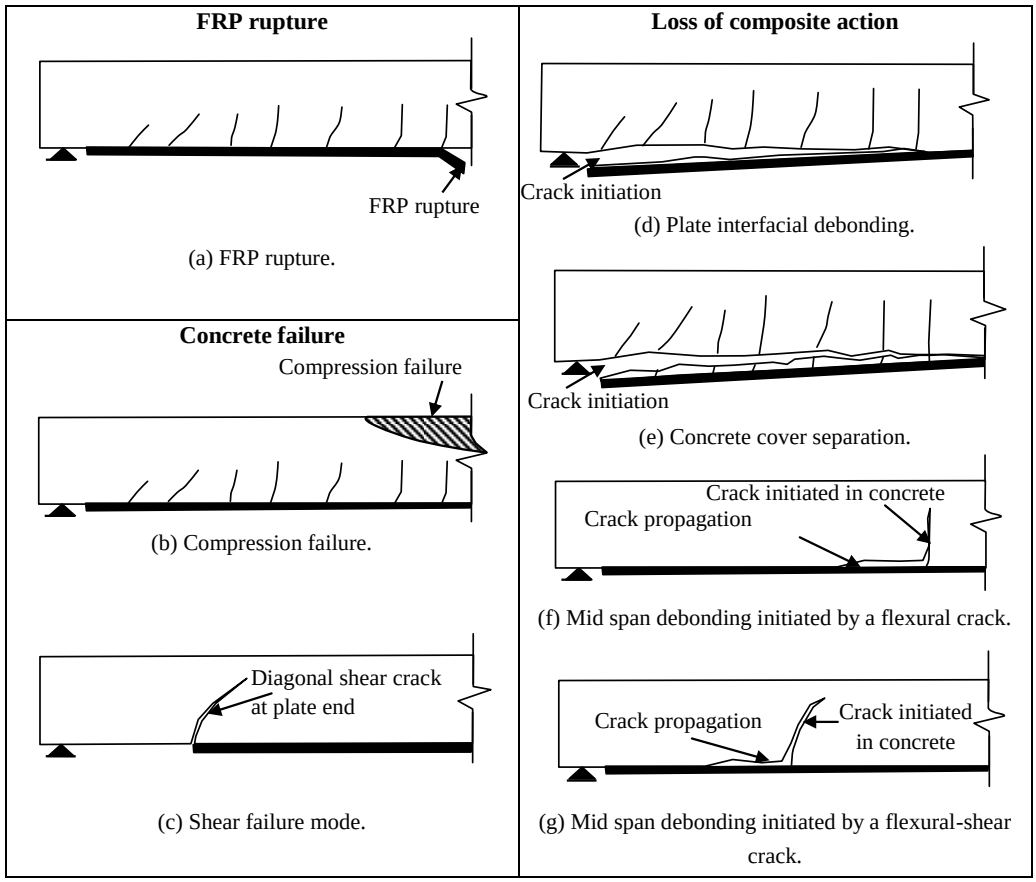

Figure 8: Failure modes in beam retrofitted for flexural strengthening.

2.2 Material behaviour

2.2.1 General

Reinforced concrete externally bonded with FRP consists of four major components: concrete, reinforcing steel, FRP and adhesive. This implies a highly nonlinear analysis challenge that involves complications such as extensive cracking and local effects.

A general approach to model such a problem is to select a suitable numerical approach to treat the response of each component separately and then obtain their combined effects by imposing the condition of material continuity. Thus, a complete analysis includes selecting a suitable numerical method, modelling each material using appropriate laws, and modelling the interaction between the materials. Therefore, the properties of each material should be known. This section provides information on concrete, steel, FRP materials and bond between FRP and concrete.

2.2.2 Concrete

Concrete is the most widely used construction material in the world. Concrete is composed of aggregate, cement, water and admixture. Concrete is generally weak in tension and strong in compression. This is due to the fact that the aggregate-mortar interface has lower strength than mortar and this yields to weak concrete under tension, Nilson et al. [21].

The stress-strain relationship for concrete under compression is initially linear elastic until micro-crack initiation. After that, the behaviour becomes nonlinear. After the ultimate compressive strength the stress decreases with increasing strain, See Figure 9a, Saenz [22].

Under uni-axial tension the stress–strain response follows a linear elastic relationship until the value of the failure stress is reached. The failure stress corresponds to the onset of micro-cracking in the concrete material. Beyond the failure stress the formation of micro-cracks is represented with a softening stress–strain response, Figure 9b. The softening curve of concrete under tension could be represented by using the model of Hillerborg [23], see Figure 10, where f_{ct} is the tensile strength and G_f is the fracture energy of concrete.

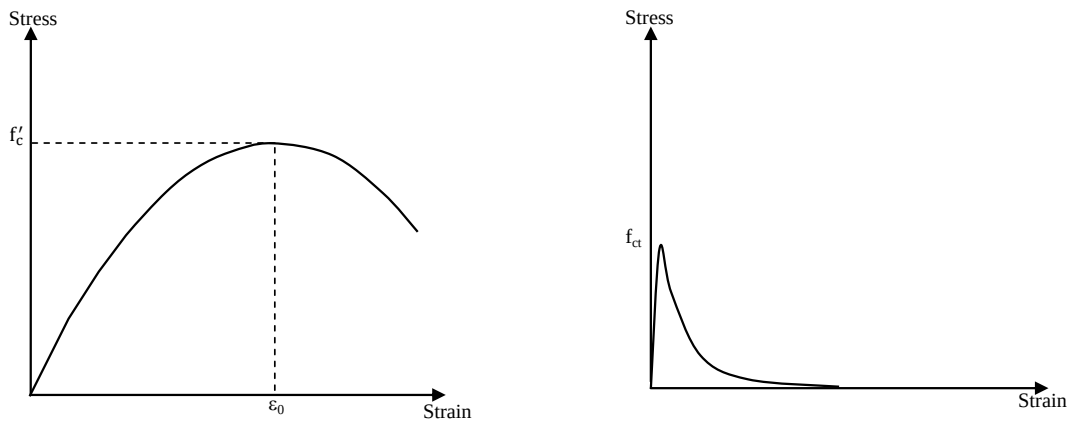

(a) Compression (b) Tension

Figure 9: Uni-axial stress-strain curves of concrete.

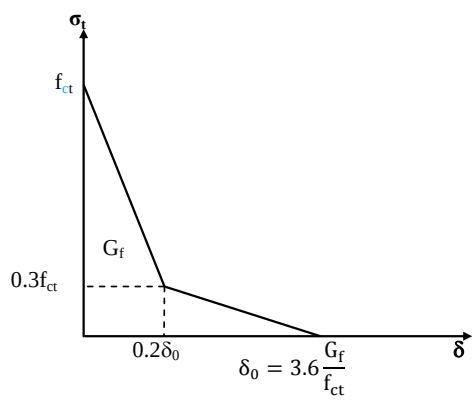

Figure 10: Softening curve of concrete under uni-axial tension, [23].

There are several frameworks of mechanics that can characterize concrete behaviour. The level of complexity of the model is directly related to the ability of the model to capture important features of mechanical behaviour of concrete such as softening. Several models are available for that.

One of the models is the discrete crack model. In this approach, the cracks are defined along element boundaries. The response of concrete in compression could be modelled by Drucker-Prager perfect plasticity, Wu and Hemdan [24].

Another model is the smeared crack model. In the smeared cracking approach, cracking of the concrete occurs when the principal tensile stress exceeds the tensile strength. The elastic modulus of the material is then assumed to be zero in the direction parallel to the principal tensile stress direction, Pham et al. [25] and Supaviriyakit et al. [26].

The third approach is a plastic damage model. Plastic damage models have been used successfully for predicting the response of standard concrete tests in both tension and compression. The nonlinear material behaviour of concrete can be attributed to two distinct material mechanical processes; plasticity and damage mechanisms. Hardening variables are used to represent the damage in concrete. Stiffness degradation is evaluated to represent the uni-axial tensile and compressive stress-strain response. This model assumes that the main two failure mechanisms are tensile cracking and compressive crushing of the concrete material, Qiao and Chen [27] and Coronado and Lopez [28].

2.2.3 Reinforcing Steel

Figure 11 shows a typical stress-strain relationship for reinforcing steel. Steel is initially linear-elastic for stress less than the initial yield stress. At ultimate tensile strain, the reinforcement begins to neck and strength is reduced. At a maximum strain, the steel reinforcement fractures and load capacity is lost, ASTM A615 [29]. This steel response may be defined by a few material parameters as identified in Figure 11. These include the elastic modulus, E_s, the yield strength, f_y, the strain at which peak strength is achieved, ε_u, the peak strength, f_u, the strain at which fracture occurs, ε_{max}, and the capacity prior to steel fracture, f_s.

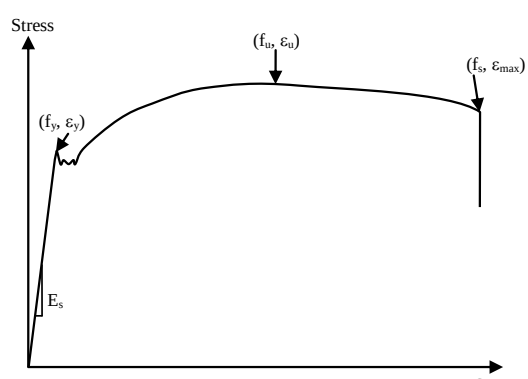

Figure 11: Tensile stress-strain curve for typical reinforcing steel bar.

For general engineering applications, an elastic-plastic constitutive relationship, either with or without strain hardening, is normally assumed for ductile reinforcing steel, as shown in Figure 12. In an elastic hardening model it is assumed that steel shows some hardening after it yields, Supaviriyakit et al. [26]. An elastic-perfectly plastic model generally yields acceptable results for the response prediction of RC members, Neale et al. [30].

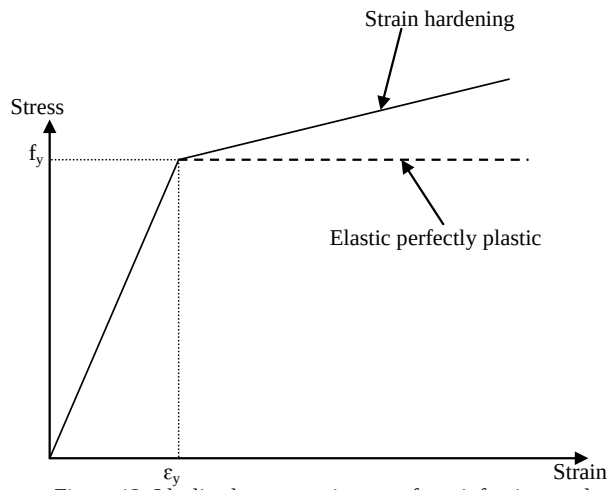

Figure 12: Idealized stress-strain curve for reinforcing steel.

2.2.4 FRP Material

Fibre reinforced polymer composites consist of high strength fibres embedded in a matrix of polymer resin as shown in Figure 13.

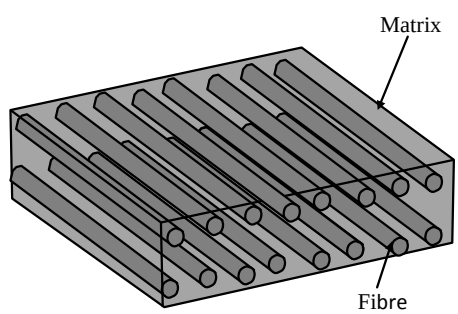

Figure 13: A schematic diagram showing a typical unidirectional FRP plate.

In FRP, the fibres provide both load carrying capacity and stiffness to the composite while the matrix is to ensure sharing of the load among fibres and to protect the fibres themselves from the environment. Typical properties for epoxy are given in Table 1. Most FRP materials

are made of fibres with high strength and stiffness, while their strain at failure is lower than that of the matrix.

Fibres typically used in FRP are glass, carbon and aramid. Typical values for properties of the fibres are given in Table 1. Carbon fibres are the stiffest, most durable and most expensive fibres. Carbon is quite resistant to most environmental impact. Glass fibres have lower strength and significantly lower stiffness but also a lower cost. Unprotected glass fibres degrade in most environments. Finally, aramid fibres have mechanical characteristics between those of glass and carbon, [31].

The fibre behaviour is linear elastic up to failure, with no significant yielding compared to steel. Figure 14 shows the stress-strain relationship for fibre, matrix and the resulting FRP material. Before the yielding of the matrix, the strain in fibre and matrix is the same. After the yielding of the matrix, a knee will appear in the stress-strain curve due to the fact that the matrix no longer contributes to the stiffness.

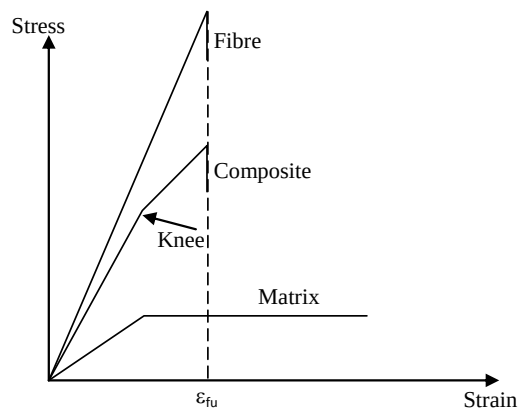

Figure 14: Stress-strain curves for typical fibre, resin and FRP composite, [31].

The mechanical properties of composites are dependent on the fibre properties, matrix properties, fibre-matrix bond properties, fibre amount and fibre orientation distribution. A composite with all fibres in one direction is designated as unidirectional. If the fibres are woven, or oriented in many directions, the composite is bi- or multidirectional.

Since it is mainly the fibres that provide stiffness and strength composites are often anisotropic with high stiffness in the fibre direction(s). In strengthening applications, unidirectional composites are predominantly used, Figure 13. The approximate stiffness and strength of a unidirectional FRP with a 65% volume fraction of carbon fibre is given in Table 1. As a comparison the corresponding properties for steel are also given.

Table 1. Typical strength and stiffness values for materials used in retrofitting, [31].

Material	Tensile strength (MPa)	Modulus of elasticity (GPa)	Density (kg/m^3)	Modulus of elasticity to density ratio (Mm^2/s^2)
Carbon	2200-5600	240-830	1800-2200	130-380
Aramid	2400-3600	130-160	1400-1500	90-110
Glass	3400-4800	70-90	2200-2500	31-33
Epoxy	60	2.5	1100-1400	1.8-2.3
CFRP	1500-3700	160-540	1400-1700	110-320
Steel	280-1900	190-210	7900	24-27

An isotropic linear elastic model is usually used to model FRP plate behaviour, if the direction of fibres is parallel to that of the principal stresses, Camata et al. [32]. Orthotropic linear elastic behaviour can be taken into consideration since the FRP material essentially has orthotropic behaviour, Hu et al. [33].

2.2.5 Bond between FRP and Concrete

Adhesives are used to attach the composites to other surfaces such as concrete. The most common adhesives are acrylics, epoxies and urethanes. Epoxies provide high bond strength with high temperature resistance, whereas acrylics provide moderate temperature resistance with good strength and rapid curing. Several considerations are involved in applying adhesives effectively. Careful surface preparation such as removing the cement paste, grinding the surface by using a disc sander, removing the dust generated by surface grinding using an air blower and careful curing are critical to bond performance, [1]. Often the most critical part of FRP application is the adhesive layer between the composite material and substrate, Figure 15.

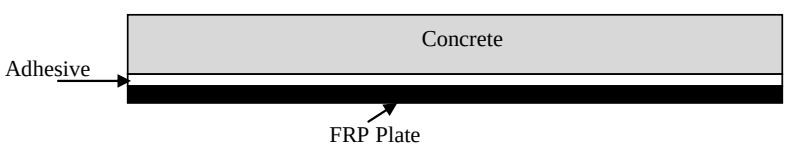

Figure 15: Concrete-FRP system.

Bond failure implies complete loss of composite action between concrete and laminate. This type of failure appears in the region of the bond as one of several types of cracking or separation patterns. Material de-cohesion and interface failure modes may occur. Material de-cohesion includes FRP delamination, cohesive failure of the adhesive and concrete substrate fracture. Interface failures are concrete-steel separation, FRP-adhesive separation and concrete-adhesive separation, which are considered to be dominating in retrofitting in most studies. Figure 16 illustrates each of the possible debonding modes.

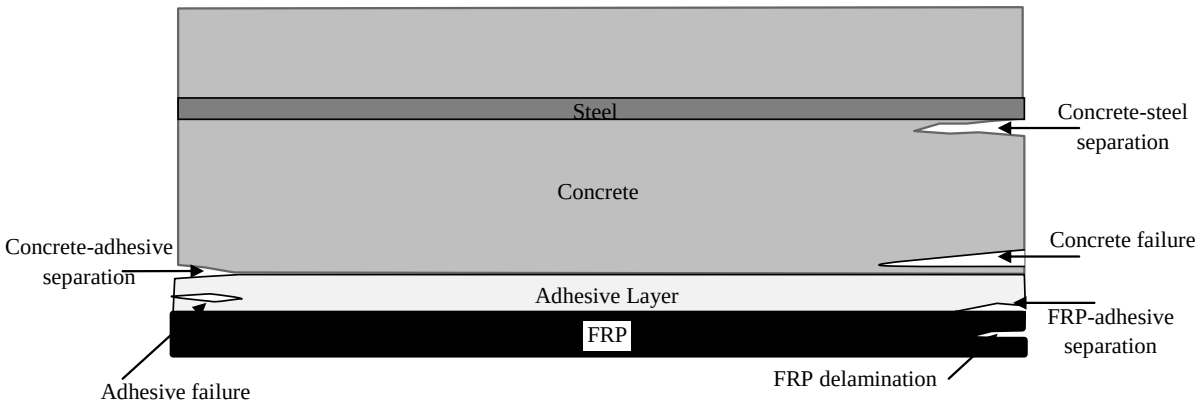

Figure 16: Failure modes at concrete plate bond.

The FRP-concrete interface is usually considered as a perfect bond, Lundqvist et al. [34] Supaviriyakit et al. [26]. However, it is important to consider the compliance of the bond between concrete and FRP since most research indicate that debonding is the dominating type of failure. Only few studies were focused on the bond, Neale et al. [30], Camata et al. [32].

The bond behaviour could be considered by using a bond-slip model to represent the behaviour of the interface layer. In most studies the bond-slip curve developed was based on axial strain measurement. The linear-brittle model was developed by Neubauer and Rostasy [35], Figure 17. This bond-slip model does not consider the softening behaviour. Therefore, the ultimate load computed using this bond-slip model is the load corresponding to initiation of interfacial micro-cracking, which in reality can be lower than the bond failure load.

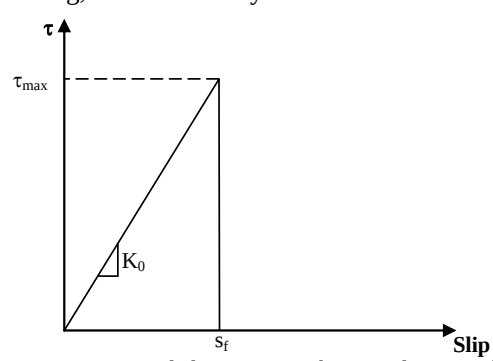

Figure 17: Bond-slip curve, Neubauer and Rostasy [35].

Bond slip should be represented by an ascending and a descending branch, Nakaba et al. [36] and Savioa et al. [37], Figure 18. A bilinear bond-slip curve was proposed by Monti et al. [38]. This model is linear up to maximum bond stress and then the stress decreases to zero stress at ultimate slip. The area underneath the stress-slip curve represents the fracture energy value.

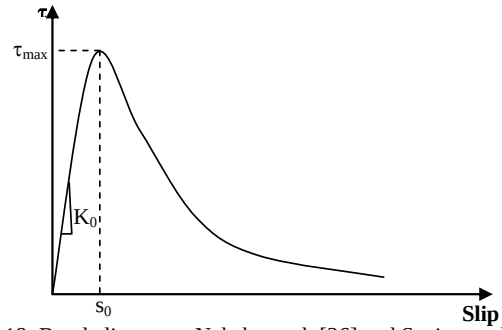

Figure 18: Bond-slip curve, Nakaba et al. [36] and Savioa et al. [37].

Lu et al. [39] simulated the behaviour of the pullout specimen by FEM. Bond stress and fracture energy parameters were obtained by fitting the simulation results of strain distribution along the FRP and ultimate load with experimental results. The bond-slip curves proposed by Lu et al. [39] are the precise model, simplified model and the bilinear model, Figures 19-21.

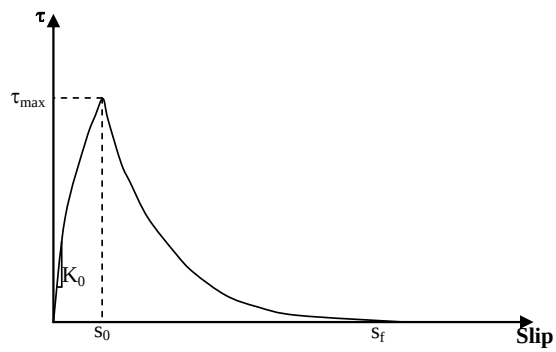

Figure 19: Bond-slip curve, precise model, Lu et al. [39].

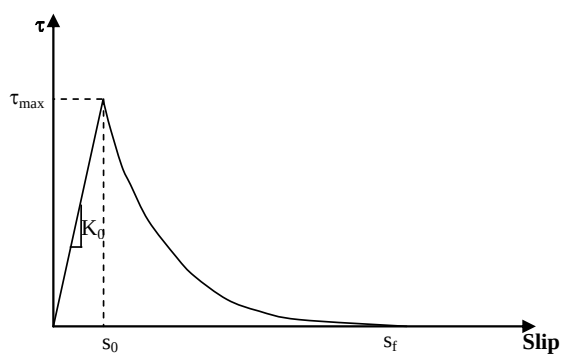

Figure 20: Bond-slip curve, simplified model, Lu et al. [39].

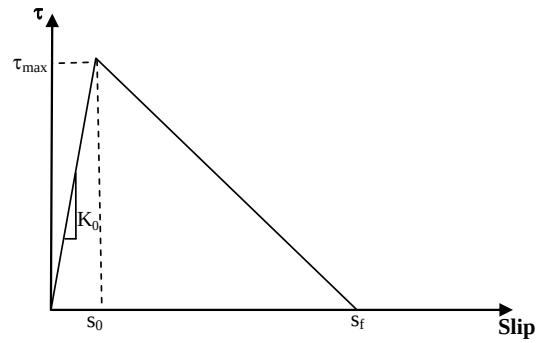

Figure 21: Bond-slip curve, bilinear model, Lu et al. [39].

Much research was focused on finding the bond strength and fracture energy. Neubauer and Rostasy [40] developed a relation to describe the bond strength and fracture energy expressed as a function of tensile strength of concrete. Brosens and Van Gemert [41], Nakaba et al. [36] and Lu et al. [39] developed a relation to describe the bond strength and the fracture energy expressed as a function of tensile strength of concrete and the ratio between the plate and the concrete width. Ulaga et al. [42] developed a relation expressed as a function of the compressive strength of concrete. Based on different types of interfacial bond stress-slip relationships, Yuan et al. [43] proved that the maximum interfacial bond force can be expressed as a function of fracture energy and FRP stiffness.

2.3 Design codes

2.3.1 General

Although the technique of externally bonded reinforcement is quite new, there are already several codes and guidelines available for engineers for planning a retrofitting project.

fib Bulletin 14 was one of the first published a guidelines, [1], in the field of externally bonded reinforcement. In the United Kingdom, already the second edition of TR55 Design guidance for strengthening concrete structures, [44], has been published. In addition CNR [45] is available in Italy. Täljsten [46] has developed a design guideline for FRP plate bonded concrete. ACI 440.2R-08 [47] also developed a guideline for the design and construction of externally bonded FRP-RC structures.

The use of FRP as external reinforcement in strengthening RC structure requires the development of design procedures that ensure adequate safety. Several failure modes could develop in retrofitted beams using FRP i.e. compression failure before or after steel yielding, FRP rupture before or after steel yielding and loss of composite action. Most of the design guidelines overcome the above failure modes in the design in different ways. The flexural capacity in guidelines comes from three parts: concrete, steel and FRP. However, details of

each of the codes are different from each other. The following sections clarify the principles of calculation for each guideline. The notation used in this section is given in section 2.5.

2.3.2 Material safety factor

In most design guidelines the design strength for material is obtained by dividing the characteristic strength by a material safety factor. ACI design guideline, however, suggests that the design strength should be determined using a reduction factor only for FRP, see Table 2.

Table 2 shows the lower and upper limit of the material safety factor and the reduction factor in each design guideline.

Table 2: Material factors.

Design guideline	Concrete	Steel	FRP	
			Safety factor	Reduction factor
fib Bulletin 14 [1]	1.5	1.15	1.2-1.5(1)	-
TR 55 [44]	1.5	1.15	1.54	-
CNR [45]	1.6	1.15	1.2-1.45(2)	-
Täljsten [46]	1.5	1.15	1.2-9.5(3)	-
ACI [47]	-	-	-	0.5-0.95(4)

(1) Depends on the application and FRP type.

(2) Depends on the application and type of failure for FRP.

(3) Depends on the uncertainties in characteristic value for strength, the uncertainties in the calculation model and existing dimension, the type of failure, the influence of control, influence of long time or short time and strengthening method.

(4) Depends on the type of FRP and environment condition.

2.3.3 Allowable strain

ACI prescribes 0.003 as allowable strain of concrete and the others use 0.0035.

2.3.4 Safety reduction

In addition, ACI uses a strength reduction for the moment. An additional strength reduction factor of 0.85 is applied to the contribution of FRP reinforcement to the moment capacity.

2.3.5 Calculation of moment

Ultimate limit state (ULS) analysis of RC members strengthened with FRP is used in all guidelines and relies on the following fundamental assumptions:

- A section plane before bending remains plane after bending.

- No relative slip between external FRP and concrete.
- Take into consideration the effect of initial load prior to strengthening; this is by considering the initial strain distribution in the calculations.

The position of the neutral axis is computed by means of a force equilibrium equation along the beam axis. The moment capacity M_d of the strengthened member can then be calculated using a moment equilibrium equation, see Figure 22.

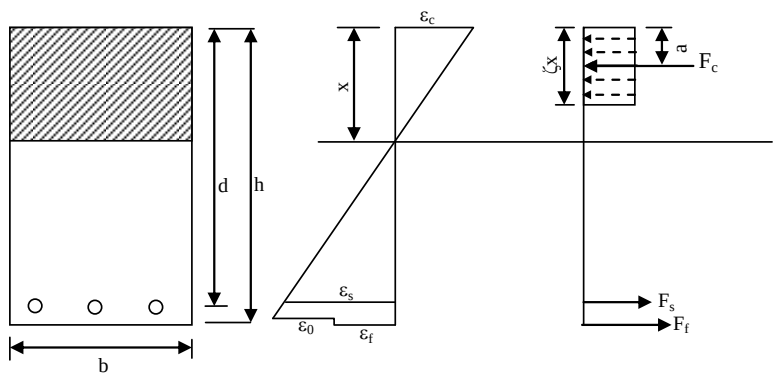

Figure 22: Stress and strain diagram for a cross-section of a rectangular beam.

There is a small difference between the design guidelines concerning the depth of the compression zone. Table 3 shows the value of ζ in each design guideline.

Table 3: Value of ζ.

Design guideline	ζ
fib Bulletin 14 [1]	0.8
TR 55 [44]	0.9
CNR [45]	0.8
Täljsten [46]	0.8
ACI [47]	0.65-0.85*

*Depends on strength of concrete.

The nominal moment capacity corresponding to the two failure modes can be expressed by:

- Steel yielding and FRP rupture:

$$M_d = A_s f_y (d - a) + A_f E_f \varepsilon_{fu} (h - a) \quad (1)$$

- Steel yielding and concrete crushing:

$$M_d = A_s f_y (d - a) + \left(\left(\frac{h - x}{x} \right) \varepsilon_{cu} - \varepsilon_0 \right) A_f E_f (h - a) \quad (2)$$

2.3.6 Composite action

(1) Plate debonding at last crack and flexural cracks:

To prevent debonding at last crack and flexural cracks the anchorage length and maximum force should be checked. Several guidelines consider this type of failure mode. The criteria in each guideline are summarized in Table 4 and Table 5 for anchorage length and maximum force, respectively.

Table 4: Anchorage length.

Design guideline	Anchorage length
fib Bulletin 14 [1]	$l_b = \sqrt{\frac{E_f t_f}{2 f_{ctm}}}$ with approach 1 and 3
	$l_b = 1.44 \sqrt{\frac{E_f t_f}{\sqrt{f_{ctm} f_{ck}}}}$ with approach 2
TR 55 [44]	$l_b = 0.7 \sqrt{\frac{E_f t_f}{f_{ctm}}}$
CNR [45]	$l_b = \sqrt{\frac{E_f t_f}{2 f_{ctm}}}$
Täljsten [46]	$l_b = \ell_{cr} \frac{0.2 f_{fd}}{\sqrt{f_{ct} E_f w / t_f}}$, $\ell_{cr} = 250$ mm, w: is the crack width, 0.5 mm.
ACI [47]	-

fib Bulletin 14, approach 1 and 3, TR55 and CNR use the same relation in calculating the anchorage length. All design guidelines take the effect of FRP geometry and FRP and concrete properties into account. In addition to that Täljsten considers the effect of tensile strength of FRP as well as crack width.

Maximum force and additional design limitations for several guidelines are also given in Table 5. fib Bulletin 14 gives three different approaches. The first approach restricts the strain in FRP. The second approach is based on calculation of the maximum increase in tensile FRP stress and the third one is based on calculation of bond shear stress. TR55 limits the strain in FRP as well as the bond shear stress. ACI design guidelines limit the strain. CNR limits the stress between subsequent cracks.

Table 5: Maximum force and additional limitations.

Design guideline	Maximum force	Additional limitations
fib Bulletin 14 [1]	$N_f = 0.64\alpha k_b b_f\sqrt{E_f t_f f_{ctm}}$, $k_b = 1.06\sqrt{\frac{2-\frac{b_f}{b_c}}{1+\frac{b_f}{400}}}$, α=0.9	$\varepsilon_f < 0.0065\text{-}0.008$
	$N_f = 0.64\alpha k_b b_f\sqrt{E_f t_f f_{ctm}}$, $k_b = 1.06\sqrt{\frac{2-\frac{b_f}{b_c}}{1+\frac{b_f}{400}}}$, α=0.9	$\varepsilon_s < \varepsilon_{yd}: \quad \frac{V_d}{0.95 d b_f\left(1+\frac{A_s E_s}{A_f E_f}\right)} \le 1.2 f_{ctk}$ $\varepsilon_s \ge \varepsilon_{yd}: \quad \frac{V_d}{0.95 d b_f} \le 1.2 f_{ctk}$
	$N_f = \frac{0.23 b_f t_f}{\gamma_c}\sqrt{\frac{E_f\sqrt{f_{ck}\, f_{ctm}}}{t_f}}$	$\sigma_f^B = \frac{0.185 E_f}{s_{rm}} - 0.285\sqrt{f_{ck}\, f_{ctm}}\frac{s_{rm}}{4t_f}$, $Max\Delta\sigma_{fd}{}^{(B)} = \frac{1}{1.5}\left[\sqrt{\frac{0.053 E_f\sqrt{f_{ck}\, f_{ctm}}}{t_f} + (\sigma_f^{(B)})^2} - \sigma_f^{(B)}\right]$, $max\Delta\sigma_{fd}{}^{(1)} = max\Delta\sigma_{fd}{}^{(A)} - \frac{\left(max\Delta\sigma_{fd}{}^{(A)} - max\Delta\sigma_{fd}{}^{(B)}\right)}{\sigma_f^{(B)}}\sigma_{fd}$, $max\Delta\sigma_{fd}{}^{(2)} = \frac{1}{1.5}\left[\sqrt{\frac{0.053 E_f\sqrt{f_{ck}\, f_{ctm}}}{t_f} + (\sigma_{fd})^2} - \sigma_{fd}\right]$, $max\Delta\sigma_{fd}{}^{(3)} = \min\left\{(f_{fd} - \sigma_{fd}), \frac{1}{1.5}\left[\sqrt{\frac{0.053 E_f\sqrt{f_{ck}\, f_{ctm}}}{t_f} + (\sigma_{fd})^2} - \sigma_{fd}\right]\right\}$ $\tau_{sm} = 1.85 f_{ctm}, \tau_{fm} = 0.44 f_{ctm}, s_{rm} = 2\frac{M_{cr}}{z_m}\frac{1}{\sum\tau_{fm} b_f + \sum\tau_{sm} d_s \pi}$, $M_{cr} = \frac{k f_{ctk,0.95} b h^2}{6}, z_m = 0.85\frac{(h E_f A_f + d E_s A_s)}{(E_f A_f + E_s A_s)}$ see Figure 23
TR55 [44]	$N_f = 0.5 b_f k_b\sqrt{E_f t_f f_{ctm}}$, $k_b = 1.06\sqrt{\frac{2-\frac{b_f}{b_c}}{1+\frac{b_f}{400}}}$	$\varepsilon_f < 0.008$ $\tau_{max} < 0.8$ MPa
CNR [45]	$N_f = \frac{1}{1.26\gamma_f}\sqrt{\frac{2\, E_f\sqrt{f_{ck}\, f_{ctm}}}{t_f}}$	$\sigma_f < \frac{3}{1.26\gamma_f}\sqrt{\frac{2\, E_f\sqrt{f_{ck}\, f_{ctm}}}{t_f}}$
Täljsten [46]	$N_f = 0.2\, f_{fd}\, b_f t_f$	-
ACI [47]	-	$\varepsilon_{fmax} = \varepsilon_{fu} k_m$ $k_m = \begin{cases}\frac{1}{60\varepsilon_{fu}}\left(1-\frac{n E_f t_f}{360000}\right) \le 0.9 & \text{for} \quad n E_f t_f \le 180000\\ \frac{1}{60\varepsilon_{fu}}\left(\frac{90000}{n E_f t_f}\right) \le 0.9 & \text{for} \quad n E_f t_f > 180000\end{cases}$

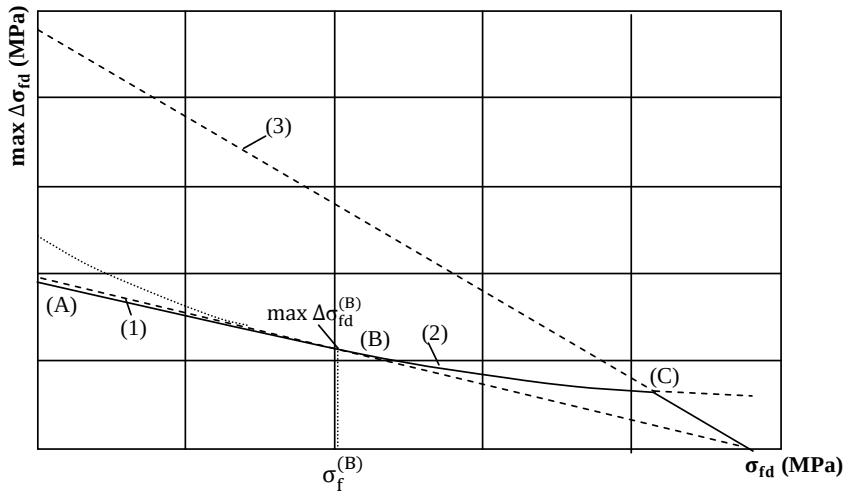

Figure 23: Diagram of the maximum possible increase in tensile stress between two subsequent cracks, Niedermeier et al. [48].

(2) Shear cracks:

Only fib Bulletin 14 takes into consideration the shear crack effect. Shear cracks in concrete elements are inclined and may result in debonding. fib Bulletin 14 uses the following to check the debonding caused by a shear crack

$$V_d \leq \tau_{rp} b_c d \tag{3}$$

where

$$\tau_{rp} = 0.38 + 151\rho_{eq} \tag{4}$$

$$\rho_{eq} = \frac{A_s + A_f \frac{E_f}{E_s}}{b_c d} \tag{5}$$

(3) Stress concentration at plate end:

Stress concentrations are especially obtained at the FRP end. Therefore bond interface crack initiation at the end of FRP should be prevented.

fib Bulletin 14 uses a simple criterion to predict shear failure at the plate end and concrete cover separation. This criterion does not depend on the material properties and geometry used in the retrofitting system. This approach employed the fictitious shear span concept, see Figure 24.

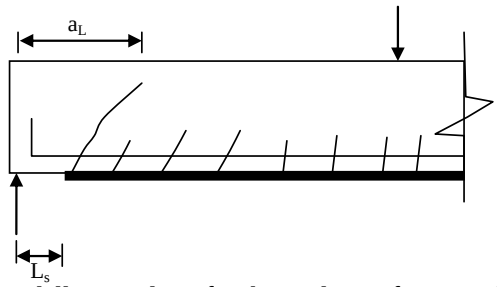

Fig. 24.Modelling analogy for the analysis of FRP-end shear failure.

$$V_{sd} \leq V_{Rd} = \tau_{Rd} b d \tag{6}$$

$$\tau_{Rd} = 0.15 \sqrt[3]{3\frac{d}{a_L}} \left(1 + \sqrt{\frac{200}{d}}\right) \sqrt[3]{100 \rho_s f_{ck}} \tag{7}$$

$$a_L = \sqrt[4]{\frac{\left(1-\sqrt{\rho_s}\right)^2}{\rho_s} d L_s^3} \tag{8}$$

Stress concentrations at the plate end are also treated in fib Bulletin 14, in the serviceability limit state, using an equation by Roberts [49]. The shear stress is limited to the characteristic tensile strength.

$$\tau_f = \left[V_{x=0} + \left(\frac{G_a}{E_f t_f t_a}\right)^{0.5} M_{x=0}\right] \frac{t_f (h - x_e)}{I} \tag{9}$$

Täljsten, [42], checks the stress concentration at the end of the plate. He assumed the failure to begin when the principal stress is equal to the concrete strength. Täljsten assumes the maximum shear stress at plate end equal to

$$\tau_{max} = \frac{G_a P}{2 t_a E_c b_c} \frac{(2\ell + a_f - b_L)}{(\ell + a_f)} \frac{(a\lambda + 1)}{\lambda^2} \tag{10}$$

$$\lambda^2 = \frac{G_a b_f}{t_a} \left[\frac{1}{E_f A_f} + \frac{1}{E_c A_c} + \frac{z_0}{E_c b_c}\right] \tag{11}$$

Normal stress is stress assumed equal to shear stress. Then the following criterion is used:

$$\sigma_y = \tau_{xy} = \tau_{max} \tag{12}$$

$$\sigma_1 < f_{ctk} \tag{13}$$

ACI controls this failure by length of FRP. It is recommended to extend the laminate to a certain distance past the point corresponding to the cracking moment, M_{cr}. In addition, the

design shear force at the termination point should not be greater than two thirds of the concrete shear strength, $V_u<0.67V_c$.

2.4 Discussion

Even though extensive work has been done on the use of FRP laminates in retrofitting there is a need for further refinement of models and further parameter studies. From the literature review, it can be concluded that the interface zone has been modelled with linear or with non-linear models.

Researchers have reported on different failure modes. It is important to understand under what circumstances a certain failure mode will occur.

Despite that many models have been developed to represent the bond strength and fracture energy, it is necessary to develop a model that depends on the adhesive properties, because these properties play a significant role in debonding failure beside concrete properties.

Main weaknesses in the available guidelines are lack of a unified design approach especially in the design rules concerning composite action. Better understanding is needed and development of simple design models for mechanisms associated with debonding is an important task. Particularly, the equation for shear stress at the end of the plate in fib Bulletin 14 guideline needs an improvement by taking into consideration a non-uniform stress distribution effect in 3D, i.e. concrete FRP width ratio effect.

2.5 Notations

A_f	Cross sectional area of FRP.
A_s	Cross sectional area of steel.
E_f	Elastic modulus of FRP.
E_s	Elastic modulus of steel.
F_c	Compression force in concrete.
F_f	Tensile force in FRP.
F_s	Tensile force in steel.
G_a	Shear modulus of the adhesive layer.
I	Second moment of area of fully composite transformed equivalent FRP plate.
I_c	Second moment of area of the cracked section.
L_s	The distance of the FRP end from the support.
M	Bending moment at the cut off point.
M_{cr}	Bending moment causing cracking.
M_d	Moment capacity for the member.
$M_{x=0}$	Bending moment at the end of the laminate plate.

V_d	Maximum shear force.
V_{Rp}	Resisting shear force at which shear crack peeling is initiated.
$V_{x=0}$	Shear force at the end of the laminate plate.
a	The depth from extreme compression fibre to the resultant force. There is a small difference between the design guideline in assuming this depth. Table 3 shows the value of α in each design guideline.
a_f	Distance between support and termination point of FRP.
b	Width of beam.
b_f	Width of FRP plate.
b_L	Distance between point load to the support.
d	Lever arms of internal forces for longitudinal steel.
d_s	Diameter of the steel bars.
f_c'	Design compressive strength of concrete in European codes and nominal strength in ACI.
f_{cbd}	Design bond shear strength.
f_{ck}	Characteristic value of the concrete compressive strength.
f_{ct}	Characteristic value of the concrete compressive strength.
f_{ctk}	Characteristic value of the concrete tensile strength.
$f_{ctk,0.95}$	Upper bound characteristic tensile strength of concrete.
f_{ctm}	Mean tensile strength of concrete.
f_{fd}	Design tensile strength of FRP.
f_y	Design yield strength of steel in European codes and nominal strength in ACI.
h	Depth from the extreme compression fibre to the externally bonded FRP.
$h - x_e$	Distance from neutral axis of the strengthened section to the plate.
k_b	Geometry factor.
ℓ	Half length of FRP.
t_a	Adhesive thickness.
t_f	FRP thickness.
s_{rm}	Unfavourable spacing of flexural cracks.
x	Depth of the neutral axis from the extreme compression fibre.
z_0	Inner lever arm which equal h-a.
α	Reduction factor taken as 0.9.
α_f	Modular ratio for FRP to concrete.
γ_f	FRP material safety factor.
ε_0	Concrete strain on tension side at time of the FRP application.
ε_c	Concrete strain in the extreme compression fibre.
ε_{cu}	Compression failure strain of concrete.
ε_f	FRP strain.

ε_{fu}	Tensile failure strain of FRP.
ε_{s}	Tensile steel strain.
ε_{yd}	Design value of the yield strain of the steel reinforcement.
σ_1	Principal stress.
σ_f	FRP stress.
σ_{fd}	Design value of FRP stress.
τ_{fm}	Mean bond stress of the external reinforcement.
τ_{Rp}	Resisting shear stress corresponding to initiation of peeling.
τ_{sm}	Mean bond stress of the internal reinforcement.

3 Overview of present work

3.1 Development of modelling framework

One main focus of this study is to develop a modelling framework representing the behaviour of beams retrofitted with FRP. This involves several aspects of theoretical and practical interest. Important issues include material models, element types, mesh, convergence and boundary conditions. A general conclusion regarding these issues is that the model must be rich enough to be able to capture the important phenomena, but it should not be more complex than necessary since this would only increase the computer time needed. To be able to verify the quality of the model, results must be compared to experimental results. How these issues were handled is described in this section.

3.1.1 FEM program

Abaqus/standard, [50], was used for the finite element modelling in this work. This FEM package includes a large variety of material models and elements including facilities necessary for this particular subject.

3.1.2 Constitutive models

(1) Concrete

In the last decades, many constitutive models which can predict the behaviour of concrete, including cracks and crushing have been developed. Two approaches are available in Abaqus to predict the behaviour of concrete: smeared crack and plastic damage models. The plastic damage model was selected for this study since it has higher potential for convergence compared to the smeared crack model.

The concrete plastic damage model assumes that the two main concrete failure mechanisms are cracking and crushing. Crack propagation is modelled by using continuum damage mechanics, stiffness degradation.

The plastic damage model requires the values of elastic modulus, Poisson's ratio, the plastic damage parameters and description of compressive and tensile behaviour. The five plastic damage parameters are the dilation angle, the flow potential eccentricity, the ratio of initial equibiaxial compressive yield stress to initial uniaxial compressive yield stress, the ratio of the second stress invariant on the tensile meridian to that on the compressive meridian and the viscosity parameter that defines viscoplastic regularization. The values of the last four parameters were recommended by the Abaqus documentation for defining concrete material and were set to 0.1, 1.16, 0.66, and 0.0, respectively. The dilation angle and Poisson's ratio were chosen to be 37° and 0.2, respectively.

Another important thing is to represent the stress-strain curve for concrete in an accurate way. For a given concrete characteristic compressive strength, the concrete stress-strain curve in compression can be described using a suitable confined concrete model such as the one developed by Sneaze [22]. The stress-strain curve can be defined beyond the ultimate stress, into the strain-softening regime. The compressive inelastic strain, $\tilde{\varepsilon}_{0c}^{in}$, is defined as the total strain minus the elastic strain, $\tilde{\varepsilon}_{0c}^{in} = \varepsilon_c - \varepsilon_{0c}^{el}$, as illustrated in Figure 25.

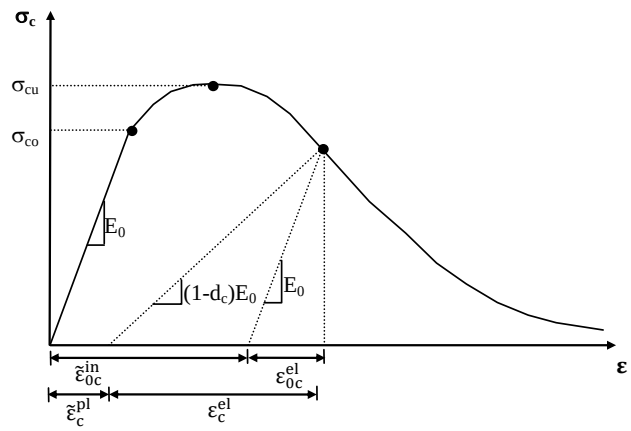

Figure 25: Response of concrete to uniaxial loading in compression.

The concrete behaviour in tension was modelled using a linear elastic approach until cracking is initiated at tensile strength. After crack initiation, the softening will start. The post-failure behaviour for direct straining is modelled with tension stiffening, which permits to define the strain-softening behaviour for cracked concrete. Tension stiffening is required in the concrete damage plasticity model. It is possible to specify tension stiffening by means of a post-failure stress-strain relation or by applying a fracture energy cracking criterion. Hillerborg's fracture energy proposal, [23], was used in this study. With this approach the behaviour is characterized by a stress-crack opening response rather than a stress-strain response.

The degradation of the elastic stiffness is characterized by two damage variables, d_t and d_c, which are assumed to be functions of the plastic strains. The damage variables can take values from zero, representing the undamaged material, to one, which represents total loss of strength. Linear relationship between the damage variable and stress was assumed.

(2) Steel reinforcement

The constitutive model used to simulate the steel reinforcement was the classical metal elastic-perfectly plastic model. The input for the steel model includes elastic modulus Poisson's ratio and yield stress. Possion's ratio was assumed to be 0.3 in this study.

(3) Interface between concrete and steel

Perfect bond between steel and concrete was assumed in this work.

(4) FRP

For FRP, linear elastic behaviour up to failure was assumed. Elastic modulus, Poisson's ratio, and tensile strength were needed for the simulations. Poisson's ratio was assumed to be 0.3 in this study. Both orthotropic and isotropic linear elasticity were evaluated. There was, however, no significant difference in the results for cases when the fibre direction was parallel to the tensile stress. Thus, it is preferable to use the more simple assumption of isotropy.

(5) Interface between concrete and FRP

The model for the interface between FRP and concrete is of essential importance. A perfect bond model and cohesive models were evaluated for describing the concrete-FRP interface. With a perfect bond between FRP and concrete the ultimate load and stiffness were overestimated, compared to experimental results. This is because degradation in the bond cannot be captured in this type of model, and it implies that a perfect bond model is not suitable in a study focusing on fracture. The cohesive model available in Abaqus is a better choice for representing the interface behaviour. The cohesive model defines surfaces of separation and describes their interaction by defining a relative displacement at each contact point. The definition of the model is characterised by the parameters, initial stiffness, shear strength, fracture energy and curve shape of the bond slip model. Input values for the cohesive model found in literature were widespread and few. In previous models the input data was only related to concrete properties, and it was considered important also to include the adhesive properties. In order to find the values of initial stiffness, shear strength and fracture energy that gave the best fit, simulations were performed and the results were compared with experimental results from literature.

The following relations for initial stiffness, K_0, shear strength, τ_{max}, and fracture energy, G_f, as a function of the adhesive and concrete properties, were proposed:

$$K_0 = 0.16\frac{G_a}{t_a} + 0.47 \tag{14}$$

$$\tau_{max} = 1.46{G_a}^{0.165}{f_{ct}}^{1.033} \tag{15}$$

$$G_f = 0.52{f_{ct}}^{0.26}{G_a}^{-0.23} \tag{16}$$

where t_a is the adhesive thickness in mm, G_a is the adhesive modulus in GPa and f_{ct} is the tensile strength of concrete in MPa.

3.1.3 Model geometry and element types

3D simulations were performed to get an accurate approximation of the overall behaviour, failure mode and the out-plane effects (e.g. width ratio between concrete and FRP) of the retrofitted structure.

Taking advantage of the double symmetry of the beam, only one quarter of the specimen was modelled.

To model specimens having internal steel bars as reinforcement, 4-node linear tetrahedral elements were used for the concrete, reinforcement steel, steel plates at supports and under the load and FRP. This element type was used because the beam has a complex geometry since there are steel bars inside the concrete. To model the interface layer, 8-node 3-D cohesive elements were used. These elements are composed of two surfaces separated by a thickness. The relative motion of the bottom and top parts of the cohesive element measured along the thickness direction represents opening or closing of the interface. The relative motion of these parts perpendicular to the thickness direction represents the transverse shear behaviour of the cohesive element. 8-node brick elements were used for specimens without internal reinforcement.

3.1.4 Mesh and convergence issues

Preliminary results obtained with a rather coarse mesh showed that it was fairly difficult to obtain convergence and the results were not acceptable. The results obtained from a fine mesh were more accurate. An even finer mesh gave almost the same result as the previous mesh but more time was needed for computations. Therefore a moderately fine mesh was chosen in this study. The solution time with this mesh is approximately 3-12 h, using processor 2 Xeon 5160 (3.0 GHz, dual core).

When performing a nonlinear analysis convergence difficulties may occur, especially when cracks start to initiate. One solution used in this study was using small enough time increments to ensure that the analysis will follow the load-deflection curve, and this improved the convergence. In addition a damping factor based on the dissipated energy fraction was used. The dissipated energy fraction has a default value of 2.0×10^{-4}. In this study 2.0×10^{-5} was used.

3.1.5 Boundary conditions

Boundary conditions that represent structural supports specify values of displacement and rotation variables at appropriate nodes. The boundary conditions for the simulated quarter of a beam are illustrated in Figure 26. Load was applied in a location corresponding to the experimental situation, either as distributed load or as a point load. For point loading

deflection increments were applied and Newton method was used. For distributed load, load increments were applied and Riks method was used.

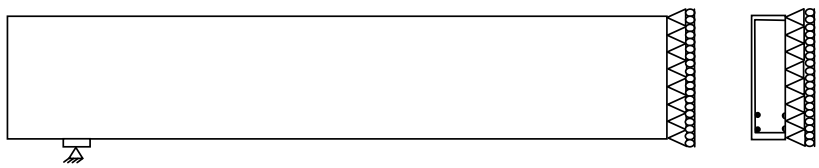

Figure 26: Boundary conditions used in numerical work.

Tied contact was used for connecting meshes. In this approach, each of the nodes on the fine mesh has the same displacement as the point on the coarse mesh to which it is closest. This allows for the modelling of normal and shear stresses along the entire tied surfaces. The tied contact was used between concrete and cohesive element, cohesive element and FRP, and concrete and steel plate under load.

3.1.6 Experimental work for verification

An experimental study of 4-point bending was made to verify the applicability of the FEM modelling framework. Two groups of beams were considered. The first group was designed to fail in flexure, while the other group was designed to fail in shear. All beams were loaded until cracks developed. Then the beams were unloaded and retrofitted with FRP. The retrofitting schemes were chosen according to the failure location. The first group was retrofitted using FRP only for flexure, while the second group was retrofitted only for shear.

3.1.7 Comparison with experimental work

From the FEM analysis the load-deflection relationships until failure, failure modes and crack pattern were obtained and compared to the experimental results. Comparison of the results showed a good agreement between FEM and experimental works, see Figures 27-29.

The FEM analysis predicts the beam to be somewhat stiffer than the experimental work shows. This can be attributed to the fact that perfect bond between concrete and steel was assumed and the estimation of the behaviour of the interface between FRP and concrete. With a perfect bond between FRP and concrete, the ultimate load and stiffness was overestimated.

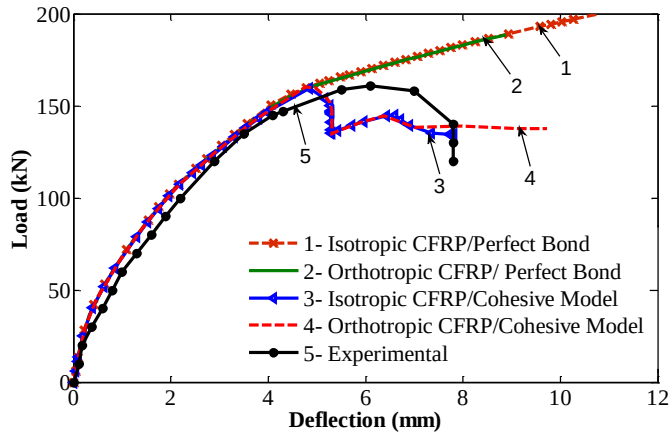

Figure 27: Load-deflection curves of beams, obtained by experiments and different models, RB1, Paper B.

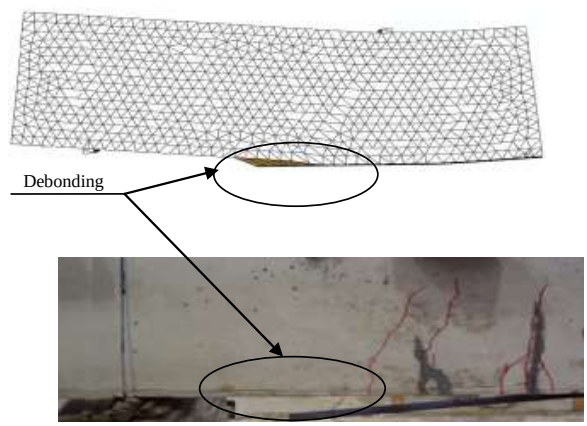

Figure 28: Comparison of failure mode from FEM analysis and experiment for beam RB2, Paper B.

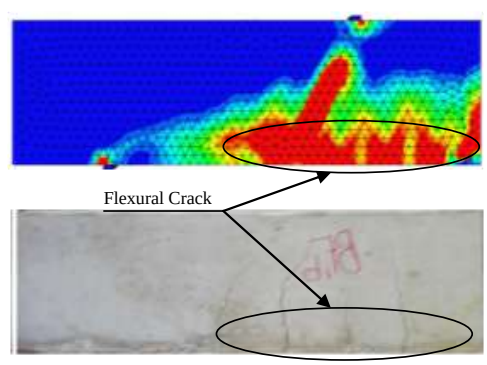

Figure 29: Comparison between plastic strain distribution from FEM analysis and crack patterns from experiments, Paper B.

3.2 Effect of parameters

The FE model developed and experimental results were used to investigate the influence of various parameters on the behaviour of retrofitted structures.

3.2.1 FRP geometry and properties

Different length, width, and stiffness of FRP were studied. The length of FRP affects significantly the behaviour of a beam retrofitted in flexure. When the length of FRP increases the load capacity increases. For a long plate the anchorage length needed is provided outside the cracking region which leads to an improved performance. Since the moment is decreasing towards the end of the beam, the shear stresses do not reach the same level in the anchorage zone.

Nonlinear finite element analyses were performed with varying orientation and length of FRP when used in shear. The results showed that it is preferable to use a length that covers the entire beam depth and FRP with orientation 45^o to the beam axis.

Simulations were also performed to examine the effect of stiffness, and width of FRP. The results showed that it is preferable to increase the amount of reinforcement by increasing the width of FRP rather than increasing the thickness of FRP, see Figure 30. This is due to the fact that when the thickness instead of the width of FRP increases, this means that the width ratios between concrete and FRP would decrease and therefore debonding risk would increase.

The stiffness of a beam increases with increased FRP stiffness. The stiffness of FRP, however, affects the failure mode of a retrofitted beam. Small stiffness results in FRP rupture. When high stiffness was used debonding occurred before steel yielding and resulted in a small ultimate load value. With medium stiffness and medium width ratio, debonding occurred after steel yielding, see Figure 31.

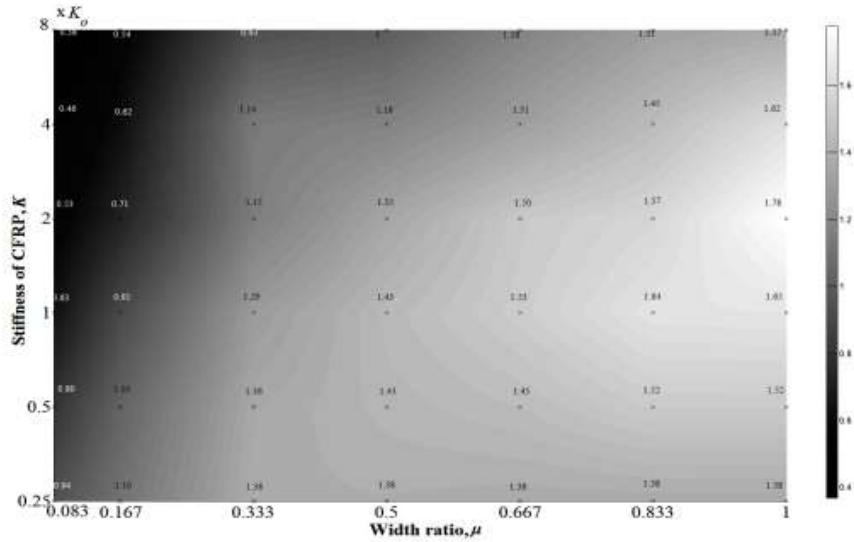

Figure 30: Maximum load ratio, α= maximum load of retrofitted beam/maximum load of control beam, versus the width ratio, $\mu = w_{CFRP}/w_{beam}$, and stiffness of CFRP, $K=E_{CFRP}\, w_{CFRP}\, t_{CFRP}$. The scale indicates the maximum load ratio, α, Paper D.

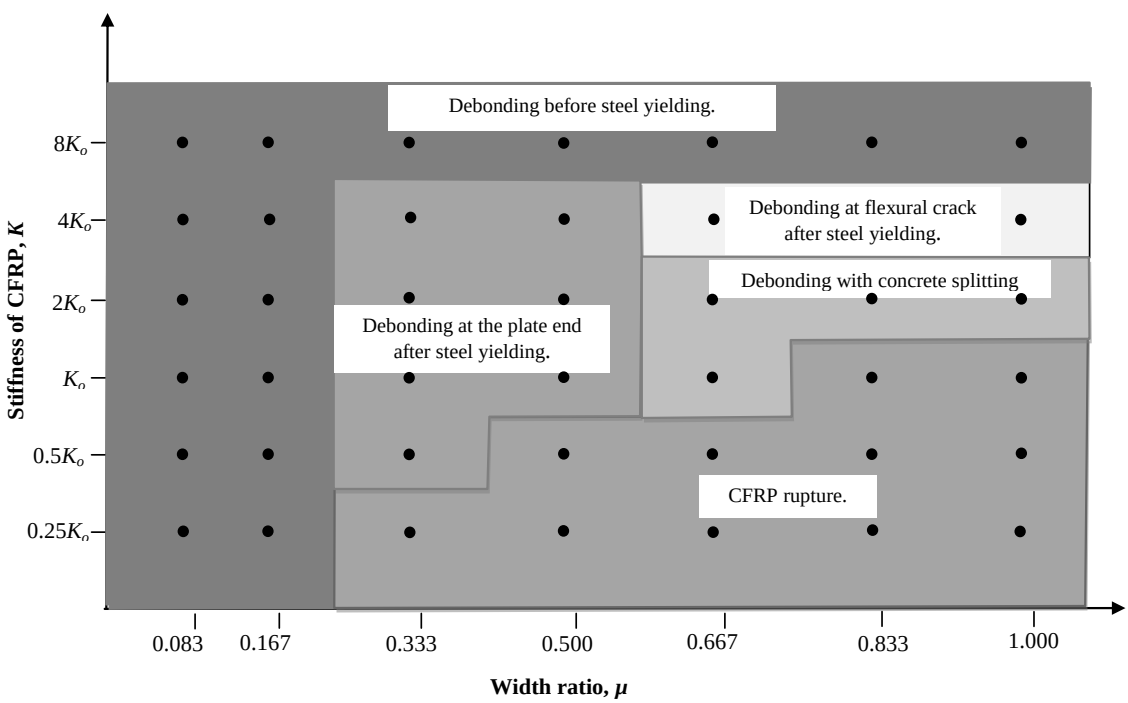

Figure 31: Failure modes of the retrofitted beams. Data points are indicated with dots, Paper D.

3.2.2 Adhesive properties

Adhesive properties affect the behaviour of a retrofitted beam when debonding dominates the failure mode. The load capacity of the beam decreases slightly with increasing shear modulus of adhesive. This is due to the fact that a high shear modulus value of the adhesive increases the rate of stress transfer between FRP and concrete, which leads to stress concentrations in the interface, which will increase the risk of debonding at lower load more than expected.

3.2.3 Influence of width ratio on plate end shear stress concentration

It was shown that the expression

$$\tau_f = \left[V_{x=0} + \left(\frac{G_a}{E_f t_f t_a}\right)^{0.5} M_{x=0}\right] \frac{t_f(h-x_e)}{I} \tag{17}$$

which is used in fib Bulletin 14 for evaluating interfacial shear stress at plate end for simply supported RC beams bonded with FRP, underestimate the value of predicted shear stress. Where $V_{x=0}$ is the shear force at the end of the FRP plate, $M_{x=0}$ is the bending moment at the end of the FRP plate, t_f is the thickness of the laminate plate, t_a is the thickness of the adhesive layer, I is the second moment of area of fully composite transformed equivalent FRP plate, $h - x_e$ is the distance from neutral axis of the strengthened section to the plate, G_a is the shear modulus of the adhesive layer and E_f is the elastic modulus of the laminate plate.

The results showed that it is necessary to include the effect of width ratio, i.e. non-uniform stress distribution in the out of plane direction due to width ratio less than 1. A modified expression was proposed

$$\tau_f = 1.22\left(\frac{b_f}{b_c}\right)^{-0.2}\left[V_{x=0} + \left(\frac{G_a}{E_f t_f t_a}\right)^{0.5} M_{x=0}\right] \frac{t_f(h-x_e)}{I} \tag{18}$$

The modification was introduced by fitting the simulation results with Eq. (17) value at certain load.

4 Conclusions and future work

4.1 Conclusions

A 3D modelling framework for simulating the behaviour of RC beams retrofitted with FRP was developed.

The plastic damage model used for concrete and the elastic-perfectly plastic model used for steel proved to be able to model the reinforced concrete, as was shown by comparing simulations to tests of control beams. A uni-axial CFRP is essentially an orthotropic material, but simulations showed that for cases where the principal stress direction coincides with the fibre direction, an isotropic model could be used with good accuracy.

Since debonding plays an important role as a limiting phenomenon for retrofitted beams, a perfect bond model is not suitable for the CFRP-concrete interface, at least not if the intention is to study the fracture behaviour. A cohesive bond model, on the other hand, can capture the debonding.

Input values found in literature were widespread and few and it was also considered important to include adhesive properties in the model. A new model for the input values for the cohesive model, shear strength, fracture energy and initial interfacial stiffness, was proposed based on fitting FEM results to experimental results from literature. Different shapes of the bond slip curve, bilinear, trilinear and exponential, were evaluated. The results showed that the curve shape has a minor effect on the behaviour of concrete-FRP specimens.

Comparison with experimental results showed that the modelling strategy can capture the behaviour of retrofitted RC beams.

Experiments and simulations showed that retrofitting can increase load capacity and stiffness and the effect is larger for retrofitting in flexure than in shear. On the other hand, simulations showed that an increase in the amount of CFRP will in some cases decrease the maximum load. This means that understanding of the behaviour of a retrofitted structure is very important since an unsuitable arrangement of CFRP can actually make the situation worse.

Experiments and simulations showed that it is important to provide a sufficient anchorage length outside the region of maximum stress to obtain full effect from the retrofitting. For retrofitting in shear, it was also shown that the best effect is obtained if fibre direction of the CFRP coincides with the principal tensile stress direction.

Simulations showed that several different failure modes can occur, depending on the geometry and stiffness properties of the CFRP. Many of the failure modes involve debonding, associated with a stress concentration in the concrete-CFRP interface zone. An important criterion when designing the CFRP arrangement is thus to avoid stress concentrations as far as is possible. A high stiffness and a low width of the CFRP will give a pronounced stress

concentration at the plate end. This should definitely be avoided since it will cause debonding before steel yielding and failure will occur at low load.

A wider CFRP plate will (for constant stiffness) always give a higher maximum load, while increased CFRP stiffness will increase the maximum load only up to a certain value of the stiffness, and thereafter it will decrease the maximum load.

The equation for shear stress at the plate end used in fib Bulletin 14 [1] was evaluated. It was found to be insufficient with respect to influence of FRP width on shear stress. A correction factor was proposed to overcome this problem.

Findings from this research were applied in a case study on a deficient structure in need for strengthening. A simulation versus design guideline comparison showed that the plate end shear stress should be evaluated in the ultimate limit state, and the equation with FRP width correction factor should be used.

4.2 Future work

Previous experimental programs have shown that the FRP plate retrofitting system enhances the capacity of deficient concrete beams. There are, however, many environmental factors involved during the life span of a retrofitted structure that need more attention. They include seasonal temperature variation, degradation of material properties, creep and so on. The durability of FRP reinforced beams under these conditions should be investigated.

Further refinement of the numerical model could be of interest. Especially concerning the modelling of the FRP-concrete interface, there is still a need for further development.

This study showed that there is a stress concentration at the end of the plate causing debonding failure. It would be interesting to study different approaches to avoid this phenomenon. Examples are tapering at end of plate and external FRP wrapping (stirrup) for reducing the stress concentration at the end of the plate.

There are many design guidelines available for retrofitted structures. These guidelines, however, have different criteria for predicting debonding. This indicates a lack of fundamental understanding of the phenomenon, and further research is needed.

References

[1] fib Bulletin 14. Externally bonded FRP reinforcement for RC structures. 2001.

[2] Lacasse, C., Labossiere, P., and Neale, K.W. FRPs for the rehabilitation of concrete beams exhibiting alkali-aggregate reactions. Proceedings of 5th International Symposium on Fibre-Reinforced (FRP) Polymer Reinforcement for Concrete Structures (FRPRCS-7), 2001; 1: 35-43.

[3] David, E, Djelal, C, and Buyle-Bodin, F. Repair and strengthening of reinforced concrete beams using composite materials. 2nd Int. PhD Symposium in Civil Engineering, Budapest, 1998.

[4] Toutanji, H., Zhao, L., and Zhang, Y. Flexural behavior of reinforced concrete beams externally strengthened with CFRP sheets bonded with an inorganic matrix. Engineering Structures. 2006; 28: 557-566.

[5] Shahawy, M.A., Arockiasamy, T.M., Beitelmant, T. and Sowrirajan, R. Reinforced concrete rectangular beams strengthened with CFRP laminates. Composites Part B: Eng. 1996; 27: 225-233.

[6] Shehata, A.E.M, Cerqueira, E.C., Pinto, C.T.M., and Coppe. Strengthening of R.C. beams in flexure and shear using CFRP laminate. Proceedings of 5th International Symposium on Fibre-Reinforced (FRP) Polymer Reinforcement for Concrete Structures (FRPRCS-7), 2001; 97-106.

[7] Wenwei W., Guo L. Experimental study and analysis of RC beams strengthened with CFRP laminates under sustaining load. International Journal of Solids and Structures, 2006; 43: 1372–1387.

[8] Grace, N.F., Soliman, A.K., Abdel-Sayed, G., and Saleh, K.R. Strengthening of continuous beams using fibre reinforced polymer laminates. Proceedings of 4th International Symposium on Fiber-Reinforced (FRP) Polymer Reinforcement for Concrete Structures (FRPRCS-7). American Concrete Institute, Farmington Hills, Mich. 1999; 647-657.

[9] Aiello, M.A., Valente, L., and Rizzo, A. Moment redistribution in continuous reinforced concrete beams strengthened with carbon fiber reinforced polymer laminates. Mechanics of Composite Materials . 2007; 43: 453-66.

[10] Karbhari, M. FRP International. The Official Newsletter of the International Institute for FRP in Construction. 2004; 1(2).

[11] Khalifa, A., Tumialan, G., Nanni, A. and Belarbi, A. Shear strengthening of continuous RC beams using externally bonded CFRP sheet. American Concrete Institute, Proc., 4th International Symposium on FRP for Reinforcement of Concrete Structures (FRPRCS4), Baltimore, MD, Nov. 1999; 995-1008.

[12] Deniaud, C., and Chang, J.J.R. Shear Behavior of Reinforced Concrete T-Beams with Externally Bonded Fiber Reinforced Polymer Sheets. ACI Structural Journal, 1998; 3: 386-494.

[13] Sundarraja, M. and Rajamohan, S. Strengthening of RC beams in shear using GFRP inclined strips – An experimental study. Construction and building materials. 2009; 23: 856-864.

[14] Norris, T., Saadatmanesh, H. and Ehsani, M. R. Shear and flexural strengthening of RC beams with carbon fibre sheets. Journal of structural engineering, 1997; 123(7): 903-911.

[15] Khalifa, A . and Nanni, A. Rehabilitation of rectangular simply supported RC beams with shear deficiencies using CFRP composites. Construction and Building Materials. 2002; 16:135-146.

[16] Esfahani, M., Kianoush, M. and Tajari, A. Flexural behaviour of reinforced concrete beams strengthened by CFRP sheets. Engineering structures. 2007, 29: 2428-2444.

[17] Ashour AF, El-Refaie S.A. and Garrity, S.W. Flexural strengthening of RC continuous beams using CFRP laminates. Cement & Concrete Composites. 2004; 26:765-775.

[18] Garden, H.N., and Hollaway, L.C. An experimental study of the influence of plate end anchorage of carbon fiber composite plates used to strengthen reinforced concrete beams. Composite Structures. 1998; 42(2): 175-88.

[19] Smith, S.T. and Teng, J.G. FRP-strengthened RC beams. I: Review of debonding strength models. Engineering Structures. 2002; 24(4): 385-95.

[20] Gao, B., Kim, J. and Leung, C. Strengthening efficiency of taper ended FRP strips bonded to RC beams. Composite science and technology. 2006; 66: 2257-2264.

[21] Nilson H, Darwin D, Dolan CW. Design of concrete structures. 13th ed. McGraw Hill Higher Education; 2004.

[22] Saenz, L. Discussion equation for the stress - strain curve of concrete, By Desayi P, Krishnan S, ACI J, 1964; 61, 1229–35.

[23] Hillerborg, A. The theoretical basis of a method to determine the fracture energy Gf of concrete. Materials and Structures, RILEM 50-FMC, 1985; 108, pp 291-296.

[24] Wu, Z., and Hemdan, S. Debonding in FRP-strengthened flexural members with different shear-span ratios. Proceedings of 7th International Symposium on Fiber-Reinforced (FRP) Polymer Reinforcement for Concrete Structures (FRPRCS-7), 2005; 411-426.

[25] Pham, H., Al- Mahaidi, R. and Saouma, V. Modelling of CFRP concrete bond using smeared and discrete cracks. Composite structure, 2006; 75: 145-150.

[26] Supaviriyakit, T., Pornpongsaroj, P. and Pimanamas, A. Finite Element Analysis of FRP Strengthened RC Beam. Songklanakarin J.Sci.Technol. 2004; 26(4): 497-507.

[27] Qiao, P., and Chen, Y. Cohesive fracture simulation and failure modes of FRP-concrete bonded interface. Theoretical and applied fracture mechanics, 2008; 49, 213-225.

[28] Coronado, C. A. and Lopez, M. M. Sensitivity analysis of reinforced concrete beams strengthened with FRP laminates. Cement and concrete composit, 2006; 28: 102-114.

[29] ASTM A615. Standard specification for deformed and plain billet steel bars for concrete reinforcing. American society for testing and material. Annual book of ASTM standard, 1995.

[30] Neale, K., Ebead, U., Abdel Baky, H., Elsayed, W. and Godat, A. Modelling of debonding phenomena in FRP-strengthened concrete beams and slabs. Proceedings of the international symposium on bond behaviour of FRP in structures (BBFS). 2005.

[31] Piggott, M. Load bearing fibre composites, 2nd Edition. Kluwer Academic Publishers, Boston/ Dordrecht/ London. 2002.

[32] Camata, G., Spacone, E. and Zarnic, R. Experimental and nonlinear finite element studies of RC beams strengthened with FRP plates. Composites: Part B. 2007, 38: 277-288.

[33] Hu, H.T., Lin, F.-M. and Jan, Y.Y. Nonlinear finite element analysis of reinforced concrete beams strengthened by fiber–reinforced plastics. Cement and concrete composite. 2006, 28: 102-114.

[34] Lundquist, J., Nordin, H., Täljsten, B. and Olofsson, T. Numerical analysis of concrete beams strengthened with CFRP-A study of anchorage lengths. In: FRP in Construction, Proceedings of the International Symposium of Bond Behaviour of FRP in Structures. 2005; 247-254.

[35] Neubauer, U. and Rostasy, F.S. Bond failure of concrete fiber reinforced polymer plates at inclined cracks-experiments and fracture mechanics model. In: Proc. of 4th international symposium on fiber reinforced polymer reinforcement for reinforced concrete structures, SP-188, Farmington Hills (MI): ACI. 1999; 369-82

[36] Nakaba, K., Kanakubo, T., Furuta, T. and Yoshizawa, H. Bond behaviour between fiber-reinforced polymer laminates and concrete, ACI Structures Journal. 2001; 98(3): 359-367

[37] Savioa, M., Farracuti, B. and Mazzotti, D. Non-linear bond-slip law for FRP-concrete interface. In: Proc. of 6th international symposium on FRP reinforcement for concrete structures. Singapore: World Scientific Publications. 2003; 163-72

[38] Monti, M., Renzelli, M. and Luciani, P. FRP adhesion in uncracked and cracked concrete zones. In: Proc. of 6th international symposium on FRP reinforcement for concrete structures. Singapore: World Scientific Publications. 2003; 183-92

[39] Lu, X. Z., Teng, J. G., Ye, L. P. and Jiang, J. J. Bond-slip models for FRP sheets/plates bonded to concrete, Engineering Structures. 2005; 27: 920-937

[40] Neubauer, U. and Rostasy, F. S. Design aspects of concrete structures strengthened with externally bonded CFRP plates, In: Proceedings of the 7th International Conference on Structural Faults and Repairs. Edinburgh, Scotland, ECS Publications. 1997; 2: 109–118.

[41] Brosens, K. and Van Gemert, D. Anchorage Design for externally bonded carbon fiber polymer laminates, In: Dolan, C. W., Rizkalla, S. H. and Nanni, A. (eds), Proceedings of the 4th International Symposium on Fiber Reinforced Polymer Reinforcement for Concrete Structures, Baltimore, USA, 1999: 635–645.

[42] Ulaga, T., Vogel, T. and Meier, U. Bilinear stress–slip bond model: Theoretical background and significance, In: Proceedings of the Sixth International Symposium on FRP Reinforcement for Concrete Structures (FRPRCS-6). 2003; 1: 153–162.

[43] Yuan, H., Wu, Z. and Yoshizawa, H. Theoretical solutions on interfacial stress transfer of externally bonded steel/composite plates, Journal of Structural Mechanics and Earthquake Engineering, JSCE. 2001; 18(1): 27-39

[44] Darby, A., Ibell, T. and Clarke, J. TR55 Design guidance for strengthening concrete structures using fibre composite materials. London: The Concrete Society, 2004.

[45] CNR-DT 200. Guide for the design and construction of externally bonded FRP systems for strengthening existing structures, Italian National Research Council, 2004.

[46] Täljsten, B. FRP Strengthening of existing concrete structures. Design Guidelines. Division of Structural Engineering, Luleå University of Technology, Luleå 2002, 228 pp, ISBN 91-89580-03-6, 2002.

[47] ACI 440.2R-08. Guide for the design and construction of externally bonded FRP systems for strengthening concrete structures. ACI Committee 440, American Concrete Institute, Farmington Hills, Mich., 2008, 76p.

[48] Niedermeier, R. Envelope line of tensile forces while using externally bonded reinforcement. Doctoral Dissertation, TU München. 2000.

[49] Roberts, T.M. Approximate analysis of shear and normal stress concentration in the adhesive layer of plated RC beams. The Structural Engineer, 1989; 67 (12/20): 229-233.

[50] Hibbitt, Karlsson, Sorensen, & Inc. ABAQUS Theory manual, User manual, Example Manual. Version 6.8. Providence, RI. 2000.

Part II

Appended Papers

Paper A

A

Retrofitting of Reinforced Concrete Beams Using Composite Laminates

Yasmeen Taleb Obaidat, Susanne Heyden, Ola Dahlblom, Ghazi Abu-Farsakh and Yahia Abdel-Jawad

Published in Construction & Building Materials, 2011; 25(2): 591-597.

Construction and Building Materials 25 (2011) 591–597

Contents lists available at ScienceDirect

Construction and Building Materials

journal homepage: www.elsevier.com/locate/conbuildmat

Review

Retrofitting of reinforced concrete beams using composite laminates

Yasmeen Taleb Obaidat [a,*], Susanne Heyden [a], Ola Dahlblom [a], Ghazi Abu-Farsakh [b], Yahia Abdel-Jawad [b]

[a] Division of Structural Mechanics, Lund University, Lund, Sweden
[b] Jordan University of Science and Technology, Irbid, Jordan

ARTICLE INFO

Article history:
Received 16 December 2009
Received in revised form 14 April 2010
Accepted 19 June 2010

Keywords:
Carbon fibre reinforced plastic (CFRP)
Strengthening
Retrofitting
Laminate
Reinforced concrete beam
Flexure
Debonding

ABSTRACT

This paper presents the results of an experimental study to investigate the behaviour of structurally damaged full-scale reinforced concrete beams retrofitted with CFRP laminates in shear or in flexure. The main variables considered were the internal reinforcement ratio, position of retrofitting and the length of CFRP. The experimental results, generally, indicate that beams retrofitted in shear and flexure by using CFRP laminates are structurally efficient and are restored to stiffness and strength values nearly equal to or greater than those of the control beams. It was found that the efficiency of the strengthening technique by CFRP in flexure varied depending on the length. The main failure mode in the experimental work was plate debonding in retrofitted beams.

Contents

1. Introduction

There are many existing structures, which do not fulfill specified requirements. This may for example be due to upgrading of the design standards, increased loading, corrosion of the reinforcement

* Corresponding author.
E-mail address: Yasmeen.Obaidat@construction.lth.se (Y.T. Obaidat).

0950-0618/$ - see front matter © 2010 Elsevier Ltd. All rights reserved.
doi:10.1016/j.conbuildmat.2010.06.082

bars, construction errors or accidents such as earthquakes. To remedy for insufficient capacity the structures need to be replaced or retrofitted.

Different types of strengthening materials are available in the market. Examples of these are ferrocement, steel plates and fibre reinforced polymer (FRP) laminate. Retrofitting of reinforced concrete (RC) structures by bonding external steel and FRP plates or sheets is an effective method for improving structural performance under both service and ultimate load conditions. It is both environmentally and economically preferable to repair or strengthen structures rather than to replace them totally. With the development of structurally effective adhesives, there have been marked increases in strengthening using steel plates and FRP laminates. FRP has become increasingly attractive compared to steel plates due to its advantageous low weight, high stiffness and strength to weight ratio, corrosion resistance, lower maintenance costs and faster installation time.

Earlier research has demonstrated that the addition of carbon fibre reinforced polymer (CFRP) laminate to reinforced concrete beams can increase stiffness and maximum load of the beams. In a study by Toutanj et al. [1] beams retrofitted with CFRP laminates showed an increased maximum load up to 170% as compared to control beams. Another study by Kachlakev and McCurry [2] shows an increase of 150% when beams were strengthened in both flexure and shear with CFRP and glass FRP laminates respectively. Other studies have also been conducted by David et al. [3], Shahawy et al. [4], Khalifa and Nanni [5], Shehata et al. [6], Khalifa et al. [7] in an attempt to quantify the flexural and shear strengthening enhancements offered by the externally bonded CFRP laminates. Ferreira [8] showed that when a beam is strengthened with CFRP sheets the stiffness increase and the tension cracking is delayed to higher loads, and Karunasena et al. [9] showed that an externally bonded composite, of either CFRP or GFRP materials, improved the moment capacity of deteriorated concrete beams.

In spite of many studies of the behaviour of retrofitted beams, the effect of the length of CFRP on the behaviour of pre-cracked beams retrofitted by CFRP in flexure and the behaviour of retrofitted beams in shear after preloading have not been explored. This study examined experimentally the flexural and the shear behaviours of RC-beams retrofitted or strengthened with CFRP laminates. To accomplish this, laboratory testing was conducted on full-size beams. The main variables in this study are the reinforcement steel ratio and CFRP length.

2. Materials and methods

The experimental work undertaken in this study consisted of four point bending tests of 12 simply supported RC beams. In addition, material tests were carried out to determine the mechanical properties of the concrete, reinforcement steel and CFRP which were used in constructing the beams.

2.1. Materials

An ordinary strength concrete mix was prepared using Ordinary Portland cement (Type I). The aggregate used consisted of coarse limestone, crushed limestone and silica sand. The gradation of coarse and fine particles met the ASTM specification (C136) [10].

The concrete mix was designed according to ACI method 211 [11], to have slump 50 mm and 28 days cylinder compressive strength of 30 MPa. The maximum aggregate size was 10 mm and the free water cement ratio was 0.55. The concrete mix is shown in Table 1.

The mean compressive strength was determined in compressive tests 28 days after casting of three 300 mm by 150 mm diameter cylinders. The average concrete compressive strength was 29 MPa. The failure of a specimen is shown in Fig. 1.

The steel bars used for longitudinal reinforcement were tested in uniaxial tension. Details of the material properties for the reinforcing steel are given in Table 2. The average elastic modulus was 209 GPa. The stirrups were fabricated using steel with nominal diameter 8 mm. This steel was not tested in the experimental work.

The CFRP used in this study was supplied by FOSROC [12]. The laminate had a thickness of 1.2 mm, a width of 50 mm and the elastic modulus 165 GPa according to the manufacturer. The plates were supplied in a roll form as shown in Fig. 2. Three specimens were prepared and tested using a tension testing machine at a rate of 2 mm/min, to determine the ultimate stress. The mean ultimate stress of the

Table 1
Concrete mix proportions, kg/m^3 concrete.

Materials	kg/m^3
Cement	332
Water	206
Coarse aggregate (5 mm $\leqslant d \leqslant$ 10 mm)	830
Fine aggregate (d < 5 mm)	662

Fig. 1. Concrete specimen in cylinder compression test.

Table 2
Mechanical properties of steel bars.

Nominal diameter (mm)	Elastic modulus (GPa)	Yield Stress (MPa)	Ultimate stress (MPa)	Ultimate strain
10	211	520	741	0.151
12	207	495	760	0.167
18	209	512	739	0.131

Fig. 2. Roll of CFRP plate.

three specimens was 2640 MPa, with the strain corresponding to the failure load being 0.0154. This test also showed that the behaviour of the CFRP is linear elastic up to failure. The failure of a specimen is shown in Fig. 3.

The material used for the bonding of CFRP plates to the concrete was an epoxy adhesive with compressive strength equal to 40 MPa according to the manufacturer and it was applied with a total thickness equal to 1 mm.

2.2. Experimental procedure

Twelve beams were tested under four point bending after curing 6 months. The beams were divided into two groups. For group RF, focus was on flexural behaviour, and for group RS focus was on shear behaviour.

For group RF, two beams were used as control beams. The other six were preloaded until flexural cracks appeared and then retrofitted with CFRP. Three different lengths of CFRP were used, with two nominally equal beams for each length. Finally, the retrofitted beams were loaded until failure and the results were compared with the control beams.

For group RS, two beams were used as control beams, and the other two were preloaded until shear cracks appeared and then retrofitted and finally tested to failure.

2.2.1. Manufacture of beams

The beams had a rectangular cross-section of 150 mm width and 300 mm height, and were 1960 mm long. The beams in group RF were designed to have insufficient flexural strength to obtain a pure flexural failure. They had tension reinforcement ($2\,\phi\,12$), compression reinforcement ($2\,\phi\,10$) and the steel bars were tied together with 8 mm stirrups c/c 100 mm along the beam, see Fig. 4a.

The beams in group RS had the same geometry, but were cast with a reduced shear reinforcement ratio and a larger longitudinal reinforcement ratio in order to obtain pure diagonal shear cracks without development of flexural cracks. The beams had tension reinforcement ($2\,\phi\,18$), compression reinforcement ($2\,\phi\,10$) and were tied with 8 mm stirrups c/c 400 mm along the beam as shown in Fig. 4. All beams were designed according to [13].

In all the beams, the clear concrete cover to the main flexural reinforcement was set to 25 mm. This cover was expected to avoid splitting bond failure. Geometry and reinforcement are shown in Fig. 4b. The beams cured for 6 months before they were tested.

2.2.2. Testing of control beams

The beams were tested in four point bending. This load case was chosen because it gives constant maximum moment and zero shear in the section between the loads, and constant maximum shear force between support and load. The moment was linearly varying between supports and load. The span between the supports was 1560 mm and the load was applied at points dividing the length into three equal parts as shown in Fig. 5. Steel plates were used under the loads to distribute the load over the width of the beam. The testing equipment was a testing machine of 400 kN capacity jack. A linearly variable differential transducer, LVDT, was used to measure the deflection at midspan, as shown in Fig. 5. Fig. 6 shows the test setup of a beam.

Deflections and load were recorded during the test. The first crack appeared in the control beams of group RF at $P = 60$ kN and flexural cracks had formed along the beam at $P = 95$ kN.

For the beams in group RS, shear cracks were initiated in both shear spans. The first shear crack was the critical crack in the beam and it started to develop at $P = 120$ kN. The load in this group is higher than for those in group RF due to intensive flexural reinforcement. A steel ratio around the balanced steel ratio was used.

2.2.3. Preloading of beams

In order to simulate damage, the beams were preloaded before retrofitting. The preloading was done with the same setup as described in Section 2.2.2. First the beams were loaded until cracks appeared; the load was 95 kN for beams in group RF and for beams in group RS the first shear crack initiated at a load of 120 kN, as determined in the control beams test. Then the load was released.

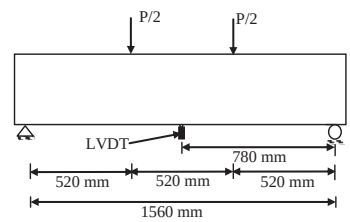

Fig. 5. Supports, loading and position of LVDT.

Fig. 3. The failure of a CFRP laminate specimen.

Fig. 6. Test setup.

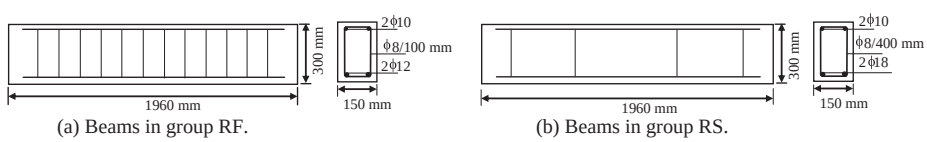

Fig. 4. Geometry and reinforcement of beams in groups RF and RS.

2.2.4. Retrofitting of beams

The beams in group RF were removed from the test machine and turned over to retrofit them with CFRP as shown in Fig. 7. The soffit of the beam was retrofitted with CFRP laminates 50 mm wide and of three different lengths, 1560 mm (series RF1), 1040 mm (series RF2) and 520 mm (series RF3) as shown in Fig. 7. The laminate was positioned at the centre of the beam width as shown in Fig. 8. The laminate was applied when the beams were subjected to a negative moment corresponding to their own dead weight. This implies a small prestressing effect which could be obtained by a jack in the case of on-site repair.

For the beams in group RS, the web of the beam was retrofitted with CFRP laminates 50 mm wide and 300 mm long on the two faces of beams as shown in Figs. 9 and 10. The same procedure was used as for the beams in group RF, but the position of the laminate was different.

In order to ensure correct application of the external strengthening materials, it was considered necessary to improve the concrete surface characteristics on the contact areas to be bonded. The surface preparation was done according to the manufacturer's instruction [12]. It included removing the cement paste, grinding the surface by using a disc sander, and removing the dust generated by surface grinding using an air blower. After that the epoxy adhesive was applied to both the CFRP and the concrete surface. Finally the CFRP plates were applied to the beams.

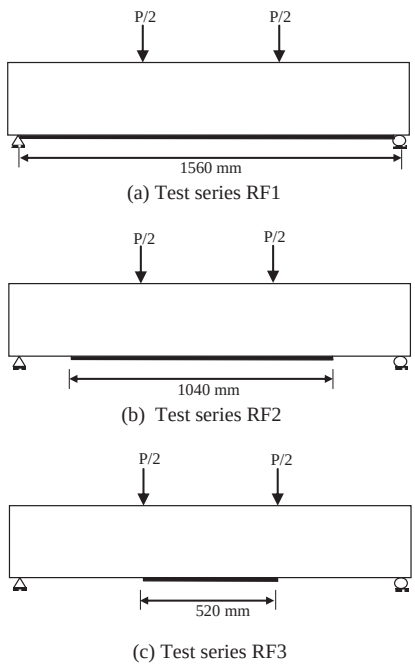

Fig. 7. Lengths of CFRP laminate in test series RF1, RF2 and RF3.

Fig. 8. Application of CFRP laminate for beams in group RF.

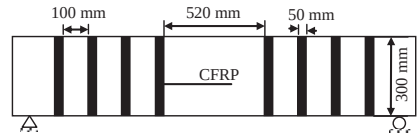

Fig. 9. The arrangement of the CFRP laminate in group RS.

Fig. 10. CFRP laminate in test series RS1.

2.2.5. Testing of retrofitted beams

After 7 days curing at ambient temperature the beams were retested under four point bending until failure occurred. The tests were performed using the same set-up as described in Section 2.2.2.

3. Results

3.1. Beams in group RF

3.1.1. Control beams

The load versus midspan deflection curves for the two control beams are shown in Fig. 11. The beams behave in a ductile manner and gives large deflection before the final failure. This is the typical behaviour of an under-reinforced RC member [14]. The difference between the two specimens is rather small, and the mean value, also indicated in the figure, will be used.

The curve includes a linear response up to the load 22 kN. The appearance of a crack was first noted at load 60 kN. The midspan

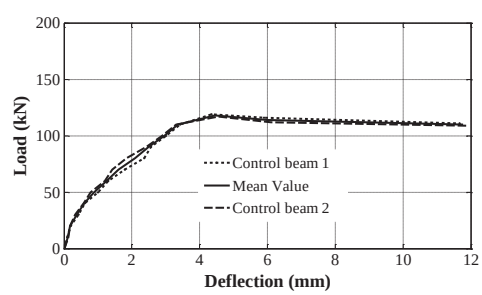

Fig. 11. Comparison between individual control beams in group RF.

deflection curve illustrates the nonlinearities at cracking of the concrete. After 95 kN load flexural cracks formed and widened as loading increased. The maximum load was 118 kN as shown in the figure. After maximum load, the cracks did not grow in length for the remainder of the test but the flexural cracks in the constant moment region widened. The failure of a control beam is shown in Fig. 12.

3.1.2. Retrofitted beams

The load–deflection curves for the individual beams in series RF1, RF2 and RF3 are shown in Fig. 13. The results from the two nominally equal beams in each series are close, which indicates that the retrofitting was performed in a well-defined manner. The mean curve will be used in the following.

The mean load–deflection curves for the retrofitted beams and for the control beams are shown in Fig. 14. As shown in the figure the stiffness of all beams at small load is almost the same. From a load around 60 kN -cracking stage- the stiffness of the control beam decreases notably due to cracking. The decrease in stiffness is smaller for the retrofitted beams since the CFRP prevents cracks to develop and widen. The longer the CFRP the stiffer the beam. This is probably because the longer CFRP strips have a full anchorage length outside the maximum moment region and are hence more efficient in the cracking zone. Some contribution to the stiffness may also be due to the stiffening of the beam caused by the CFRP outside the cracking region.

It should be noted that if a control beam would be loaded until cracking, unloaded, and then subjected to load again, the stiffness would be somewhat lower the second time due to the damage in the beam. This means that even if the curve of series RF3 is similar to that of the control beam the CFRP has improved the beam and restored the stiffness to the level of the control beam.

The curves reveal that the strengthening process has significantly increased the maximum load in series RF1 and RF2. The maximum load in series RF1 was 166 kN, which is a more than 33% increase compared to the control beam. The maximum load for series RF2 was 142 kN, 20% higher than for the control beam. For series RF3 the maximum load was 128 kN which corresponds to a 7% increase in maximum load.

All beams experienced a brittle failure mechanism, however in this case sudden debonding of the CFRP plate from the concrete occurred without concrete splitting. This failure was due to high shear stress occurring at the ends of the CFR. The properties of the adhesive are probably important in relation to the debonding failure. A lower stiffness and higher fracture energy will probably weaken the tendency of debonding. For RF2 and RF3 debonding occurred earlier than for RF1. The main reason leading to this is that RF2 and RF3 do not have a full anchorage length outside the maximum moment region, hence higher shear stress concentration will occur compared to for the longest CFRP, Fig. 15. The crack propagation and the final crack pattern of the beam are greatly different from that of the control beam. The control beam had few flexural cracks with large width, and the retrofitted beam had many flexural cracks with smaller width. This indicates that the propagation

Fig. 12. Flexural failure for control beam.

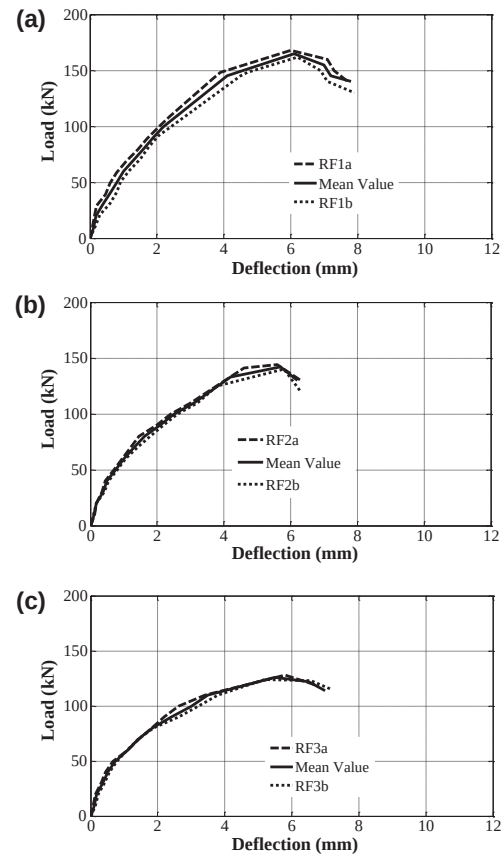

Fig. 13. Comparison between load–deflection curves for individual retrofitted beams in group RF. (a) Series RF1. (b) Series RF2. (c) Series RF3.

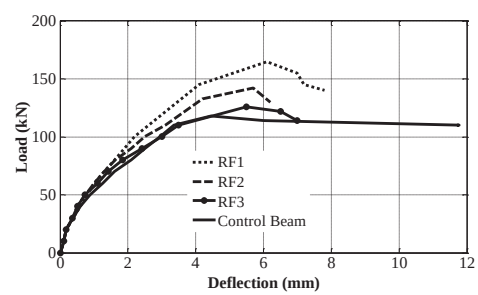

Fig. 14. Comparison between mean load–deflection curves for retrofitted beams and control beam in group RF.

Fig. 15. Debonding failures in group RF.

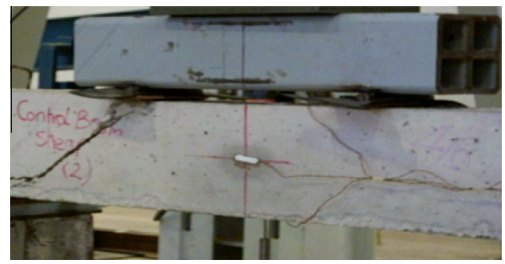

Fig. 17. Shear failure for control beam.

of cracks was confined by the CFRP laminates. In addition, the cracks in series RF1 were fewer and had smaller width than in the other retrofitted beams.

The results indicate that the externally bonded CFRP has increased the stiffness and maximum load of the beam. In addition, the crack width and the deflection have decreased. The efficiency of the strengthening by CFRP in flexure varied depending on the length of the CFRP.

3.2. Beams in group RS

3.2.1. Control beam

The load versus midspan deflection curves for the control beams are shown in Fig. 16. It is clear that the beam failed in a brittle manner and has a low energy absorption before failure. This is the typical behaviour of an ordinary RC member with insufficient shear steel [15]. The difference between the two specimens is rather small, and the mean value, also indicated in the figure, will be used.

The curve has linear response until 60 kN. The ultimate load of the control beams was 220 kN. The cracking patterns consist of a pure diagonal shear crack in the constant shear spans, Fig. 17. This is due to the reduced amount of shear reinforcement.

3.2.2. Retrofitted beams

A debonding failure occurred for all beams also in this group. The debonding mode is due to cracking of the concrete underneath the CFRP plate. The beam after failure appears in Fig. 18, which clearly shows the shear crack cross the bond area in the concrete.

The load–deflection curves for the two beams and the mean value are shown in Fig. 19. Also here, the variation between the individual beams was small.

Fig. 18. Debonding and shear failures in group RS.

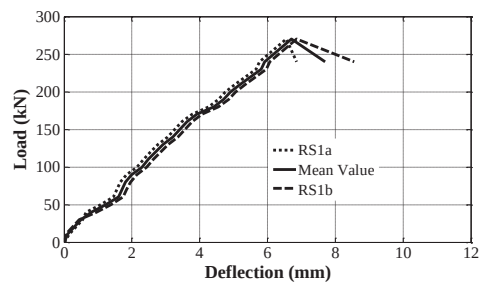

Fig. 19. Comparison between load–deflection curves for individual retrofitted beams in group RS.

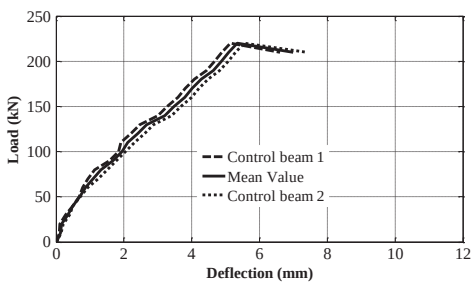

Fig. 16. Comparison between load–deflection curves for individual control beams in group RS.

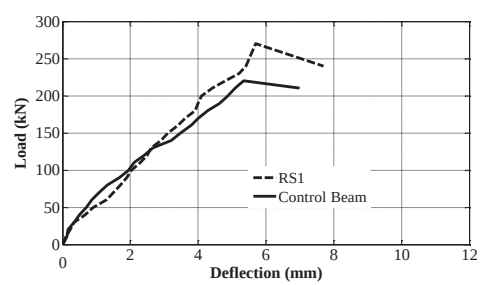

Fig. 20. Comparison between mean load–deflection curves for retrofitted beams and control beam in group RS.

The load versus midspan deflection curve for the mean value of the retrofitted beams is compared with the response of the control beams in Fig. 20.

The control beam shows more softening due to crack propagation, while in the retrofitted beam, the cracks are arrested by the CFRP, and this makes the curve of the retrofitted beam somewhat straighter than the control beam curve. The maximum load of the strengthened beam was 270 kN. It may be observed that strengthening increases the maximum load by over 23%, when compared with the control beam.

4. Concluding and remarks

The paper investigated the flexural and shear behaviour of reinforced beams retrofitted with CFRP after preloading. The following conclusions are drawn from this experimental study:

- The stiffness of the CFRP-retrofitted beams is increased compared to that of the control beams.
- Employing externally bonded CFRP plates resulted in an increase in maximum load. The increase in maximum load of the retrofitted specimens reached values of about 23% for retrofitting in shear and between 7% and 33% for retrofitting in flexure. Moreover, retrofitting shifts the mode of failure to be brittle.
- The crack width for the retrofitted beams is decreased compared to the control beams.
- Experimental results showed that increasing the CFRP plate length in flexural retrofitting can make the CFRP more effective for concrete repair and strengthening. This means that insufficient strengthening lengths do not produce the intended strengthening effect.
- The results showed that the main failure mode was plate debonding which reduces the efficiency of retrofitting.

Based on this conclusion deeper studies should be performed to investigate the behaviour of the interface layer between the CFRP and concrete. Also numerical work should be done to predict the behaviour of retrofitted beams and to evaluate the influence of different parameters on the overall behaviour of the beams.

References

[1] Toutanji H, Zhao L, Zhang Y. Flexural behaviour of reinforced concrete beams externally strengthened with CFRP sheets bonded with an inorganic matrix. Eng Struct 2006;28(March):557–66.
[2] Kachlakev D, McCurry DD. Behavior of full-scale reinforced concrete beams retrofitted for shear and flexural with FRP laminates. Composites 2000;31:445–52.
[3] David E, Djelal C, Buyle-Bodin F. Repair and strengthening of reinforced concrete beams using composite materials. In: 2nd Int PhD symposium in civil engineering, Budapest; 1998.
[4] Shahawy MA, Arockiasamy TM, Beitelmant T, Sowrirajan R. Reinforced concrete rectangular beams strengthened with CFRP laminates. Composites 1996;27:225–33.
[5] Khalifa A, Nanni A. Rehabilitation of rectangular simply supported RC beams with shear deficiencies using CFRP composites. Constr Build Mater 2002;16:135–46.
[6] Shehata AEM, Cerqueira EC, Pinto CTM, Coppe. Strengthening of RC beams in flexure and shear using CFRP laminate. Fiber Reinf Plast Reinf Concr Struct 2001;1:97–106.
[7] Khalifa A, Tumialan G, Nanni A, Belarbi A. Shear strengthening of continuous RC beams using externally bonded CFRP sheets. American Concrete Institute. In: Proceedings of the 4th international symposium on FRP for reinforcement of concrete structures (FRPRCS4), Baltimore, MD; November 1999. p. 995–1008.
[8] Ferreira AJM. On the shear-deformation theories for the analysis of concrete shells reinforced with external composite laminates. Strength Mater 2003;35(2):128–35.
[9] Karunasena W, Hardeo P, Bosnich G. Rehabilitation of concrete beams by externally bonding fiber composite reinforcement. In composite systems: macrocomposites, microcomposites, nanocomposites. In: Proceedings of the ACUN-4, international composites conference, 4th, Sydney, Australia; July 21–25 2002. p. 222–226.
[10] ASTM C136. Standard test method for sieve analysis of fine and coarse aggregates. American Society for Testing and Materials; 2004.
[11] ACI Committee 211.1-91. Standard practice for selecting proportion for normal, heavy weight and mass concrete. ACI manual of concrete practice. Part 1; 1996.
[12] http://www.fosroc.com [16.12.09].
[13] ACI Comittee 318. Building code requirements for structural concrete and commentary (ACI 318-99). American concrete institute detroit, MI; 1999.
[14] Nilson H, Darwin D, Dolan CW. Design of concrete structures. 13th ed. McGraw Hill Higher Education; 2004.
[15] Nielsen MP. Limit analysis and concrete plasticity. 2nd ed. CRC Press; 1999.

Paper B

B

The Effect of CFRP and CFRP/Concrete Interface Models when Modelling Retrofitted RC Beams with FEM.

Yasmeen Taleb Obaidat, Susanne Heyden and Ola Dahlblom

Published in Composite Structures, 2010; 92: 1391–1398.

Composite Structures 92 (2010) 1391–1398

Contents lists available at ScienceDirect

Composite Structures

journal homepage: www.elsevier.com/locate/compstruct

The effect of CFRP and CFRP/concrete interface models when modelling retrofitted RC beams with FEM

Yasmeen Taleb Obaidat *, Susanne Heyden, Ola Dahlblom

Division of Structural Mechanics, Lund University, Lund, Sweden

ARTICLE INFO

Article history:
Available online 14 November 2009

Keywords:
Carbon fibre reinforced plastic (CFRP)
Strengthening
Laminate
Cohesive model
Reinforced concrete beam
Finite element analysis (FEA)

ABSTRACT

Concrete structures retrofitted with fibre reinforced plastic (FRP) applications have become widespread in the last decade due to the economic benefit from it. This paper presents a finite element analysis which is validated against laboratory tests of eight beams. All beams had the same rectangular cross-section geometry and were loaded under four point bending, but differed in the length of the carbon fibre reinforced plastic (CFRP) plate. The commercial numerical analysis tool Abaqus was used, and different material models were evaluated with respect to their ability to describe the behaviour of the beams. Linear elastic isotropic and orthotropic models were used for the CFRP and a perfect bond model and a cohesive bond model was used for the concrete–CFRP interface. A plastic damage model was used for the concrete. The analyses results show good agreement with the experimental data regarding load–displacement response, crack pattern and debonding failure mode when the cohesive bond model is used. The perfect bond model failed to capture the softening behaviour of the beams. There is no significant difference between the elastic isotropic and orthotropic models for the CFRP.

1. Introduction

Upgrading of reinforced concrete structures may be required for many different reasons. The concrete may have become structurally inadequate for example, due to deterioration of materials, poor initial design and/or construction, lack of maintenance, upgrading of design loads or accident events such as earthquakes. In recent years, the development of strong epoxy glue has led to a technique which has great potential in the field of upgrading structures. Basically the technique involves gluing steel or FRP plates to the surface of the concrete. The plates then act compositely with the concrete and help to carry the loads.

The use of FRP to repair and rehabilitate damaged steel and concrete structures has become increasingly attractive due to the well-known good mechanical properties of this material, with particular reference to its very high strength to density ratio. Other advantages are corrosion resistance, reduced maintenance costs and faster installation time compared to conventional materials.

The application of CFRP as external reinforcement to strengthen concrete beams has received much attention from researchers [1–5], but only very few studies have focused on structural members strengthened after preloading [6,7]. The behaviour of structures which have been preloaded until cracking initiates deserves more attention, since this corresponds to the real-life use of CFRP retrofitting.

Researchers have observed new types of failures that can reduce the performance of CFRP when used in retrofitting structures [8]. These failures are often brittle, and include debonding of concrete layers, delamination of CFRP and shear collapse. Brittle debonding has particularly been observed at laminate ends, due to high concentration of shear stresses at discontinuities, where shear cracks in the concrete are likely to develop [9]. Thus, it is necessary to study and understand the behaviour of CFRP strengthened reinforced concrete members, including those failures.

Several researchers have simulated the behaviour of the concrete–CFRP interface through using a very fine mesh to simulate the adhesive layer defined as a linear elastic material [10]. However, they have not used any failure criterion for the adhesive layer. Most researchers who have studied the behaviour of retrofitted structures have, however, not considered the effect of the interfacial behaviour at all [11–13].

In this paper, we use the finite element method to model the behaviour of beams strengthened with CFRP. For validation, the study was carried out using a series of beams that had been experimentally tested for flexural behaviour and reported by Obaidat [14]. Two different models for the CFRP and two different models for the concrete–CFRP interface are investigated. The models are used for analysing beams with different lengths of CFRP applied.

* Corresponding author.
E-mail address: Yasmeen.Obaidat@byggmek.lth.se (Y.T. Obaidat).

0263-8223/$ - see front matter © 2009 Elsevier Ltd. All rights reserved.
doi:10.1016/j.compstruct.2009.11.008

2. Experimental work

Experimental data was obtained from previous work by Obaidat [14]. Eight identical RC beams were loaded with a four point bending configuration with a span of 1560 mm, and distance between loads of 520 mm. All beams were 300-mm high, 150-mm wide, and 1960-mm long. The longitudinal reinforcement consisted of two ϕ 12 for tension and two ϕ 10 for compression. Shear reinforcement was sufficiently provided and consisted of ϕ 8 c/c 100 mm, as seen in Fig. 1.

Two control beams were loaded to failure and the other beams were loaded until cracks appeared, then retrofitted using different lengths of CFRP, see Fig. 2. The CFRP was adhered to the bottom surface of the beams with their fibre direction oriented in the axial direction of the beam. Each CFRP plate was 1.2 mm thick and 50 mm wide. Finally the beams were retested, while the deflection and load were monitored.

A comparison of load–deflection curves of retrofitted beams and control beams is presented in Fig. 3. The experimental results showed that the retrofitting using CFRP increased the strength of the beam and the effect increased with the length of the CFRP plate. All retrofitted beams failed due to debonding of the CFRP.

3. Finite element analysis

Finite element failure analysis was performed to model the nonlinear behaviour of the beams. The FEM package Abaqus/standard [15] was used for the analysis.

3.1. Material properties and constitutive models

3.1.1. Concrete

A plastic damage model was used to model the concrete behaviour. This model assumes that the main two failure modes are tensile cracking and compressive crushing [15]. Under uni-axial tension the stress–strain response follows a linear elastic relationship until the value of the failure stress is reached. The failure stress corresponds to the onset of micro-cracking in the concrete material. Beyond the failure stress the formation of micro-cracks is represented with a softening stress–strain response. Hence, the elastic parameters required to establish the first part of the relation are elastic modulus, E_c, and tensile strength, f_{ct}, Fig. 4a. The compressive strength, f_c', was in the experimental work measured to be 30 MPa. E_c and f_{ct} were then calculated by [16]:

$$E_c = 4700\sqrt{f_c'} = 26{,}000 \text{ MPa} \quad (1)$$

$$f_{ct} = 0.33\sqrt{f_c'} = 1.81 \text{ MPa} \quad (2)$$

where f_c', is given in MPa.

To specify the post-peak tension failure behaviour of concrete the fracture energy method was used. The fracture energy for mode I, G_f, is the area under the softening curve and was assumed equal to 90 J/m^2, see Fig. 4b.

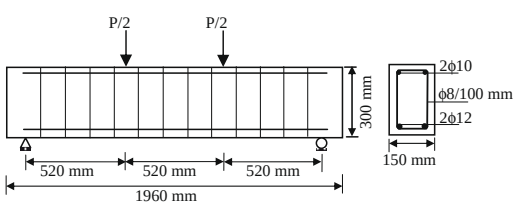

Fig. 1. Geometry, reinforcement and load of the tested beams.

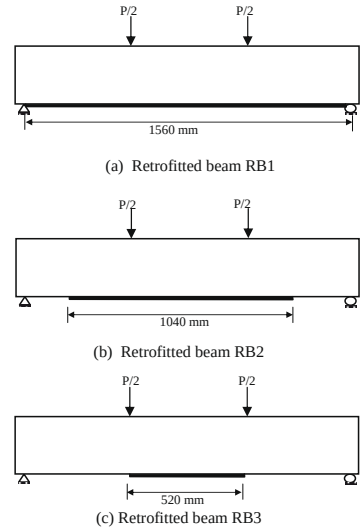

Fig. 2. Length of CFRP laminates in test series RB1, RB2 and RB3.

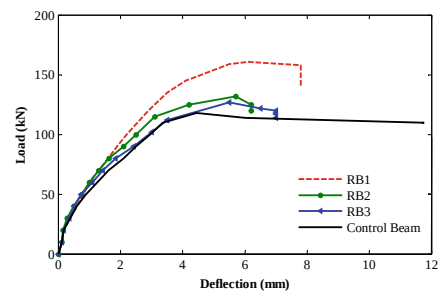

Fig. 3. Load versus mid-span deflection for un-strengthened and strengthened beams.

The stress–strain relationship proposed by Saenz [17] was used to construct the uni-axial compressive stress–strain curve for concrete:

$$\sigma_c = \frac{E_c\varepsilon_c}{1 + (R + R_E - 2)\left(\frac{\varepsilon_c}{\varepsilon_0}\right) - (2R - 1)\left(\frac{\varepsilon_c}{\varepsilon_0}\right)^2 + R\left(\frac{\varepsilon_c}{\varepsilon_0}\right)^3} \quad (3)$$

where

$$R = \frac{R_E(R_\sigma - 1)}{(R_\varepsilon - 1)^2} - \frac{1}{R_\varepsilon}, \quad R_E = \frac{E_c}{E_0}, \quad E_0 = \frac{f_c'}{\varepsilon_0} \quad (4)$$

and, $\varepsilon_0 = 0.0025$, $R_\varepsilon = 4$, $R_\sigma = 4$ as reported in [18]. The stress–strain relationship in compression for concrete is represented in Fig. 5.

Poisson's ratio for concrete was assumed to be 0.2.

3.1.2. Steel reinforcement

The steel was assumed to be an elastic–perfectly plastic material and identical in tension and compression as shown in Fig. 6.

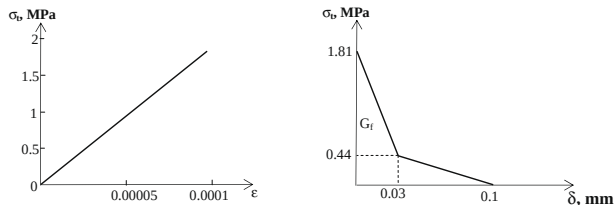

(a) Stress-strain relationship up to ultimate load. (b) Post-peak stress deformation relationship.

Fig. 4. Concrete under uni-axial tension.

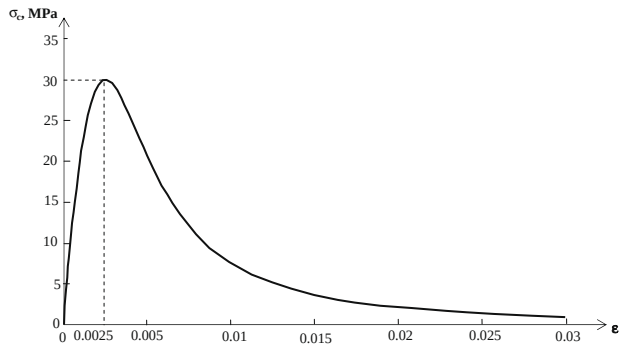

Fig. 5. Stress–strain relationship for concrete under uni-axial compression.

The elastic modulus, E_s, and yield stress, f_y, were measured in the experimental study and the values obtained were $E_s = 209$ GPa and $f_y = 507$ MPa. These values were used in the FEM model. A Poisson's ratio of 0.3 was used for the steel reinforcement. The bond between steel reinforcement and concrete was assumed as a perfect bond.

3.1.3. CFRP

Two different models for the CFRP were used in this study. In the first model, the CFRP material was considered as linear elastic isotropic until failure. In the second model, the CFRP was modelled as a linear elastic orthotropic material. Since the composite is unidirectional it is obvious that the behaviour is essentially orthotropic. In a case like this however, where the composite is primarily stressed in the fibre direction, it is probable that the modulus in the fibre direction is the more important parameter. This is why an isotropic model is considered suitable. The elastic modulus in the fibre direction of the unidirectional CFRP material used in the experimental study was specified by the manufacturer as 165 GPa. This value for E and $v = 0.3$ was used for the isotropic model. For the orthotropic material model E_{11} was set to 165 GPa. Using Rule of Mixture [19], $E_{epoxy} = 2.5$ GPa and that the fibre volume fraction was 75%, E_{fibre} was found to be 219 GPa and $v_{12} = v_{13} = 0.3$. By use of Inverse Rule of Mixture [19], $E_{22} = E_{33} = 9.65$ GPa and $G_{12} = G_{13} = 5.2$ GPa. v_{23} and G_{23} were set to 0.45 and 3.4, respectively.

3.1.4. CFRP–concrete interface

Two different models were used to represent the interface between concrete and CFRP. In the first model the interface was modelled as a perfect bond while in the second it was modelled using a cohesive zone model. Fig. 7 shows a graphic interpretation of a simple bilinear traction–separation law written in terms of the effective traction τ and effective opening displacement δ. The interface is modelled as a rich zone of small thickness and the initial stiffness K_0 is defined as [20]:

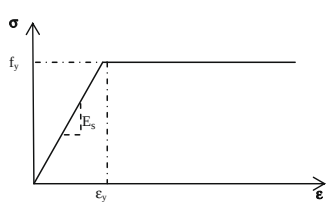

Fig. 6. Stress strain behaviour of steel.

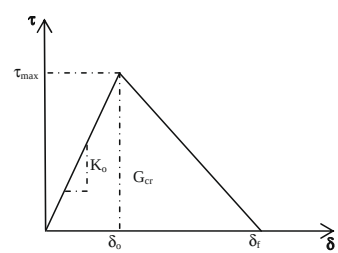

Fig. 7. Bilinear traction–separation constitutive law.

$$K_0 = \frac{1}{\frac{t_i}{G_i} + \frac{t_c}{G_c}} \tag{5}$$

where t_i is the resin thickness, t_c is the concrete thickness, and G_i and G_c are the shear modulus of resin and concrete respectively. The values used for this study were t_i = 1 mm, t_c = 5 mm, G_i = 0.665 GPa, and G_c = 10.8 GPa.

From Fig. 7, it is obvious that the relationship between the traction stress and effective opening displacement is defined by the stiffness, K_0, the local strength of the material, τ_{max}, a characteristic opening displacement at fracture, δ_f, and the energy needed for opening the crack, G_{cr}, which is equal to the area under the traction–displacement curve. Eq. (6), [21], provides an upper limit for the maximum shear stress, τ_{max}, giving τ_{max} = 3 MPa in this case:

$$\tau_{max} = 1.5\beta_w f_t \tag{6}$$

where

$$\beta_w = \sqrt{\left(2.25 - \frac{b_f}{b_c}\right) \Big/ \left(1.25 + \frac{b_f}{b_c}\right)}$$

and b_f is CFRP plate width, b_c is concrete width and f_{ct} is concrete tensile strength.

Numerical simulations showed that this value is too high; since CFRP rupture or concrete crushing induced the failure, instead of the CFRP debonding that occurred in the experimental study, see Fig. 8. The two curves representing τ_{max} = 3 MPa show increasing load up to failure, and the simulations ended with CFRP rupture or concrete crushing. Hence, τ_{max} was reduced to 1.5 MPa.

For fracture energy, G_{cr}, previous researches have indicated values from 300 J/m^2 up to 1500 J/m^2 [22,23]. To investigate to what extent G_{cr} affects the results, numerical simulations were performed for G_{cr} = 500 J/m^2 and 900 J/m^2. The simulations showed that G_{cr} has in this case only a moderate influence on the load–deformation behaviour, as seen in Fig. 8. For this study the value 900 J/m^2, in the middle of the interval proposed by previous studies, was used.

The initiation of damage was assumed to occur when a quadratic traction function involving the nominal stress ratios reached the value one. This criterion can be represented by [15]:

$$\left\{\frac{\sigma_n}{\sigma_n^0}\right\}^2 + \left\{\frac{\tau_n}{\tau_s^0}\right\}^2 + \left\{\frac{\tau_t}{\tau_t^0}\right\}^2 = 1 \tag{7}$$

where σ_n is the cohesive tensile and τ_s and τ_t are shear stresses of the interface, and n, s, and t refer to the direction of the stress component, see Fig. 9b. The values used for this study were $\sigma_n^0 = f_{ct}$ = 1.81 MPa, and $\tau_s^0 = \tau_t^0$ = 1.5 MPa.

Interface damage evolution was expressed in terms of energy release. The description of this model is available in the Abaqus material library [15]. The dependence of the fracture energy on the mode mix was defined based on the Benzaggah–Kenane fracture criterion [15]. Benzaggah–Kenane fracture criterion is particularly useful when the critical fracture energies during deformation purely along the first and the second shear directions are the same; i.e., $G_s^C = G_t^C$. It is given by:

$$G_n^C + \left(G_s^C - G_n^C\right)\left\{\frac{G_{\mathscr{S}}}{G_{\mathscr{T}}}\right\}^{\eta} = G^C \tag{8}$$

where $G_{\mathscr{S}} = G_S + G_t$, $G_{\mathscr{T}} = G_n + G_s$, and η are the material parameter. G_n, G_s and G_t refer to the work done by the traction and its conjugate separation in the normal, the first and the second shear directions, respectively. The values used for this study were G_n^C = 90 J/m^2, $G_t^C = G_s^C$ = 900 J/m^2, and η = 1.45.

3.2. Numerical analysis

4-Node linear tetrahedral elements were used for the reinforced concrete, reinforcement steel, steel plates at supports and under the load, and CFRP in this model. The element configuration is shown in Fig. 9a. 8-Node 3-D cohesive elements were used to model the interface layer. The cohesive interface elements are composed of two surfaces separated by a thickness, Fig. 9b. The relative motion of the bottom and top parts of the cohesive element measured along the thickness direction represents opening or closing of the interface. The relative motion of these parts represents the transverse shear behaviour of the cohesive element.

To show the effect of the bond model and the behaviour of CFRP, four combinations of bond model and CFRP model were analysed; Perfect bond with isotropic CFRP, perfect bond with orthotropic CFRP, cohesive bond model with isotropic CFRP, and cohesive bond model with orthotropic CFRP.

One quarter of the specimen was modelled, as shown in Fig. 10, by taking advantage of the double symmetry of the beam. The boundary conditions are illustrated in Fig.11. A fine mesh is needed to obtain results of sufficient accuracy. The pre-crack was modelled by making a gap of 0.1 mm width and 10 mm depth between the continuum elements, 20 mm from the centre of the beam. Table 1 shows the number of elements, number of degrees of freedom and CPU time. The processor type used for this study was 2 Xeon 5160 (3.0 GHz, dual core).

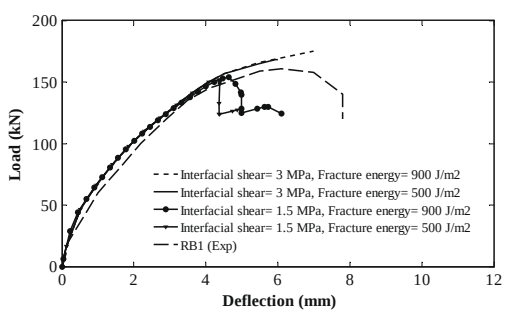

Fig. 8. Comparison between the experimental and the FE analysis results for different model of interfacial behaviour and isotropic behaviour for CFRP for beam RB1.

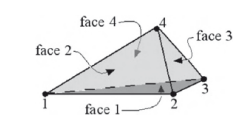

(a) 4-node linear tetrahedral element.

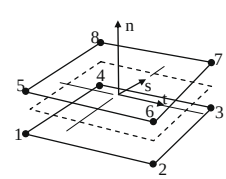

(b) 8-node 3-D cohesive element.

Fig. 9. Elements used in the numerical analysis.

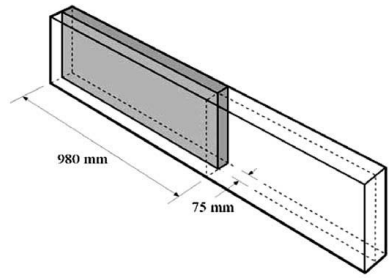

(a) By use of symmetry, one quarter of the beam was modelled.

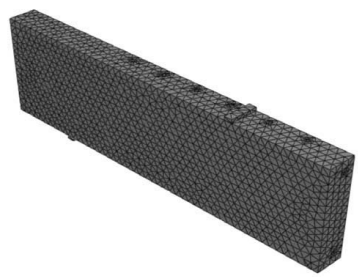

(b) Finite element mesh of quarter of beam.

Fig. 10. Geometry and elements used in the numerical analysis.

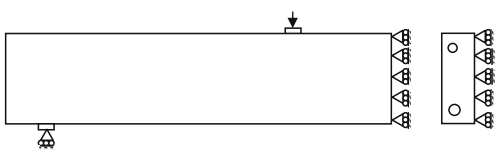

Fig. 11. Boundary conditions used in numerical work.

Table 1
Model size and computational time.

Model	Number of elements	Number of degrees of freedom (DOF)	CPU time (h)
Control beam	150,813	79,428	2:54
Isotropic CFRP/ perfect bond			
RB1	168,630	89,595	3:41
RB2	169,019	89,583	4:25
RB3	168,917	89,406	4:05
Orthotropic CFRP/ perfect bond			
RB1	168,630	89,595	6:36
RB2	169,019	89,583	2:57
RB3	168,917	89,406	2:40
Isotropic CFRP/ cohesive model			
RB1	168,669	90,075	4:06
RB2	169,656	90,189	3:08
RB3	170,307	90,240	2:30
Orthotropic CFRP/ cohesive model			
RB1	168,669	90,075	3:41
RB2	169,656	90,189	2:50
RB3	170,307	90,240	2:52

3.3. Nonlinear solution

In this study the total deflection applied was divided into a series of deflection increments. Newton method iterations provide convergence, within tolerance limits, at the end of each deflection increment. During concrete cracking, steel yielding and the ultimate stage where a large number of cracks occur, the deflections are applied with gradually smaller increments. Automatic stabilization and small time increment were also used to avoid a diverged solution.

4. Results

4.1. Load–deflection curves

The load–deflection curves obtained for control beam and retrofitted beams from experiments and FEM analysis are shown in Fig. 12. Four different combinations of models for CFRP and concrete/CFRP bond were used.

There is good agreement between FEM and experimental results for the control beam, Fig. 12a. The FEM analysis predicts the beam to be slightly stiffer and stronger, probably because of the assumed perfect bond between concrete and reinforcement. The good agreement indicates that the constitutive models used for concrete and reinforcement can capture the fracture behaviour well.

When comparing Fig. 12a–d, it can be seen that the length of the CFRP significantly influences the behaviour of the beam. The longer CFRP, the higher is the maximum load.

For the retrofitted beams, the results from the four different FEM models are close to identical during the first part of the curve, all slightly stiffer than the experimental results, Fig. 12b–d.

After cracks start appearing, the perfect bond models increasingly overestimate the stiffness of the beam. This is due to the fact that the perfect bond does not take the shear strain between the concrete and CFRP into consideration. This shear strain increases when cracks appear and causes the beam to become less stiff.

The perfect bond models also fail to capture the softening of the beam, a fact that is most obvious for RB1. Debonding failure, which occurred in the experiments, is not possible with the perfect bond model. Thus, it is possible to increase the load further until another mode of failure occurs. In this case shear flexural crack failure or CFRP rupture. The curves for isotropic and orthotropic perfect bond models are close to coincident, but the orthotropic perfect bond model gives a maximum load value that is slightly smaller than the isotropic perfect bond model. This is possibly because the unrealistically high stiffness in the transverse direction and shear of the isotropic CFRP provides a strengthening confinement.

The cohesive models show good agreement with the experimental results. There are only small differences between the isotropic and orthotropic cohesive models.

There are several possible causes for the differences between the experimental data and the finite element analysis. One is, as for the control beam, the assumed perfect bond between concrete and steel reinforcement. In addition, the location and dimensions of the pre-crack were not represented exactly as it appeared in the experimental work; another reason is due to the estimation of the behaviour of the interface between CFRP and concrete. This may lead to the overestimation of the stiffness and capacity of the reinforced concrete structural element.

The results show that a cohesive model gives good agreement with experimental results, but the perfect bond model does not, at least not for high load levels. The results also show that it is not necessary to take into account the orthotropic properties of the unidirectional CFRP.

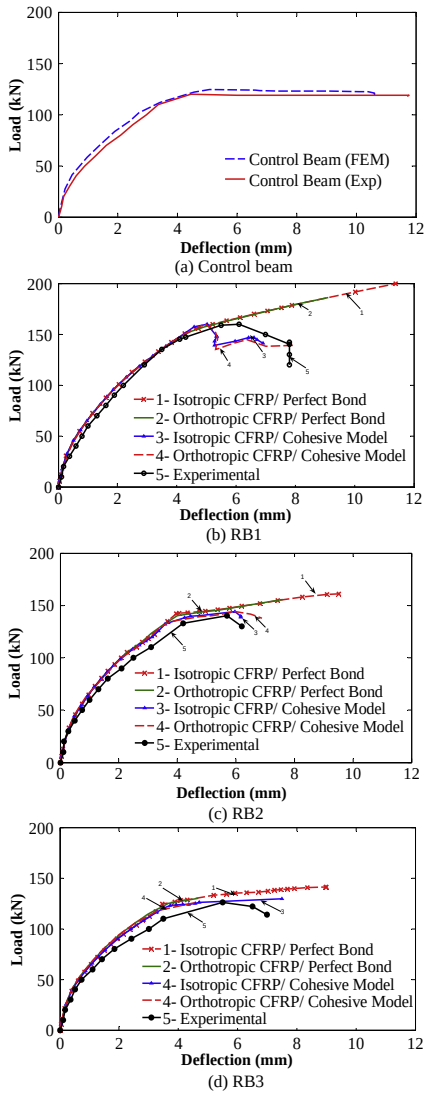

Fig. 12. Load–deflection curves of beams, obtained by experiments and different models.

4.2. Effect of retrofitting on the stress

Fig. 13 shows the differences between the axial stress for the control specimens and the retrofitted beam RB2 at load equal to 10 kN. All models which were used in this study gave the same indication for this point. Also the parts of the strengthened beams a long distance from the CFRP have a different stress distribution compared to those of the un-strengthened specimens at the corresponding location. This indicates that the effect of the strengthening is not local but it affects the stress distribution of the beam as a whole.

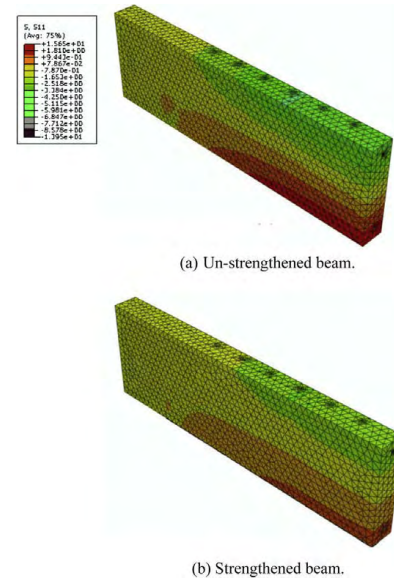

Fig. 13. Comparison of axial stress distribution between un-strengthened beam and strengthened beam, RB2.

4.3. Evolution of cracks

As the concrete damage plasticity model does not have a notation of cracks developing at the material integration point, it was assumed that cracking initiates at the points where the maximum principal plastic strain is positive, following Lubliner et al. [24]. Fig. 14 shows a comparison between plastic strain distributions obtained from the finite element analysis and crack patterns obtained from the experiments for the control beam and strengthened beams. The cracks obtained in the experiments and in the simulations are similar, which indicates that the model can capture the mechanisms of fracture in the beams.

4.4. Failure mode

The perfect bond model does not include fracture of the bond, and is thus unable to model the debonding fracture mode which the experiments showed. The cohesive model, on the other hand, can represent debonding. When the cohesive bond model was used debonding fracture occurred, just like in the experiments. This is illustrated in Fig. 15.

4.5. Stress in bond layer

Debonding of CFRP is likely to initiate at the stress concentration in the bond layer, which occur in the plate end region and around cracks. A simplified illustration of the axial stress in the composite and the corresponding shear stress in the bond layer for a beam with a constant moment and a mid-span crack is shown in Fig. 16. In the anchorage zone the axial stress in the composite is increasing and the axial force is transmitted to the composite through shear stress in the bond layer. In the crack zone axial force cannot be sustained by the beam itself and axial force is thus transmitted to the composite, resulting in shear stress in the bond layer.

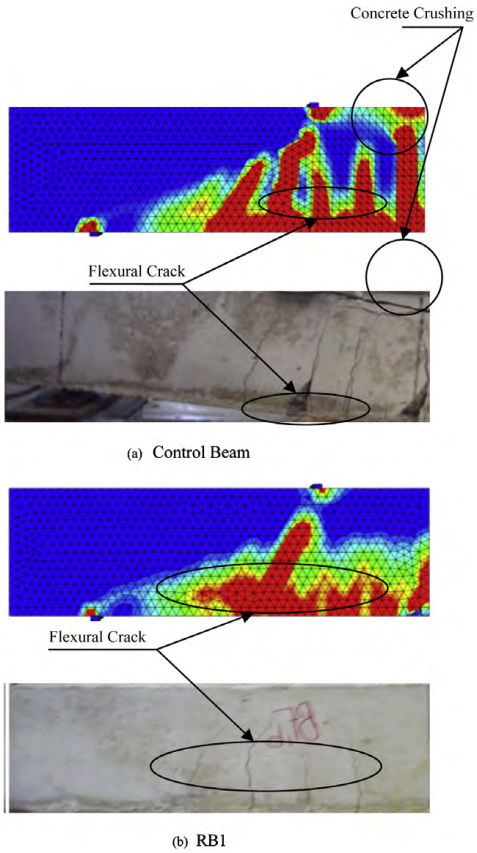

Fig. 14. Comparison between plastic strain distribution from FEM analysis and crack patterns from experiments.

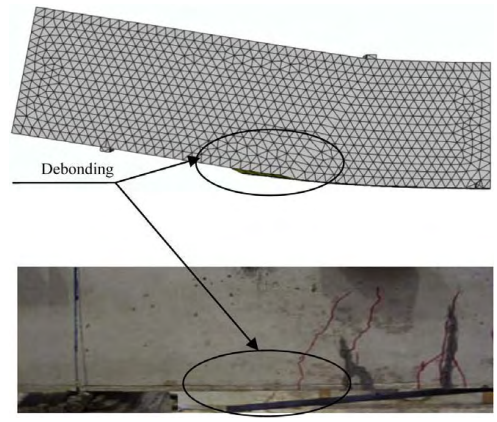

Fig. 15. Comparison of failure mode from FEM analysis and experiment for beam RB2.

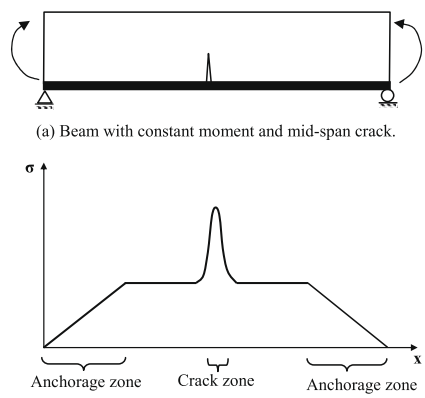

Fig. 16. Axial stress in composite material and shear stress in bond layer.

The stress state in the bond layer in the analysed beams is more complicated due to a complex crack pattern and 3-D effects. Still, it is possible to see the phenomena illustrated in Fig. 16.

Fig. 17 illustrates the shear stress in the cohesive layer for RB2 at different load levels. Note that due to symmetry only one half of the beam is represented. From Fig. 17, it can be seen that when the load is equal to 8 kN (i.e., before cracking) there are shear stress concentrations at the pre-cracked region and at the plate end. By increasing the load up to 100 kN (i.e., after the cracks are initiated) the interfacial shear stress increases, and has a maximum value at the plate end. The shear stress also reaches maximum value around the pre-cracked zone due to rapidly transmitted force between the concrete and CFRP. At the ultimate load, 140 kN, debonding has occurred at the plate end, and the maximum shear stress shifts to the mid-span which becomes a new anchorage zone and where the flexural cracks propagate.

Fig. 18 shows the shear stress in the cohesive layer for different CFRP lengths at a load of 100 kN. At this load cracking has initiated. It is clear that when the CFRP length is short, the entire plate is an anchorage zone and the shear stress is high and almost constant, see RB3. For RB1, the anchorage length needed is provided outside the cracking region which leads to an improved performance. Since the moment is decreasing towards the end of the beam, the shear stresses do not reach the same level in the anchorage zone as for RB2 and RB3.

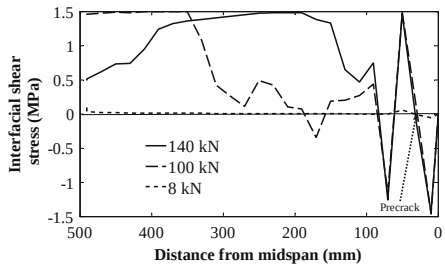

Fig. 17. Shear stress of the interface layer at different loads for beam RB2.

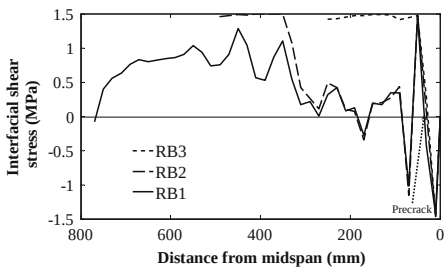

Fig. 18. Shear stress of the interface layer for different beams at 100 kN.

5. Conclusions

A finite element model was developed to analyse beams retrofitted with CFRP. The finite element results show good agreement with the experimental results. Elastic orthotropic and isotropic behaviours were used to represent the CFRP behaviour; also a cohesive model was used to address the interfacial behaviour between CFRP and concrete. The following conclusions can be drawn from this study:

- The behaviour of the retrofitted beams is significantly influenced by the length of CFRP. This is clear in experimental results as well as in numerical analysis. The ultimate load increases with the length of the CFRP.
- The perfect bond model failed to capture the softening of the beams.
- No significant differences were observed when different assumptions were used for CFRP with the cohesive bond model.
- The cohesive model proved able to represent the bond behaviour between CFRP and concrete. The predicted ultimate loads and the debonding failure mode were in excellent correlation with the experimental work.

References

[1] Kachlakev D, Mccurry DD. Behavior of full-scale reinforced concrete beams retrofitted for shear and flexural with FRP laminates. Compos J 2000;31:445–52.
[2] Valivonis J, Skuturna T. Cracking and strength of reinforced concrete structures in flexure strengthened with carbon fibre laminates. Civ Eng Manage J 2006;13(4):317–33.
[3] Yeong-soo S, Chadon L. Flexural behavior of reinforced concrete beams strengthened with carbon fiber-reinforced polymer laminates at different levels of sustaining load. ACI Struct J 2003;100:231–40.
[4] Aram MR, Gzaderski C, Motavalli M. Debonding failure modes of flexural FRP-strengthened RC beam. Compos Part B 2008;39:826–41.
[5] Ashour AF, El-Refaie SA, Garrity SW. Flexural strengthening of RC continuous beams using CFRP laminates. Cement Concr Compos 2004;26:765–75.
[6] Ai-hui Z, Wei-Liang J, Gui-bing L. Behaviour of preloaded RC beams strengthened with CFRP laminates. J Zhejiang Univ Sci A 2006:436–44.
[7] Wenwei W, Guo L. Experimental study of RC beams strengthened with CFRP sheets under sustaining loads. Wuhan Univ Technol – Mater Sci Ed J 2006;21(3).
[8] Esfahani M, Kianoush M, Tajari A. Flexural behaviour of reinforced concrete beams strengthened by CFRP sheets. Eng Struct 2007;29:2428–44.
[9] Teng JG, Smith ST, Yao J, Chen JF. Intermediate crack-introduced debonding in beams and slabs. Construct Build Mater J 2003;17(6–7):447–62.
[10] Ebead U, Marzouk H. Tension–stiffening model for FRP strengthened RC concrete two-way slab. Mater Struct 2004:193–200.
[11] Hu H-T, Lin F-M, Jan Y-Y. Nonlinear finite element analysis of reinforced concrete beams strengthened by fibre-reinforced plastic. Compos Struct J 2004;63:271–81.
[12] Lundquist J, Nordin H, Täljsten B, Olafsson T. Numerical analysis of concrete beams strengthened with CFRP – a study of anchorage lengths. In: FRP in construction, Proceeding of the international symposium of bond behaviour of FRP in structures; 2005. p. 247–54.
[13] Santhakumar R, Chandrasekaran E. Analysis of retrofitted reinforced concrete shear beams using carbon fibre composite. Electron J Struct Eng 2004;4:66–74.
[14] Obaidat Y. Retrofitting of reinforced concrete beams using composite laminates. Master Thesis, Jordan University of Science and Technology; 2007.
[15] Hibbitt, Karlsson, and Sorensen, Inc. ABAQUS Theory manual, User manual and Example Manual, Version 6.7. Providence, RI; 2000.
[16] ACI Committee 318. Building code requirements for structural concrete and commentary (ACI 318-99). Detroit (MI): American Concrete Institute; 1999.
[17] Saenz, LP. Discussion of "Equation for the stress-strain curve of concrete" by Desayi P, Krishnan S. ACI Journal 1964;61:1229–35.
[18] Hu H-T, Schnobrich WC. Constitutive modelling of concrete by using nonassociated plasticity. J Mater Civil Eng (ASCE) 1989;1(4):199–216.
[19] Piggott M. Load bearing fibre composites. 2nd ed. Boston/Dordrecht/London: Kluwer Academic Publishers; 2002.
[20] Guo ZG, Cao SY, Sun WM, Lin XY. Experimental study on bond stress-slip behaviour between FRP sheets and concrete. In: FRP in construction, proceedings of the international symposium on bond behaviour of FRP in structures; 2005. p. 77–84.
[21] Lu XZ, Ten JG, Ye LP, Jaing JJ. Bond-slip models for FRP sheets/plates bonded to concrete. Eng Struct 2005;24(5):920–37.
[22] JCI. Technical report on continuos fibre reinforced concrete. JCI TC952 on continuos reinforced concrete; 1998. p. 116–24.
[23] JCI. Technical report on retrofit technology for concrete structures. Technical committee on retrofitting technology for concrete structures; 2003. p. 79–97.
[24] Lubliner J, Oliver J, Oller S, Oñate E. A plastic-damage model for concrete. Int J Solids Struct 1989;25:299–329.

Paper C

C

Nonlinear FE Modelling of Shear Behaviour in RC Beam Retrofitted with CFRP

Yasmeen Taleb Obaidat, Ola Dahlblom and Susanne Heyden

Published in proceedings of Computational Modelling of Concrete Structures (EURO-C 2010), Austria, 2010, 671-677.

Computational Modelling of Concrete Structures – Bićanić et al. (eds)

Nonlinear FE modelling of shear behaviour in RC beam retrofitted with CFRP

Yasmeen Taleb Obaidat, Ola Dahlblom & Susanne Heyden
Division of Structural Mechanics, Lund University, Lund, Sweden

ABSTRACT: A nonlinear 3-D numerical model has been developed using the ABAQUS finite element program, and it was used to examine the shear behaviour of beams retrofitted by CFRP. Two models were used to represent the interface between CFRP and concrete, a perfect bond model and a cohesive model. Validation of the model was performed using data obtained from an experimental study. The results showed that the cohesive model is able to simulate the composite behaviour of reinforced concrete beams retrofitted by CFRP in shear correctly. The model is then used to examine the influence of length and orientation of CFRP. It is shown that the length of CFRP and the orientation strongly influence on the behaviour of the retrofitted beams.

1 INTRODUCTION

Reinforced concrete (RC) structural elements such as beams are subjected to significant flexure and shear. Strengthening or upgrading becomes necessary when these structural elements are not able to provide satisfactory strength and serviceability. Shear failure of RC beams could occur without any warning. Many existing RC members are found to be deficient in shear strength and need to be repaired. Shear deficiencies in reinforced concrete beams may occur due to many factors such as inadequate shear reinforcement, reduction in steel area due to corrosion, use of outdated design codes, increased service load and design faults.

The application of carbon fibre reinforced polymer (CFRP) as an external reinforcement has become widely used recently. It is found to be important for improving the structural performance of reinforced concrete structures. A beam can be bonded with CFRP plates on either the soffit or the web. Generally, the soffit bonding is preferred for flexural retrofitting of beams, while web bonding is performed for shear retrofitting. For shear retrofitting of beams, different schemes can be employed, such as bonding vertical or inclined strips, or bonding continuous plates on the web. Most of the research done in the past on strengthening of existing RC beams focused on flexural strengthening (Ashour et al. 2004), (Esfahani et al. 2007), (Wang & Zhang 2008) (Wenwei & Guo 2006) and (Obaidat et al. 2009) and very few studies have specifically addressed the topic of shear strengthening (Sales & Melo 2001), (Santhakumar & Chandrasekaran 2004) and (Sundarraja & Rajamohan 2009).

While experimental methods of investigation are extremely useful in obtaining information about the composite behaviour of FRP and reinforced concrete, the use of numerical models helps in developing a good understanding of the behaviour at lower costs.

In this paper, the efficiency of applying CFRP as external reinforcement to enhance the shear capacity of RC beams was investigated by the finite element method. ABAQUS (Hibbitt, Karlsson, & Sorensen Inc. 2000) is used to model the behaviour of a retrofitted beam; in the first part of the paper validation of the model is done using four beams tested by Obaidat (Obaidat 2007). The second part is to investigate the effect of different parameters on shear retrofitting. The test parameters included a variable length and orientation of CFRP.

2 EXPERIMENTAL DATA

The experimental data was obtained from (Obaidat 2007). This work consisted of four beams subjected to four point bending. All beams were identical in geometry and reinforcement. The geometry of the beams is shown in Figure 1 and the material properties are given in Table 1. Two beams were used as control beams and the rest were retrofitted on both sides of the beams with CFRP. The CFRP had 50 mm width and 300 mm length and the spacing was 100 mm, see Figures 2 and 3.

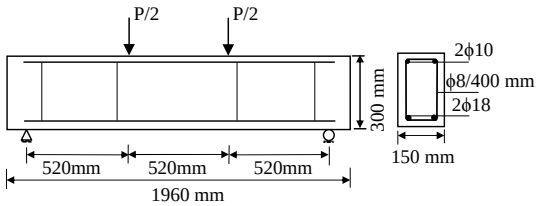

Figure 1. Geometry, arrangement of reinforcement and load of the tested beams.

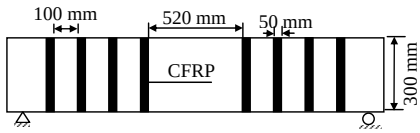

Figure 2. The arrangement of the CFRP laminate in retrofitted beams.

Figure 3. Installation CFRP in experimental work.

Table.1. Mechanical properties of materials used.

Steel	f_v	507 MPa
	E_s	210 GPa
	ν	0.3
Concrete	f_c'	30 MPa
CFRP	E_f	165 GPa
	f_f	2 GPa

3 NUMERICAL SIMULATIONS

3.1 *Studied bodies*

In order to study how the length and orientation of CFRP affect the shear behaviour of retrofitted beams, numerical simulations were conducted for the cases shown in Figure 4. Three different lengths of CFRP were used in the simulations. The orientation of the CFRP was also varied keeping the amount of CFRP as in 90º by using 35 mm width of CFRP. Two different models for the concrete-CFRP interface were evaluated in the validation.

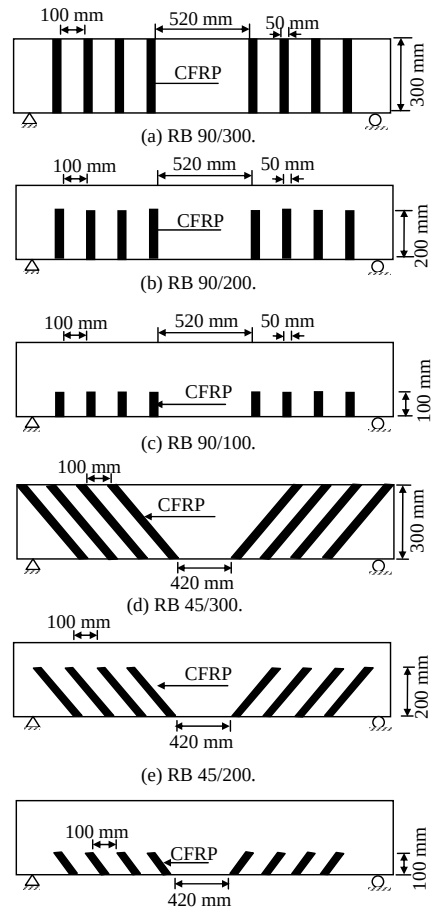

Figure 4. Studied CFRP configurations.

3.2 *Material Models*

3.2.1 *Concrete*

A plastic damage model was used to represent the behaviour of concrete. The model assumes that the two main failure mechanisms are tensile cracking and compressive crushing of the concrete material.

The softening curve of concrete under tension is shown in Figure 5, where f_{ct} is the tensile strength, and G_f is the fracture energy of concrete, (Hillerborg 1985). The tensile strength of concrete can be obtained from Equation 1 (ACI Comitte 318. 1999), and the fracture energy was assumed equal to 90 J/m^2.

$$f_{ct} = 0.35\sqrt{f_c'} = 1.81 \text{ MPa} \quad (1)$$

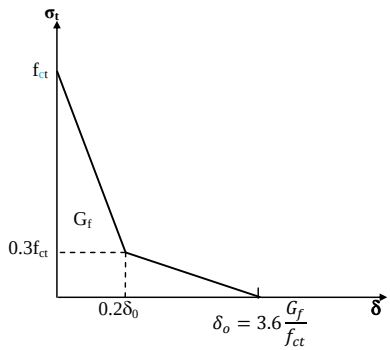

Figure 5. Softening curve of concrete under uni-axial tension.

The stress-strain curve under uni-axial compression is shown in Figure 6, (Saenz 1964). The modulus of elasticity was obtained using (ACI Comitte 318. 1999)

$$E_c = 4700\sqrt{f_c'} = 26000 \text{ MPa} \quad (2)$$

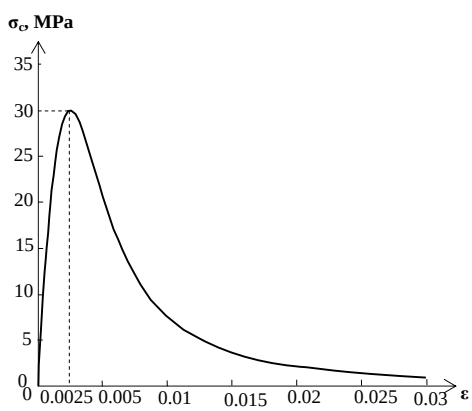

Figure 6. Stress-strain behaviour of concrete under uniaxial compression.

3.2.2 *Steel reinforcement*

The constitutive behaviour of steel was modelled using an elastic perfectly plastic model, see Figure 7. The parameters used to define this model are elastic modulus E_s, yield stress, f_y, and Poisson's ratio, ν. The parameters from the experimental study were used; see Table 1. Perfect bond was assumed between the steel and the concrete.

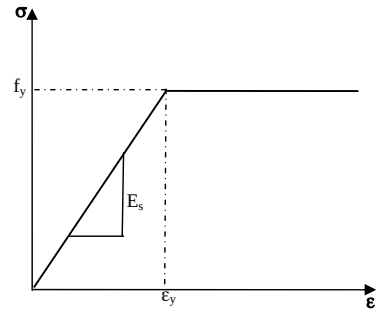

Figure 7. Stress-strain curve for the reinforcement steel.

3.2.3 *CFRP*

The CFRP was assumed to be a linear elastic orthotropic material. The elastic modulus in the fibre direction of the unidirectional CFRP material used in the experimental study was specified by the manufacturer as 165 GPa. For the orthotropic material model E_{11} was set to 165 GPa. Using Rule of Mixture (Piggott 2002), E_{epoxy}= 2.5 GPa and the fibre volume fraction 75 %, E_{fibre} was found to be 219 GPa and $\nu_{12}= \nu_{13}$= 0.3. By use of Inverse Rule of Mixture (Piggott 2002), $E_{22}= E_{33}$= 9.65 GPa and $G_{12}=G_{13}$= 5.2 GPa. ν_{23} and G_{23} were set to 0.45 and 3.4 GPa, respectively.

3.2.4 *CFRP-concrete interface*

Two different models for the interface between CFRP and concrete were used in this study. In the first model, the interface was considered as a perfect bond. In the second model, the interface was modelled using a cohesive zone model.

Cohesive elements were used together with a traction separation law which defines the traction as a function of the separation distance between the interface elements, see Figure 8. The material has an initial linear elastic behaviour. The elastic response is followed by damage initiation and evolution until total degradation of the elements.

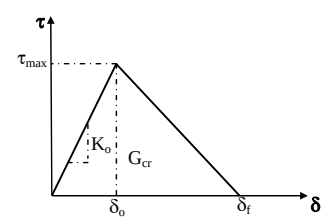

Figure 8. Bilinear traction–separation constitutive law.

The nominal traction stress vector consists of three components: σ_n, τ_t, τ_s, which represents the normal and shear tractions, respectively.

The initial stiffness matrix is directly related to the thickness of the cohesive layer and to the material stiffness G. A general expression of this relation is:

$$K_o = \frac{1}{\frac{t_i}{G_i} + \frac{t_c}{G_c}} \quad (3)$$

where t_i is the adhesive thickness, t_c is the concrete thickness, and G_i and G_c are the shear modulus of adhesive and concrete respectively.

An upper limit for the maximum shear stress, τ_{max}, is provided by the expression (Ye, Lu & Chen 2005):

$$\tau_{max} = 1.2\,\beta_w f_{ct} \quad (4)$$

where:

$$\beta_w = \sqrt{\left(2.25 - {}^{w_f}/_{s_f}\right)/\left(1.25 + {}^{w_f}/_{s_f}\right)}$$

and w_f is CFRP plate width, s_f is spacing of CFRP strips and f_{ct} is concrete tensile strength.

This equation gives τ_{max}= 2.17 MPa. Numerical simulations showed that this value is too high; since CFRP rupture or concrete crushing induced the failure, instead of the CFRP debonding that occurred in the experimental study. Hence, τ_{max} was reduced to 1.5 MPa.

For fracture energy, G_{cr}, previous studies have indicated values from 300 J/m^2 up to 1500 J/m^2 (JCI 1998) and (JCI 2003). For this study the value 900 J/m^2, in the middle of the interval proposed by previous studies, was used.

During separation of the cohesive element surfaces, the thickness increases and the stiffness degrades. The quadratic nominal stress criterion was used as damage initiation criterion:

$$\left\{\frac{\langle\sigma_n\rangle}{\sigma_n^o}\right\}^2 + \left\{\frac{\langle\tau_s\rangle}{\tau_s^o}\right\}^2 + \left\{\frac{\langle\tau_t\rangle}{\tau_t^o}\right\}^2 = 1 \quad (5)$$

where σ_n and τ_s, τ_t are the cohesive tensile and shear strengths of the interface. The values used for this study were σ_n^o= f_{ct}= 1.81 MPa, and τ_s^o= τ_t^o=1.5 MPa.

3.3 *Finite Element Analysis*

The concrete and the steel were modelled using a linear tetrahedral element. This element has four nodes with three degrees of freedom at each node– translation in the x, y, and z directions. The element used is capable of plastic deformation and cracking in three orthogonal directions. An eight node reduced-integration element was used to model the CFRP composite and the steel plates under the load and at the support. This element also has three degrees of freedom at each node. Eight-node 3-D cohesive elements were used to model the interface layer. The cohesive interface elements are composed of two surfaces separated by a thickness. The relative motion of the bottom and top parts of the cohesive element measured along the thickness direction represents opening or closing of the interface. The relative motion of these parts represents the transverse shear behaviour of the cohesive element.

Abaqus/standard (Hibbitt, Karlsson, & Sorensen Inc. 2000) was used for these simulations. The total deflection applied was divided into a series of deflection increments. In addition automatic stabilization and small time increments were used to avoid a diverged solution. Since the geometry of the beams, loading and boundary conditions were symmetrical, only one quarter of a beam was modelled with typical finite element mesh as shown in Figure 9. Boundary conditions are shown in Figure 10.

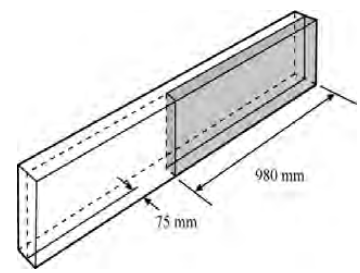

(a) By use of symmetry, one quarter of the beam was modelled.

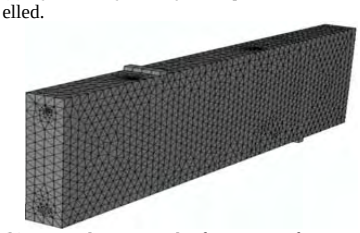

(b) Finite element mesh of a quarter of a control beam.

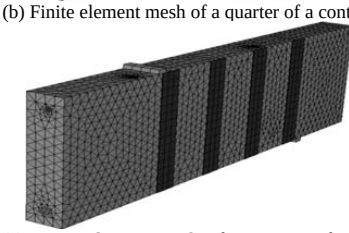

(c) Finite element mesh of a quarter of a strengthened beam.

Figure 9. Geometry and elements used in the numerical analysis.

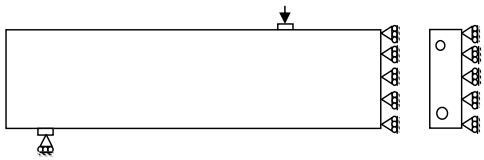

Figure 10. Boundary conditions used in numerical work.

4 VERIFICATION OF FINITE ELEMENT MODEL

To verify the finite element model of the reinforced concrete retrofitted with CFRP, four beams from an experimental study (Obaidat 2007) were simulated. The results from the FEM analysis were then compared with the experimental results.

The load-deflection curves for the control beams are shown in Figure 11. In the linear part the FEM results are slightly stiffer than the experimental results. One explanation for this may be the assumption of perfect bond between concrete and steel.

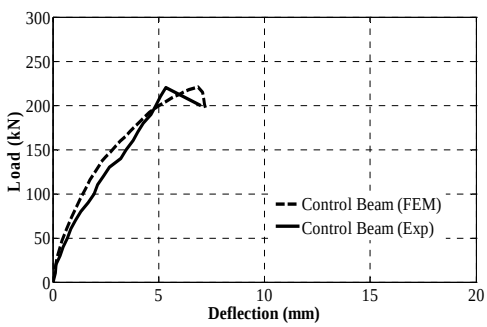

Figure 11. Load-deflection curves of control beams obtained by experiments and FEM.

As shown in Figure 12 there is good agreement between the cohesive model and the perfect bond model in the first part of the curve, but when the crack starts to propagate the cohesive bond model gives a stronger softening effect in the beam. It is also clear from the figure that the cohesive model shows a very satisfactory agreement with the experimental response. The perfect bond model overestimates the ultimate load and deflection. This can be attributed to the fact that the perfect bond model fails to capture the softening of the beam and it is not able to represent the debonding failure that occurred in the experimental work.

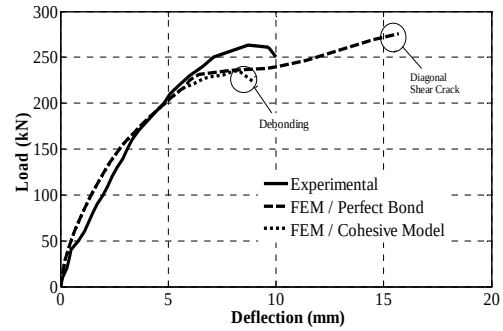

Figure 12. Load-deflection curves of retrofitted beams obtained by experiments and FEM.

The cohesive model also shows good agreement with the experimental work in the debonding failure mode as shown in Figure 13. The following results have been obtained using the cohesive model.

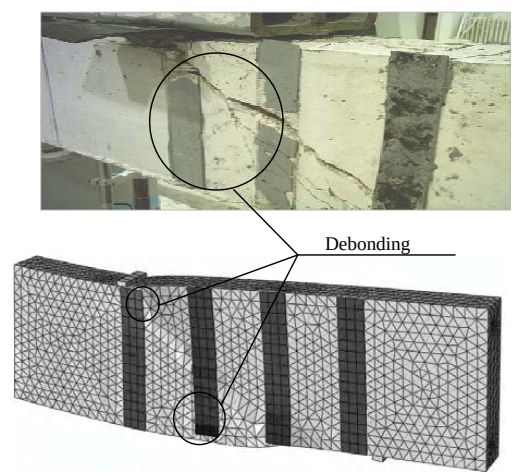

Figure 13. Comparison of failure mode from FEM analysis and experiment.

5 RESULTS AND DISCUSSION

5.1 *Effect of length of CFRP*

To study the effect of CFRP length, three lengths were investigated, 100 mm (lower third of web of beam, RB 90/100), 200 mm (lower two thirds of web of beam, RB 90/200) and 300 mm (entire web of beam, RB 90/300).

Figure 14 shows the load versus the mid-span deflection of a reinforced concrete beam retrofitted with CFRP. In all beams the failure mode was debonding due to concentration of shear stress resulting from the diagonal crack.

Generally the stiffness and load capacity of the beam increases when the length of CFRP is equal to the web of the beam as shown in Figure 14.

In Figure 14, it can be seen that for RB 90/200 and RB 90/100 the reinforcement seems not to strengthen the beam; this is due to the fact that the crack crossed the strips close to their end. This result supports what (Monti and Liotta 2005) found. For these cases the formation of such a crack was accompanied by yielding of internal shear reinforcement. The steel yielding caused the drop in the beam stiffness compared to the control beam as shown in Figure 14. Before the yielding any increase in loading is shared by the reinforcing steel and CFRP. After the yielding most of the increased loading has to be carried by the plate until debonding occurs.

It can be seen also that RB 90/200 failed at a lower load than RB 90/100. This is attributed to the fact that the area in the middle of the web is critical in the failure process and that the end of plate in RB 90/200 is in that area. Hence the stress concentration is more pronounced in this beam and debonding occurs earlier.

This analysis, regarding the length of CFRP, verifies that the strip, when the orientation is 90 degrees, should cover the whole web of the beam to provide an improvement of beam behaviour.

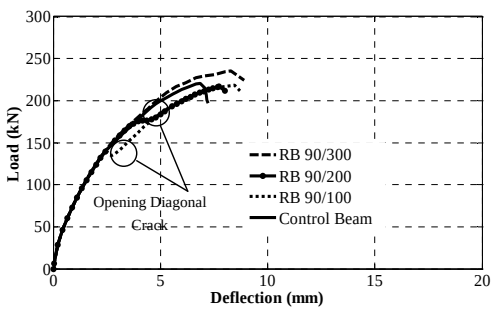

Figure 14. Load-deflection curves for different lengths of CFRP, obtained by FEM.

5.2 *Effect of orientation of CFRP*

Since a shear crack propagates in a diagonal manner the orientation of the CFRP may affect the behaviour of a retrofitted beam. Two orientations, 90º and 45º were studied.

For the longest CFRP the failure mode was a shear crack while for the other beams the failure mode was debonding.

It is clear from Figure 15 that when the angle of orientation was 45º the retrofitted beam carries more load for all lengths.

It is interesting to note that the load capacity for RB 45/300, RB 45/200 and RB 45/100 was increased by 20.1 %, 2% and 5% respectively, compared to the control beam while the change was 11.9% for RB 90/300, -1.8% for RB 45/200 and -1.1% for RB 90/100. This indicates that the performance of a beam retrofitted with CFRP is influenced by the orientation of the CFRP. When the CFRP did not cover the full depth of the beam the load capacity was actually decreased for 90º, while a small increase was obtained for 45º.

From Figure 16, it can be concluded that the orientation of CFRP has a strong effect on the behaviour of the retrofitted beam for the same total amount of CFRP. A 45º orientation gives a better effect in terms of maximum load and deflection.

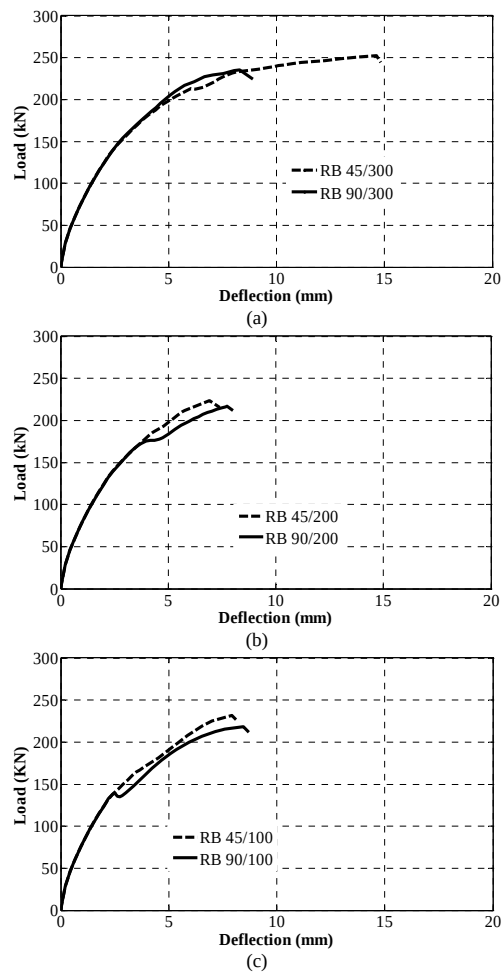

Figure 15. Load-deflection curves of 90º and 45º of CFRP obtained by FEM.

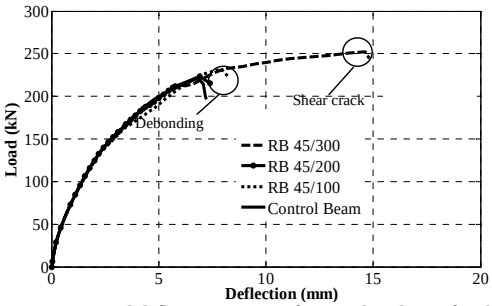

Figure 16. Load-deflection curves of Control and retrofitted beams with 45^o of CFRP and different lengths, obtained FEM.

6 CONCLUSION

An FE model was used to investigate the behaviour of RC beams retrofitted in shear with CFRP by using the commercial program ABAQUS. The results from FE model were compared with experimental work by Obaidat (Obaidat 2007) to assess the accuracy of the proposed FEM model. The present numerical study has shown that the proposed FEM model is suitable for predicting the behaviour of RC beams retrofitted with CFRP plates in shear. It should also be noted that the perfect bond model cannot account for debonding failure of CFRP since this model does not take in to account the behaviour of the interface between the CFRP and the concrete. On the other hand, the cohesive model is capable to predict the debonding failure. This study also presents results of an investigation of the effects of length and orientation of CFRP. The following can be concluded:

(1) Change in length of CFRP reinforcement may result in different behaviours of retrofitted beams. The longest CFRP presents a high stiffness and high load while when the CFRP strip do not cover the full depth of beam the load capacity decrease for 90º. Therefore it is not advisable to use a CFRP strip not covering the entire beam depth when retrofitting for shear.

(2) The peak load and deflection is slightly affected by the orientation of CFRP. For 45º CFRP orientation, a larger increase in load capacity is obtained compared to 90 º.

7 REFERENCES

ACI Comitte 318. 1999. Building Code Requirements for Structural Concrete and Commentary (ACI 318-99). American Concrete Institute Detroit, MI.

Ashour, AF, El-Refaie, SA & Garrity, SW. 2004. Flexural strengthening of RC continuous beams using CFRP laminates. *Cement & Concrete Composites;* 26: 765- 775.

Esfahani, M., Kianoush, M., & Tajari. 2007. A. Flexural behaviour of reinforced concrete beams strengthened by CFRP sheets. *Engineering Structures*; 29: 2428-2444.

Hibbitt, Karlsson, & Sorensen, Inc. 2000. ABAQUS Theory manual, User manual Example Manual, Version 6.7. Providence, RI.

Hillerborg, A. (1985). The theoretical basis of a method to determine the fracture energy G_f of concrete. Materials and Structures, RILEM 50-FMC, 108, pp 291-296.

JCI. Technical report on continous fibre reinforced concrete. JCI TC952 on Continous Reinforced Concrete 1998; 116-124.

JCI. Technical report on retrofit technology for concrete structures. Technical Committee on Retrofitting Technology for Concrete Structures 2003; 79-97.

Monti, G., & Liotta, M. A. 2005. FRP strengthening in shear: Test and design equations. *Proceeding of 7th International Symposium on Fiber Reinforce Polymer for Reinforced Concrete Structures (FRPRCS-7)*; 543-562.

Obaidat,Y. 2007. Retrofitting of reinforced concrete beams using composite laminates, *Master Thesis, Jordan University of Science and Technology.*

Obaidat,Y.,Heyden,S., & Dahlblom, O. 2009.The Effect of CFRP and CFRP/ Concrete Interface Models when Modelling Retrofitted RC Beams with FEM. Accepted for publication in *Composite Structures.*

Piggott, M. Load bearing fibre composites, 2nd Edition. Kluwer Academic Publishers, Boston/ Dordrecht/ London, 2002.

Saenz, L. Equation for the stress-strain curve of concrete. Desayi P, Krishnan S. ACI Journal 1964; 61:1229–35.

Salles Neto, M., Melo, G.S., Nagato, Y., T Beams Strengthened in shear with carbon sheet laminates, Fiber-reinforced Plastic for Reinforced Concrete Structure 2001; 1: 239-248.

Santhakumar, R., & Chandrasekaran, E. 2004. Analysis of retrofitted reinforced concrete shear beams using carbon fibre composite. Electronic *Journal of Structural Engineering,* 4: 66-74.

Sundarraja, M., & Rajamohan, S. 2009. Strengthening of RC beams in shear using GFRP inclined strips – An experimental study. C*onstruction and building materials,* 23: 856-864.

Wang, J., & Zhang, C. 2008. Nonlinear fracture mechanics of flexural- shear crack induced debonding of FRP strengthened concrete beams. I*nternational journal of solid and structures,* 45: 2916-2936.

Wenwei W., Guo L. 2006. Experimental study and analysis of RC beams strengthened with CFRP

laminates under sustaining load. *International Journal of Solids and Structures* 2006; 43: 1372–1387.

Ye, L. P., Lu, X. Z, and Chen, J. F. Design proposals for the debonding strengths of FRP strengthened RC beams in the chinese design code. *Proceeding of International Symposium on Bond Behaviour of FRP in Structures* (BBFS 2005); 45-54.

Paper D

D

FEM Study on the Effect of CFRP Stiffness and Width on Retrofitted Reinforced Concrete Beam Behaviour

Yasmeen Taleb Obaidat, Susanne Heyden and Ola Dahlblom

Submitted for publication

FEM Study on the Effect of CFRP Stiffness and Width on Retrofitted Reinforced Concrete Beam Behaviour

Yasmeen Taleb Obaidat*, Susanne Heyden and Ola Dahlblom

Division of Structural Mechanics, Lund University, Lund, Sweden

Abstract

The finite element program ABAQUS was used to study the effect of different parameters on the behaviour of an RC beam retrofitted with carbon fibre reinforced polymer (CFRP). These parameters were the stiffness and width of the CFRP. A linear elastic isotropic model was used for the CFRP and a cohesive bond model was used for the concrete–CFRP interface. A plastic damage model was used for the concrete. The material models were validated against experimental work and the results showed good agreement between experimental data and numerical results. Observations indicate that the CFRP width to beam width ratio and CFRP stiffness influence the type of failure mode of a beam retrofitted with CFRP. For small width and for large value of stiffness debonding will occur before steel yielding due to stress concentration at the end of the plate. For small values of stiffness, rupture of CFRP will occur. It was found that when the stiffness of CFRP increases the maximum load increases until a certain value of stiffness, then the maximum load decreases again. Simulations also show that the external load at steel yielding and the maximum load increase with the CFRP width.

Keywords: Carbon fibre reinforced polymer (CFRP), FEM (finite element method), Retrofitting, Reinforced concrete beam, Debonding.

1. Introduction

Upgrading of reinforced concrete structures may be required for many different reasons. The concrete may have become structurally inadequate, for example due to deterioration of materials, poor initial design and/or construction, lack of maintenance, upgrading of design loads or accident events such as earthquakes.

Retrofitting of concrete structures with externally bonded reinforcement is generally done by using either steel plates or fibre reinforced polymer (FRP) laminates. FRP can be convenient compared to steel for a number of reasons. They are lighter than the equivalent steel plates. They can be formed on site into complicated shapes and they can also be easily cut to length on site. The installation is easier and temporary support until the adhesive gains

* Corresponding author.
E-mail address: Yasmeen.Obaidat@construction.lth.se

its strength is not required due to the light weight of FRP. Earlier research has demonstrated that the addition of FRP laminate to reinforced concrete beams can increase stiffness and maximum load and reduce crack widths (Ai-hui et al. 2006, Ashour et al. (2004), Esfahani et al. (2007) and Pham et al. (2004)) and the technique is often used for upgrading concrete structures.

Nonlinear finite element analysis can be used to study the behaviour of retrofitted structures. This reduces the time and cost needed for experimental work. Many researchers have simulated the behaviour of retrofitted reinforced structures by using the finite element method. Several different approaches have been considered. Some models use nonlinear elasticity or plasticity models to capture the more complicated effects and predict the behaviour of reinforced concrete retrofitted by FRP in a general sense, (Camata et al. (2007), Coronado et al. (2006), Ebead and Marzouk (2004), Lundquist et al. (2005) and Pannirselvam et al. (2008)). An important issue is the influence of the properties of the interface between the carbon fibre reinforced polymer (CFRP) and the concrete. This was modelled in Obaidat et al. (2010). In this paper the model developed in Obaidat et al. (2010) was used for a parametric study.

The lack of design standards is disadvantageous to external strengthening of structures with CFRP. Developing rational design guidelines requires a fundamental understanding of the performance of structures strengthened with CFRP. The aim of this paper is to contribute to the understanding of the influence of CFRP width and stiffness on the performance of a strengthened beam.

2. Full Scale Experiment

Reinforced beams that were previously tested, Obaidat (2007), were used to validate the FE procedure discussed in the following sections. Fig. 1 shows the tested beams. A summary of the properties of materials as reported by Obaidat (2007) is shown in Table. 1. Two control beams were loaded to failure. Two other beams were loaded until cracks appeared, then retrofitted with unidirectional CFRP laminates attached to the bottom and finally loaded to failure. The fibres were oriented along the length of the beam. The laminates were 1560 mm long, 50 mm wide and 1.2 mm thick.

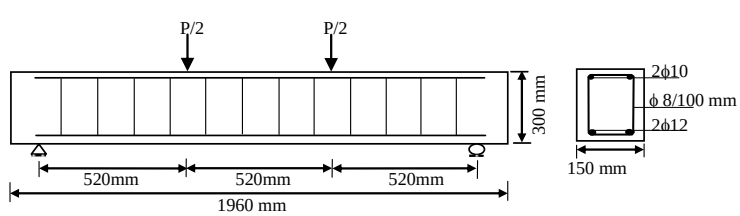

Fig. 1. Geometry, arrangement of reinforcement and load of the tested beams.

Table 1. Mechanical properties of materials used.

		Obaidat [11]	
Steel	f_y	507	MPa
	E_s	210	GPa
	ν	0.3	
Concrete	$f_c^{'}$	30	MPa
CFRP	E_{CFRP}	165	GPa
	f_{CFRP}	2	GPa

3. Finite Element Model

Beams with the same geometry, reinforcement and loading as in the experimental study, Fig. 1, were modelled by means of the finite element method. To account for the cracks that were present at retrofitting, a pre-crack was introduced close to midspan.

The analysis was performed using the general purpose finite element computer program ABAQUS (Hibbitt et al. (2000)). By taking advantage of the symmetry of the beams, a quarter of the full beam was used for modelling, see Fig. 2. This approach reduced computational time and computer disk space requirements significantly.

The reinforced concrete and steel loading plate were modelled using linear tetrahedral elements. The pre-crack was modelled by making a gap of 0.1 mm width and 10 mm depth between the continuum elements, 20 mm from the centre of beam.

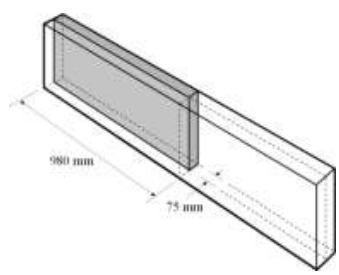

(a) A quarter of the beam was modelled.

(b) Finite element mesh of quarter of beam.

Fig. 2. Geometry and mesh used in the numerical analysis.

4. Material Properties

4.1. Concrete

The damage plasticity concrete model in ABAQUS/Standard, Hibbitt et al. (2000), assumes that the main two failure mechanisms are tensile cracking and compressive crushing. The evolution of the yield (or failure) surface is linked to failure mechanisms under tension and compression loading.

Under uniaxial tension the stress-strain response follows a linear elastic relationship until the value of the failure stress, f_{ct} is reached. The failure stress corresponds to the onset of micro-cracking in the concrete material. Beyond the failure stress the formation of micro-cracks is represented macroscopically with a softening stress-strain response. Hence, the parameters required to establish the first part of the relation are elastic modulus, E_c, and tensile strength, f_{ct}. From the compressive strength which is reported in Obaidat (2007), the elastic modulus and concrete tensile strength are calculated according to ACI Comitte 318. (1999).

$$f_{ct} = 0.33\sqrt{f_c'} \tag{1}$$

$$E_c = 4700\sqrt{f_c'} \tag{2}$$

where f_c', f_{ct} and E_c are given in MPa.

The parameter associated with the softening part of the curve is fracture energy, G_f. The fracture energy for mode I, G_f, is the area under the softening curve and is according to Beton (1993) estimated as

$$G_f = G_{fo}\left(\frac{f_c'}{10}\right)^{0.7} \tag{3}$$

where G_{fo} is a constant value related to maximum aggregate size and f_c' is given in MPa The crack opening is calculated from the fracture energy; see Fig. 3 (Hillerborg (1985)).

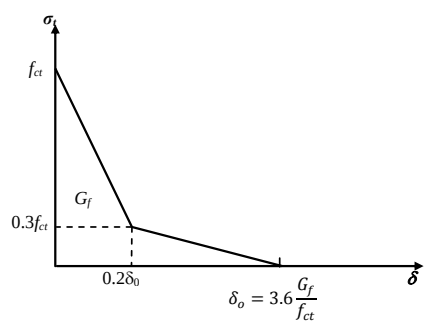

Fig. 3. Softening curve of concrete under uni-axial tension.

Under uniaxial compression the response is linear until the value of initial yield, f_{co}. In the plastic regime the response is typically characterized by stress hardening followed by strain softening beyond the ultimate stress, $f_c^{'}$. The stress–strain relationship proposed by Saenz (1964) was used to describe the uniaxial compressive stress–strain curve for concrete:

$$\sigma_c = \frac{E_c \varepsilon_c}{1 + (R + R_E - 2)\left(\frac{\varepsilon_c}{\varepsilon_o}\right) - (2R - 1)\left(\frac{\varepsilon_c}{\varepsilon_o}\right)^2 + R\left(\frac{\varepsilon_c}{\varepsilon_o}\right)^3} \tag{4}$$

where:

$$R = \frac{R_E(R_\sigma - 1)}{(R_\varepsilon - 1)^2} - \frac{1}{R_\varepsilon}, \quad R_E = \frac{E_c}{E_o}, \quad E_o = \frac{f_c^{'}}{\varepsilon_o}$$

and,

$R_\varepsilon = 4$, $R_\sigma = 4$ as reported in Hu and Schnobrich (1989), and ε_o=0.0025.

4.2 Steel reinforcement and steel plate

The steel was assumed to be elastic-perfectly plastic and identical in compression and tension. Perfect bond was assumed between the steel and concrete.

4.3 CFRP composite

The CFRP was modelled as an isotropic linear elastic material throughout this study. The unidirectional CFRP composite actually shows an orthotropic behaviour, but it was shown in Obaidat et al. (2010) that only the axial modulus is of importance in an application of this type. The elastic modulus and strength were taken to be E_{CFRP}=165 GPa and f_{CFRP}=2 GPa respectively, as found in the experimental study. The Poisson ratio of the CFRP composite was assumed to be ν_{CFRP}=0.30.

4.4. Interface Layer

Since Obaidat et al. (2010) found that a cohesive model is able to describe the failure mode and load capacity accurately, this was used to represent the interface between the concrete and CFRP in this study.

Cohesive elements were used together with a traction separation law which defines the traction function of the separation distance between interface elements (Camanho et al. (2002)), Fig. 4. The material has an initial linear elastic behaviour. The elastic response is followed by damage initiation and evolution until total degradation of the elements.

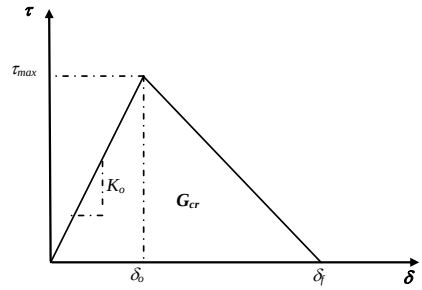

Fig. 4. Bilinear traction – separation constitutive law.

The behaviour of the interface prior to initiation of damage is described as linear-elastic. The nominal traction vector consists of three components in three-dimensional problems: σ_n, τ_t, τ_s, which represent the normal and shear tractions, respectively. The stiffness is determined according to

$$K_o = \frac{1}{t_i/G_i + t_c/G_c} \tag{5}$$

where t_i is the adhesive thickness, t_c is the effective thickness of concrete whose deformation forms part of the interfacial slip and was taken as 5 mm, and G_i= 0.667 GPa and G_c=10.8 GPa are the shear modulus of adhesive and concrete respectively.

The quadratic nominal stress criterion was used as damage initiation criterion

$$\left\{\frac{\sigma_n}{\sigma_n^o}\right\}^2 + \left\{\frac{\tau_s}{\tau_s^o}\right\}^2 + \left\{\frac{\tau_t}{\tau_t^o}\right\}^2 = 1 \tag{6}$$

where σ_n, τ_s and τ_t are the cohesive tensile and shear stresses of the interface, and the subscript refers to the direction of the stress component. The values used for this study were $\sigma_n^o = f_{ct}$= 1.81 MPa and $\tau_s^o = \tau_t^o = \tau_{max}$. An upper limit for the maximum shear stress, τ_{max}, is provided by the expression (Lu et al. (2005))

$$\tau_{max} = 1.5\,\beta_w f_{ct} \tag{7}$$

where

$$\beta_w = \sqrt{(2.25 - w_{CFRP}/w_{beam})/(1.25 + w_{CFRP}/w_{beam})}$$

and w_{CFRP} is CFRP plate width, w_{beam} is beam width and f_{ct} is concrete tensile strength. This equation gives τ_{max}= 3 MPa for w_{CFRP}= 50 mm. In numerical simulations using this value, failure is initiated by CFRP rupture or concrete crushing, instead of the CFRP debonding that occurred in the experimental study, indicating that this value is too high; hence, τ_{max} was reduced to 1.5 MPa.

For fracture energy, G_{cr}, previous studies have indicated values from 300 J/m^2 up to 1500 J/m^2 (. JCI (1998) and JCI (2003)). For this study the value 900 J/m^2, in the middle of the interval proposed by previous studies, was used.

5. Validation of numerical model

The numerical model used for the parametric study was validated against the experimental results. Fig. 5a shows the load versus deflection curves at mid-span for the control beam. There is a good correlation between the experimental results and the numerical results. In Fig. 5b the load versus deflection curves at mid-span for the retrofitted beams are shown. It is clear that there is only a slight deviation between experimental data and numerical results. Hence, the proposed model proved to be able to simulate the composite behaviour of reinforced concrete beams retrofitted by CFRP successfully.

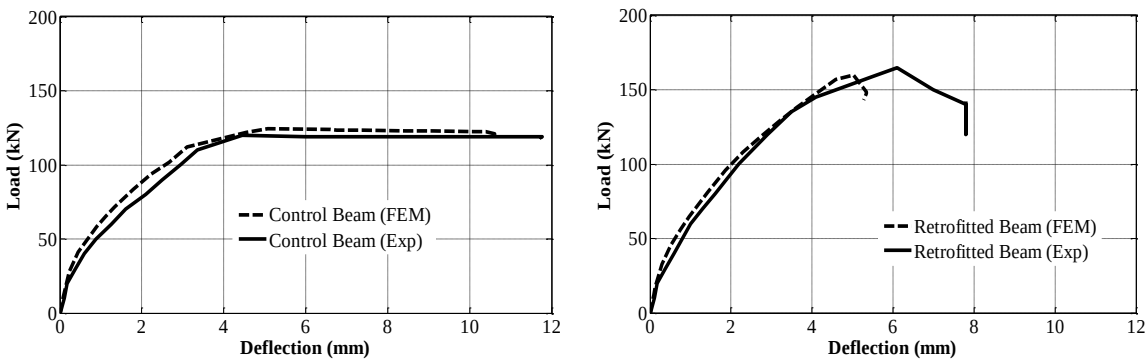

(a) Control Beam (b) Retrofitted Beam

Fig. 5. Comparison between load versus deflection curves from experimental and numerical studies.

6. Parametric Study

In order to study the effects of different parameters on a beam retrofitted with CFRP, numerical simulations were conducted. The most obvious parameter to vary is the total amount of external reinforcement, which is here quantified by the stiffness

$$K = E_{CFRP} \cdot w_{CFRP} \cdot t_{CFRP} \tag{8}$$

where E_{CFRP} is elastic modulus of CFRP, w_{CFRP} is CFRP width and t_{CFRP} is CFRP thickness. The value of the stiffness used in the experimental study is denoted K_o and has the numerical value

$$K_o = 165 \cdot 10^3 \text{ N/mm}^2 \cdot 50\text{mm} \cdot 1.2 \text{ mm} = 9900 \text{ N} \tag{9}$$

The series of different stiffnesses used to study the effect of varying stiffness, K, on retrofitted beams were: $0.25K_o$, $0.5K_o$, K_o, $2K_o$, $4K_o$ and $8K_o$. The values for the stiffness K used in the parametric study are shown on the vertical axis in Fig. 6.

Since there are three-dimensional effects present, the width of CFRP is also expected to be important. The width ratio, defined as

$$\mu = \frac{w_{CFRP}}{w_{beam}} \tag{10}$$

where w_{beam} is the beam width, was used as a measure for this. In the experimental study a width ratio of $\mu = \frac{50}{150} = \frac{1}{3}$ was used, and the values of μ used in the parameter study are shown on the horizontal axis in Fig. 6.

For varying the width ratio with constant stiffness, the thickness was chosen to adjust with the width, since simulation results show the same behaviour when adjusting either elastic modulus or thickness of CFRP to keep the stiffness, K, constant.

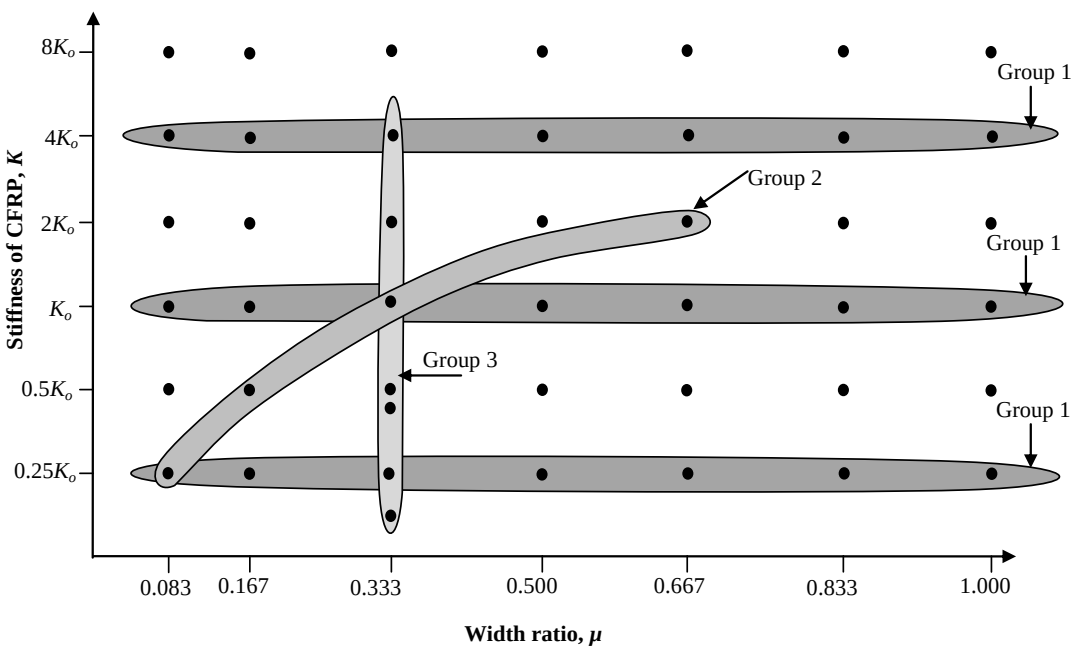

Fig. 6. Values for stiffness, K, and width ratio, μ, used in the parametric study. Dots indicate simulations.

The dots in Fig. 6 indicate the points for which the load-deflection behaviour of the beam was simulated. For presenting the results, different groups were selected to study the effect of different parameters. In Group 1 the effect of varying width ratio with constant stiffness was examined. In Group 2 the effect of varying CFRP width was studied and Group 3 deals with the effect of varying thickness.

7. Result and Discussion

As mentioned in section 6, the results were studied in three groups. Here the result of these groups will be discussed separately:

7.1. Group 1: Constant stiffness and varying width ratio

The main objective of this group is to obtain a clear understanding of how a certain amount of external reinforcement should be applied to get the best effect, and also under what circumstances more external reinforcement will give a better performance. Several different failure modes were observed in this study. Fig. 7 illustrates under what circumstances the different failure modes occurred:

- *Debonding before steel yielding:*

This failure was observed for high values of stiffness and for small width ratios. The plate end region could be regarded as an anchorage zone. In this zone axial force in the CFRP is built up through transfer of shear force in the CFRP-concrete bond. The stiffer the CFRP, the faster the increase in axial force, and hence the larger the shear stress in the bond. It is this stress concentration in the plate end region that causes the debonding when the CFRP stiffness is high. The smaller the width ratio, the smaller is the bond area available to take part in the transfer of shear force. This is why this fracture mode tends to be limiting for small width ratios. As discussed in connection to Fig. 12, the stress transfer is somewhat higher for a higher width ratio, but this is a secondary effect.

- *Debonding at the plate end after steel yielding:*

This failure was observed for medium width ratios and medium stiffness. For these cases, where the CFRP stiffness is not so high and the width ratio is not so small, a larger build up of force is allowed in the CFRP before debonding occurs. This means that the bending moment can be increased to the extent that steel yielding occurs. At further load increase, however, debonding will occur in the plate end region.

- *Debonding at flexural crack after steel yielding:*

This failure was observed for high width ratios and medium stiffness. In this case, debonding due to stress concentration in the plate end region is not a limiting phenomenon. Also in this case the bending moment can be increased to the extent that steel yielding occurs. At further load increase, there is debonding but in this case it starts from maximum moment region and propagates towards the plate end. This is the result of high interfacial shear stresses at a flexural crack in the maximum moment region.

- *Debonding with concrete splitting:*

This failure was observed when using high width ratio with medium stiffness (lower stiffness than for the previous case). After steel yielding, a flexural shear crack will develop in the concrete. The crack will propagate to the level of the tensile reinforcement and extend horizontally along the bottom of the tension steel reinforcement. With increasing external load, the horizontal crack propagates to cause parts of the concrete cover to split with the CFRP plate.

- *CFRP rupture:*

This failure was observed for small stiffness with large width ratio. After steel yielding is initiated, the force carried by the steel cannot increase anymore. Hence further increase in bending moment will result in large force in the CFRP which leads to CFRP rupture in the mid-span region.

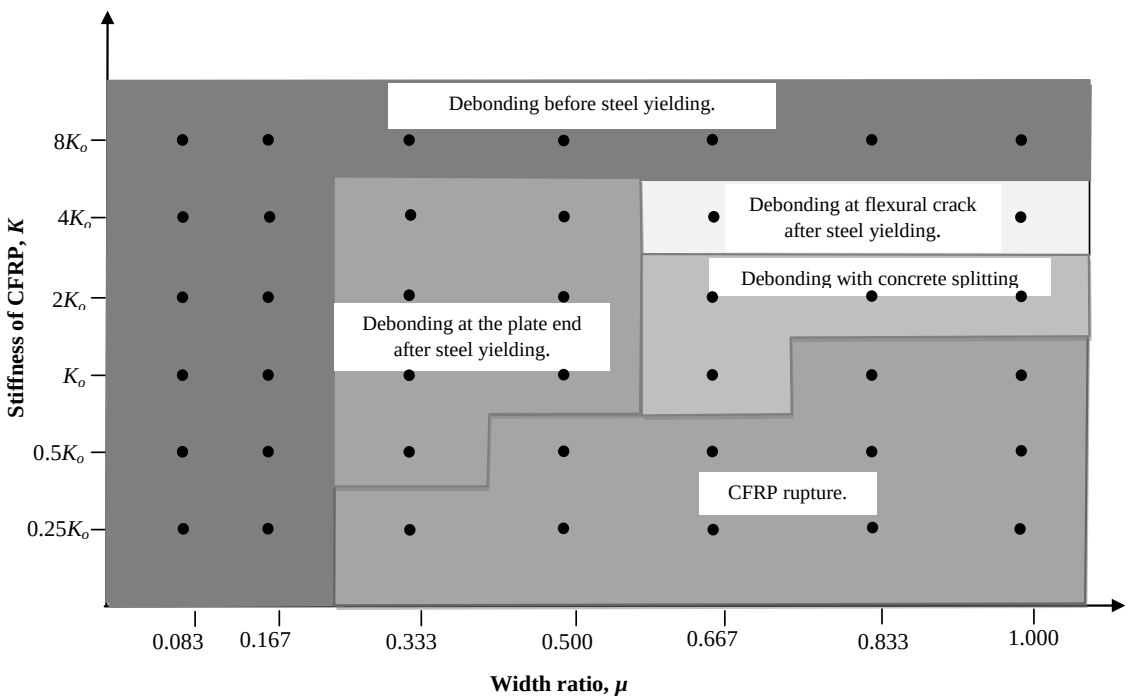

Fig. 7. Failure modes of the retrofitted beams. Data points are indicated with dots.

As is clear in Fig. 7, the width ratio and stiffness have a significant impact on the failure mode of the retrofitted beam.

The maximum load ratio is denoted α and defined as:

$$\alpha = \frac{\text{Maximum load, retrofitted beam}}{\text{Maximum load, control beam}}$$

Fig. 8a illustrates α as a function of the width ratio, μ, for stiffness values K=K_o, 0.5K_o and 0.25K_o, and Fig. 8b shows the corresponding values for stiffness values K=K_o, 2K_o, 4K_o and 8K_o.

For small stiffness values, Fig. 8a, the maximum load ratio, α, increases with the width ratio due to increase in the bond area between the concrete and CFRP. This allows the interfacial stress to distribute over a larger area, which means a less pronounced stress concentration and higher load before failure. When the failure mode shifts to CFRP rupture, which is for high width ratios, there is, however, no further increase in the maximum load ratio. CFRP rupture is governed by the CFRP cross section area rather than the bond area. When the cross section area is held constant (constant stiffness is equivalent to constant cross section area) as the width ratio increases there is thus no increase in maximum load. This means that when CFRP rupture is the limiting phenomenon no positive effect is obtained from increasing the width ratio. For large width ratios the maximum load ratio increases with increased stiffness while the opposite occurs when the width ratio has a low value. This can be attributed to the fact that when using small width with high value of stiffness a stress concentration occurs at the plate end and debonding occurs earlier. Fig. 8b shows maximum load ratio for high stiffness values. It is interesting to note that an increase in stiffness above K_o will actually give a decrease in maximum load ratio, at least if the width ratio is kept constant. For one data point this conclusion is, however, not valid. K= 2 K_o gives a higher value of α for μ= 1.

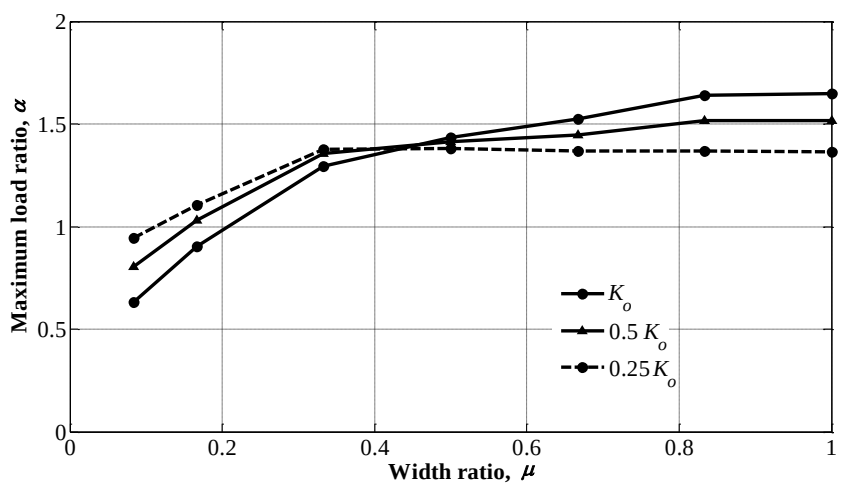

(a) Small stiffness values.

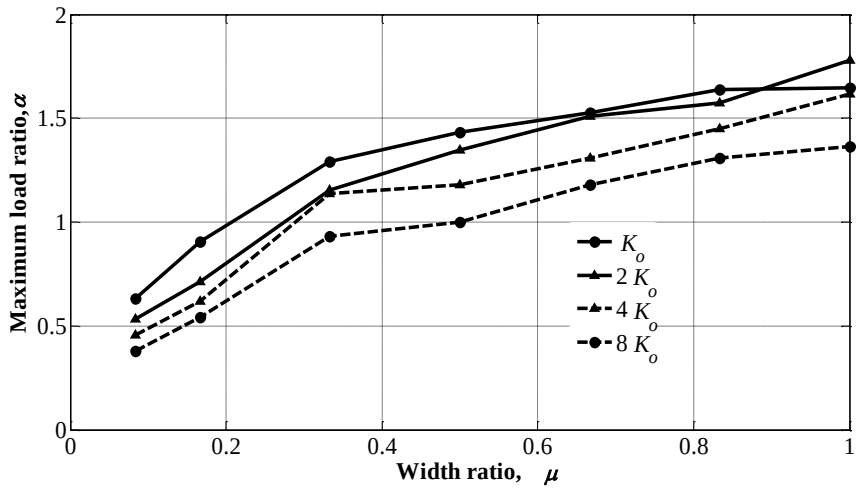

(b) Large stiffness values.

Fig. 8. Maximum load ratio, α, as a function of CFRP stiffness, K, and width ratio, μ.

In Fig. 9, Fig. 10 and Fig. 11, normalised load-deflection curves are shown for different width ratios for K=0.25K_o, K_o and 4K_o respectively. From the figures it can be observed that the load at steel yielding, maximum load and corresponding deflection increase with the width ratio.

A decrease in maximum load compared to the control beam was observed for small width ratio for all stiffness values. This is due to the fact that debonding occurs already at a small load. After debonding, these beams will probably behave like the control beam. Due to numerical instability at the debonding it is however not possible to follow the path towards the control beam curve.

It can be seen from Fig. 9, that when the stiffness, K, is small all beams have almost the same stiffness in the first part and it is close to the control beams. After cracks appear and steel yielding occurs in the control beam this looses in stiffness while the retrofitted beams can take a further load increase.

From Figs. 10 and 11 it can be seen, for the retrofitted beams, all curves are close to identical during the first part and slightly stiffer than the control beam. After the steel yielding and the debonding occur the curves drop and the deviation in stiffness appears.

In Figs. 9, 10, and 11 it can be seen that the width ratio affects the load at steel yielding. In order to clarify that a larger width ratio causes a larger part of the axial load to be carried by the CFRP, the axial stress in the centre of the CFRP along the beam is plotted in Fig. 12, at an external load level of 40 kN for K= 4K_o. From the plate end (right end of figure) the axial stress increases due to stress transfer from the concrete and due to increasing bending moment. In the maximum moment region the increase in stress is less pronounced. The peak stress close to midspan is a stress concentration occurring at the pre-crack.

It is clear from the figure that when the width ratio increases the CFRP axial stress increases. The main reason for this is probably a 3D-effect in the beam width direction. For a small width ratio, see Fig.13a, there is a tendency that the CFRP carries the axial load in the centre part of the beam cross section and the steel carries the axial load in the left and right parts. For a large width ratio on the other hand, see Fig. 13b, there is CFRP directly beneath the steel, and hence the CFRP will take more part in carrying the load. The importance of this effect is related to the position of the steel bars; if the bars are more evenly distributed over the beam width the effect may be less pronounced.

Another reason may be that a larger width ratio implies a wider bond. Even though the CFRP stiffness is constant a larger width ratio implies a wider bond. This means a larger stiffness in the bond which leads to a faster increase in axial stress in the CFRP.

When a larger part of the axial stress is carried by the CFRP, steel yielding will take place at a higher external load level. Since steel yielding is often the initiation of the final fracture process this also means that the beam will be able to carry a larger load.

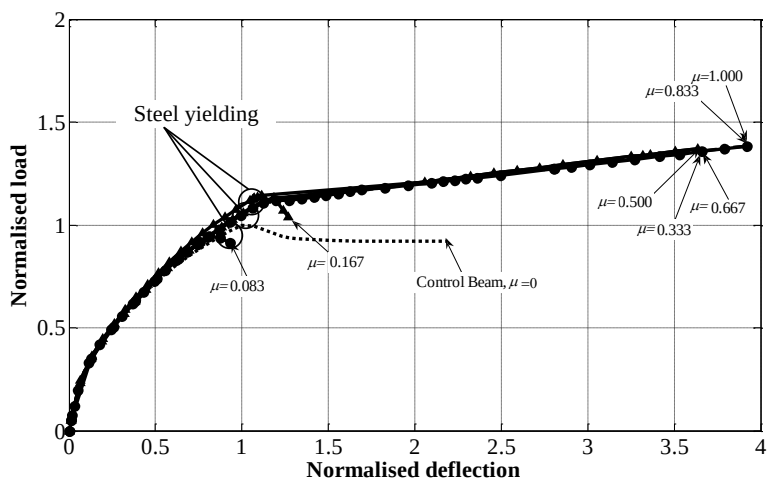

Fig. 9. Normalised load-deflection curves for different width ratios, μ, and constant stiffness, K=0.25K_o.

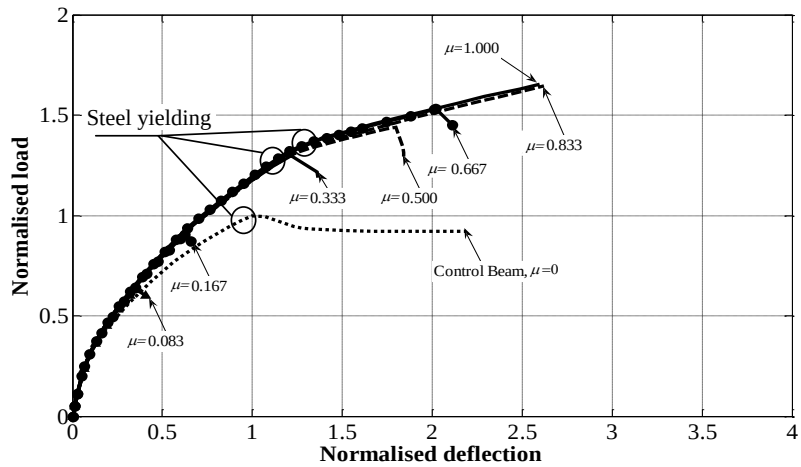

Fig. 10. Normalised load-deflection curves for different width ratios, μ, and constant stiffness, $K=K_o$.

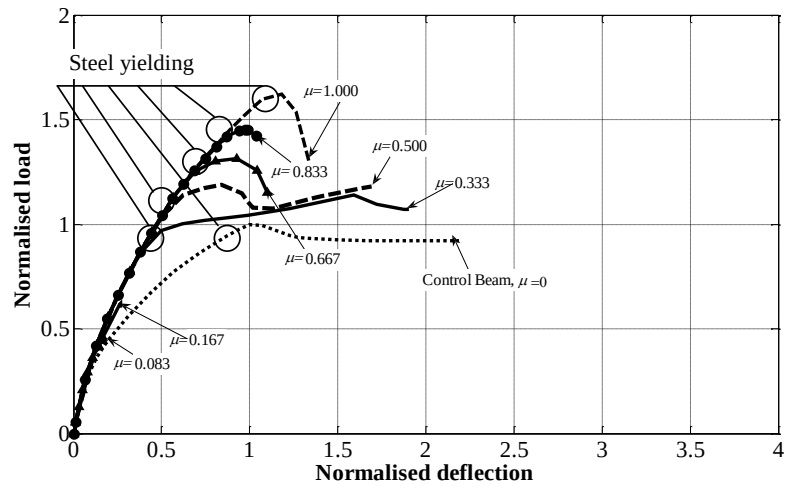

Fig. 11. Normalised load-deflection curves for different width ratios, μ, and constant stiffness, $K=4K_o$.

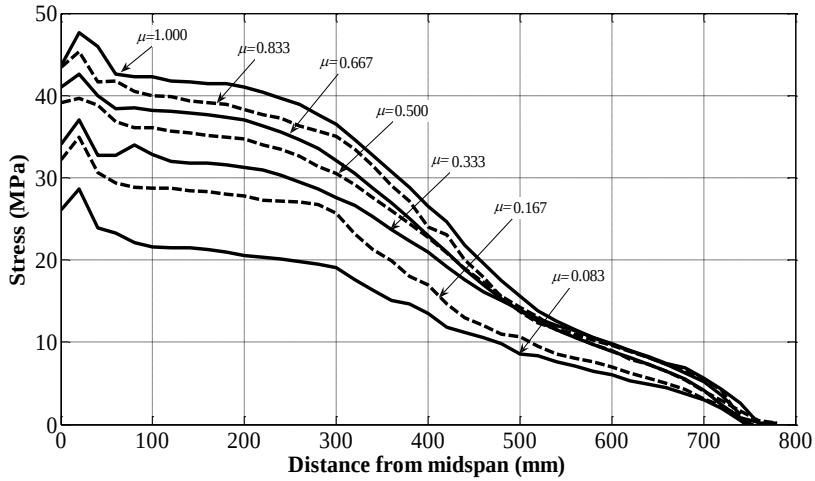

Fig. 12. Axial stress distribution in the CFRP plate at load 40 kN, for $4K_o$.

(a) Small width ratio (b) Large width ratio

Fig. 13. Comparison of geometry for small and large width ratios.

Fig. 14 illustrates the maximum load ratio for different values of stiffness and width ratio. It can be seen that for small width ratio with any value of stiffness, the maximum load ratio is less than 1, implying that a small width ratio will decrease, or at least not increase, the load bearing capacity of the beam. This is due to the debonding of CFRP before steel yielding, as mentioned before. For small stiffness with any value of the width ratio the load increases until a certain value of width ratio is reached, and then there is no further increase in load. This is due to the fact that the failure mode at this value of the width ratio shifts to rupture of CFRP, thus the use of large width ratio with small stiffness does not give any further increase of the maximum load. It is obvious that the medium stiffness with plate width equal to beam width gives maximum of maximum load ratio. The maximum value of α=1.78 was obtained for K=2K_o and μ=1. The cost of CFRP is probably not a critical factor, but it is still interesting that K=0.25K_o and μ=1 gives α=1.38. This means that 12.5% of the amount of reinforcement gives 78% of the maximum load ratio.

It can also be seen that for μ<0.5 the maximum load ratio increases with decreasing stiffness. This is due to the fact that debonding occurs earlier when increasing the stiffness with a small value of μ, then the utilization of CFRP decreases. For $\mu\geq$0.5 the maximum load

ratio increases with stiffness of CFRP, until a certain value of the stiffness, and then it decreases due to the fact that debonding after this value occurs earlier.

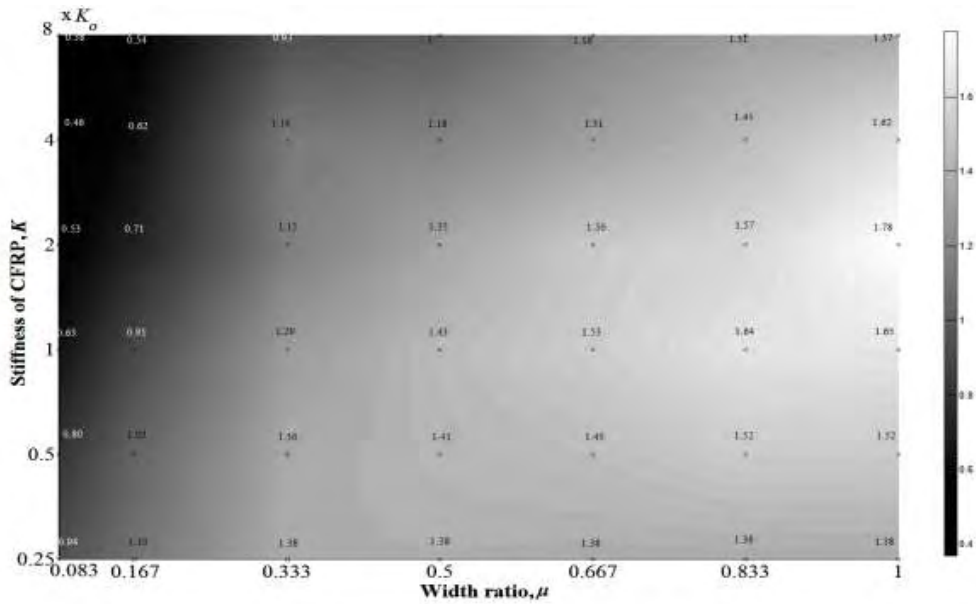

Fig. 14. Maximum load ratio, α, versus the width ratio, μ, and stiffness of CFRP, K. The scale indicates the maximum load ratio.

7.2. Group 2: Effect of varying CFRP width

In group 2 and 3 the starting point is the CFRP geometry used in the experimental study (w_{CFRP}=50 mm, t_{CFRP}=1.2 mm and E_{CFRP}=165 GPa). The results illustrate the effect of changing CFRP width (group2) and changing CFRP thickness (group3).

In group 2 the CFRP width is varied at constant thickness, implying that both the width ratio and stiffness vary, Fig. 6.

The beam stiffness increases with CFRP width. This is caused by the increase in CFRP stiffness, Figs. 9-11. Beams with small CFRP width fail at low load as was previously noted. The maximum load increases with CFRP width. This implies that the effect of increased width ratio (which generally increases the maximum load) is stronger than the effect of increased stiffness (which decreases the maximum load for the values of K and μ used here).

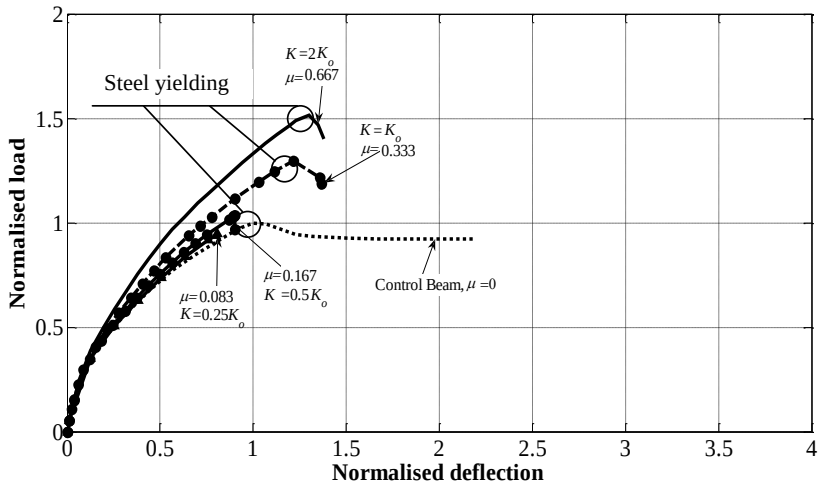

Fig. 15. Normalised load-deflection curves for different width ratios at constant thickness.

7.3. Group 3: Effect of varying CFRP thickness

In group 3 the CFRP thickness is varied at constant width, implying that CFRP stiffness is varied but the width ratio is kept constant.

As shown in Fig. 16, the maximum load ratio increases up to a certain value of the stiffness and then decreases. This is due to the same reasons as mentioned in section 7.1. A higher value of the maximum load ratio is however obtained here compared to Fig. 14, due to a higher resolution in the input values. It is interesting to note that when increasing the amount of external reinforcement by increasing the thickness, the maximum load ratio does not always increase as in the previous section. This means that it is preferable to increase the amount of reinforcement by increasing the width of CFRP rather than increasing the thickness. For example it is better to attach two CFRP plates side by side than on top of each other. As mentioned before, for small thickness (stiffness) the failure mode was CFRP rupture while for large thickness it was debonding. This result supports what Toutanji, et al. (2006) found.

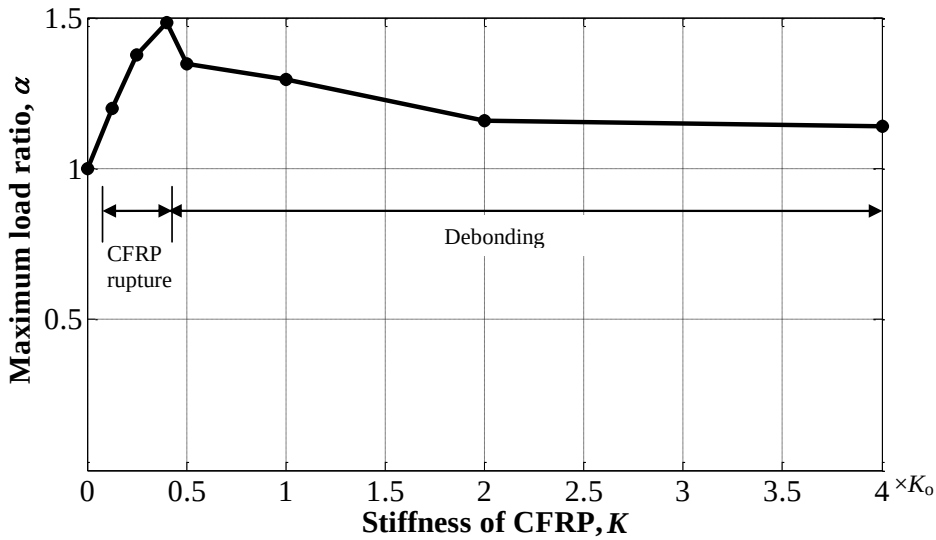

Fig. 16. Maximum load ratio versus stiffness of CFRP at constant width ratio.

8. Conclusion

A finite element model accounting for material non-linearity has been developed and successfully verified against experimental work. A parametric study has been performed to study the effects of stiffness and width of CFRP. The following conclusions are drawn:

- An increase in CFRP stiffness always gives an increase in beam stiffness.
- Different failure modes will occur depending on the values of CFRP stiffness and width ratio. High stiffness and low width ratio will result in debonding failure before steel yielding due to stress concentration at the plate end. This failure occurs at a small load value and should always be avoided.
- When the CFRP stiffness is small, there will be CFRP rupture after steel yielding. In this case, the width ratio will not have an influence on the maximum load. No clear conclusion can be made regarding if a higher maximum load will be obtained or not if the CFRP stiffness is increased to the extent that CFRP rupture will no longer occur. For some width ratios there is an increase in maximum load and for others there is a decrease.
- For medium stiffness and medium to high width ratio, debonding failure will occur after steel yielding. Debonding may initiate at the plate end or at a flexural crack and will in some cases include concrete splitting.
- Maximum load ratio increases with increasing CFRP stiffness until a certain value of the stiffness, thereafter the maximum load ratio decreases with increasing CFRP stiffness. The higher the width ratio, the higher is the optimal CFRP stiffness.

- Except when CFRP rupture is the limiting phenomenon, a higher width ratio will always give a higher maximum load ratio. One reason for this is that a high width ratio will decrease stress concentrations which otherwise may limit the load bearing capacity. Another reason is that a high width ratio will lead to that a larger part of the axial load is carried by the CFRP, which means that steel yielding will occur at a higher external load.
- The best maximum load ratio obtained in this study was 1.78, and it was reached for a CFRP stiffness of $2K_o$ and a width ratio of 1.

9. References

1. Ai-hui, Z., Wei-Liang, J., & Gui-bing, L. (2006), "Behaviour of preloaded RC beams strengthened with CFRP laminates", *Journal of Zhejiang University Science*, 436-444.
2. Ashour, AF., El-Refaie, S.A., and Garrity, SW. (2004), "Flexural strengthening of RC continuous beams using CFRP laminates", *Cement & Concrete Composites*, **26**, 765-775.
3. Esfahani, M., Kianoush, M., & Tajari, A. (2007), "Flexural behaviour of reinforced concrete beams strengthened by CFRP sheets", *Engineering Structures*, **29**, 2428-2444.
4. Pham, H., & Al- Mahaidi, R. (2004), "Experimental investigation into flextural retrofitting of reinforced concrete bridge beams using FRP compoistes", Composite Structures, **66**, 617-625.
5. Camata, G., Spacone, E., & Zarnic, R. (2007), "Experimental and nonlinear finite element studies of RC beams strengthened with FRP plates", Composites: Part B, **38**, 277-288.
6. Coronado, C. A., & Lopez, M. M. (2006), "Sensitivity analysis of reinforced concrete beams strengthened with FRP laminates", *Cement and Concrete Composites*, **28**, 102-114.
7. Ebead, U., & Marzouk, H. (2004), "Tension - stiffening model for FRP strengthend RC concrete two-way slab, *Materials and Structures"*, 193-200.
8. Lundquist, J., Nordin, H., Täljsten, B., & Olafsson, T. (2005), "Numerical analyis of concrete beams sterengthened with CFRP- A Study of anchorage lengths", *In: FRP in Construction, Proceeding of The International Symposium of Bond Behaviour of FRP in Structures*, 247-254.
9. Pannirselvam, N., Raghunath, P., & Suguna, K. (2008), "Strength Modeling of Reinforced Concrete Beam with Externally Bonded Fibre Reinforcement Polymer Reinforcement", *American J. of Engineering and Applied Science*, **1**(3): 192-199.
10. Obaidat,Y., Heyden, S., & Dahlblom, O. (2010), "The Effect of CFRP and CFRP/Concrete Interface Models when Modelling Retrofitted RC Beams with FEM", *Composite Structures*, **92**: 1391–1398.
11. Obaidat,Y. (2007), Retrofitting of reinforced concrete beams using composite laminates, Master Thesis, Jordan University of Science and Technology.

12. Hibbitt, Karlsson, Sorensen, & Inc. (2000), ABAQUS Theory manual, User manual, Example Manual, Version 6.7. Providence, RI.
13. ACI Comitte 318. (1999), Building Code Requirements for Structural Concrete and Commentary (ACI 318-99), American Concrete Institute, Detroit, MI.
14. Beton, C. E.-I. (1993), CEB-FIP Model Code 1990 (CEB-FIP MC90), Bulletin D'Information, No.215, Lausanne.
15. Hillerborg, A. (1985), "The theoretical basis of a method to determine the fracture energy G_f of concrete", *Materials and Structures*, RILEM 50-FMC, **108**, 291-296.
16. Saenz, L. (1964), "Discussion equation for the stress - strain curve of concrete", By Desayi P, Krishnan S, *ACI J*, **61**, 1229–35.
17. Hu H.-T., Schnobrich W.C. (1989), "Constitutive modelling of concrete by using nonassociated plasticity", *J Mater Civil Eng (ASCE)*, **1**(4), 199–216.
18. Camanho, P. P., and C. G. Davila. (2002), "Mixed-Mode Decohesion Finite Elements for the Simulation of Delamination in Composite Materials", *NASA/TM-2002–211737*, 1-37.
19. Lu, X. Z., Ten, J. G., Ye, L. P. and Jaing, J. J. (2005), "Bond-slip models for FRP sheets/plates bonded to concrete", *Engineering Structures*, **24** (5), 920-937.
20. JCI. (1998), Technical report on continous fibre reinforced concrete, JCI TC952 on Continous Reinforced Concrete, 116-124.
21. JCI. (2003), Technical report on retrofit technology for concrete structures, Technical Committee on Retrofitting Technology for Concrete Structures, 79-97.
22. Toutanji, H., Zhao, L., and Zhang, Y. (2006), "Flexural behavior of reinforced concrete beams externally strengthened with CFRP sheets bonded with an inorganic matrix", *Engineering Structures*, **28**, 557-566.

Paper E

E

Bond Action Between FRP and Concrete – A New Model

Yasmeen Taleb Obaidat, Susanne Heyden and Ola Dahlblom

Submitted for publication

Bond Action Between FRP and Concrete – A New Model

Yasmeen Taleb Obaidat*, Susanne Heyden and Ola Dahlblom

Division of Structural Mechanics, Lund University, Lund, Sweden

Abstract:

In this study, based on fitting a non-linear finite element model to experimental results from literature, a new model of the behaviour of the interface between concrete and fibre reinforced polymer (FRP) was proposed. An initial interface stiffness model was proposed based on the adhesive properties, to predict the strain distribution at low load. Comparison between the proposed model, test results and a previous model was performed to demonstrate the accuracy of the proposed model in predicting strain distribution at low load. The proposed model showed better agreement with test results of strain at low load than the previous model. In addition, shear strength and fracture energy models based on tensile strength of concrete and the adhesive shear modulus were proposed. According to the analysis the models provide a good estimation of ultimate load and strain distribution in FRP compared to test results. Finally, bilinear, trilinear and exponential bond-slip curves were compared. The results showed that the bond-slip curve shape has a minor effect on the behaviour of the concrete-FRP specimen.

Keywords*:* Fibre reinforced polymer (FRP); Strengthening; Interfacial stiffness; Concrete; Debonding; Cohesive Model; Fracture energy

1. Introduction

There are many methods for strengthening or rehabilitation of reinforced concrete (RC) structures, such as externally bonded steel plates and fibre reinforced plastic (FRP). FRP have recently found their way into civil engineering infrastructure and are preferred over steel plates mainly due to their high tensile strength, high strength-to-weight ratio and corrosion resistance.

There is, however, a problem of possible premature failures due to debonding of the FRP plates from the concrete. Debonding is a critical problem associated with strengthened structures using FRP and it prevents the full utilization of the FRP. Therefore, issues on how to improve the interfacial load transfer performance and how to improve the strength efficiency of FRP materials are important. The bond between the FRP and concrete plays a significant role in transferring the stress between concrete structures and externally bonded

* Corresponding author.
E-mail address: Yasmeen.Obaidat@construction.lth.se

FRP plates. The properties of this interaction depend on several factors, such as bond strength, interfacial stiffness and fracture energy.

A large amount of bond tests for FRP-concrete interfaces under shear have been carried out in the past decades to determine such properties. As is shown in Fig. 1, test methods used include single lap pullout test Chajes et al. (1996), double lap pullout tests Sato et al. (2001) and bending tests Lorenzis et al. (2001).

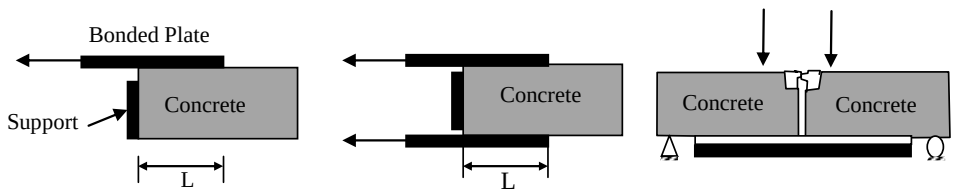

(a) single lap pullout test (b) double lap pullout test (c) bending test

Fig. 1. Type of bond test method.

Analytical and numerical models have also been developed to predict the bond stress-slip response of a concrete-FRP system. However, 3D effects and properties of adhesive effects were not considered properly. Therefore, in this study, a series of experiments from literature were selected and a numerical model was proposed based on the FEM results and experimental results. The proposed model takes into consideration 3D effects and the adhesive properties. The parameters of the model were initial interfacial stiffness, shear strength, fracture energy, and shape of bond-slip curve.

2. Local bond slip model

Numerical modelling using the finite element method is a very powerful tool for performing parameter studies in order to improve understanding of physical phenomena, like for example debonding in FRP reinforced concrete structures. Within this framework the concept of a constitutive model describing the behaviour of a material, at the material point level, is of great importance. This paper focuses on a constitutive model describing the bond between FRP and concrete, often called a local bond slip model.

Constitutive models are determined by means of experimental tests of the material in question. This is a simple enough principle, but difficulties are substantial. The main reason for this is that it is often impossible to obtain a homogeneous stress state in the specimen. Because of this, various indirect methods have been used for constructing local bond slip models.

One approach that has been used Yang et al. (2007) is measuring the strain using closely spaced strain gauges along the FRP in a pullout test. Assuming the elastic properties of the

FRP are known, the shear stress in the bond layer can be obtained by differentiating the axial stress in the FRP. This also relies on the assumption that shear deformation in the FRP is negligible, so that the strain on the surface, which is measured, equals the strain on the side towards the bond. To obtain slip at a local point, the strain along the FRP can be integrated. This is a sound approach, but it suffers from large variability due to the variability in strain along the FRP because of e.g. cracks.

Lu et al. (2005) assumed a local bond slip model determined by a few key parameters and simulated the behaviour of the pullout specimen by FEM. The key parameters were then obtained by fitting the simulation results of strain distribution along the FRP and ultimate load with experimental results. Lu et al. obtained models with a good fit with experimental results. However, the FEM simulations were performed assuming a plane stress state. The stress state in a pullout test is in general not plane stress, and to account for 3D effects, geometry parameters related to the out-of-plane dimension were included in the parameters of the local bond slip model.

One of the fundamental ideas when it comes to finite element analysis is that the effect of the geometry is accounted for by using a mesh that represents the real geometry, and the effect of the material properties is accounted for by using a proper constitutive model. In this way, the behaviour of any geometry can be simulated. That is, the constitutive model does not need to be modified when a different geometry is considered. In this paper, the approach of Lu et al. (2005) is used, but 3D FE simulations are used and the objective is to only include parameters that are related to the bond material in the bond slip model.

A local bond slip curve describes the relation between shear stress and slip at a point in the bond layer. The general shape of a typical bond-slip curve is indicated in Fig. 2. After an ascending part with successively lower stiffness the local shear strength, τ_{max}, is reached at slip s_0. Then there is softening, implying that the curve descends towards zero stress. In this study, three simplified bond-slip curve shapes with different softening behaviour are examined, see Fig. 3. All models have an ascending part defined by initial stiffness, K_0 and local shear strength τ_{max}. The area under the curves corresponds to the fracture energy G_f. In the exponential model, s_f is defined as the slip when the stress reaches $\tau=0.001\tau_{max.}$

The objective of this paper is to find the curve shape and values for K_0, τ_{max} and G_f that give the best fit with experimental results. A number of experimental results of strain distribution in the FRP and ultimate load are compared with the corresponding results from 3D FEM simulations, in order to find the model parameters giving the best fit.

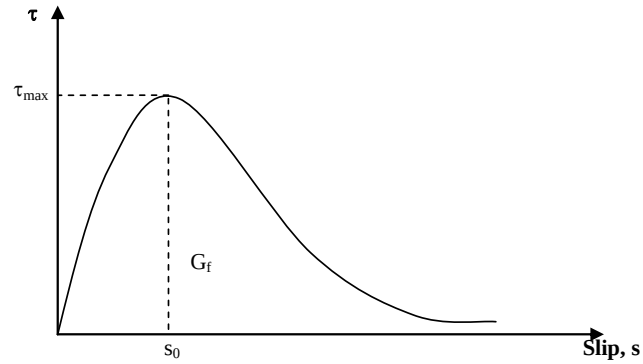

Fig. 2. Typical bond-slip curve shape.

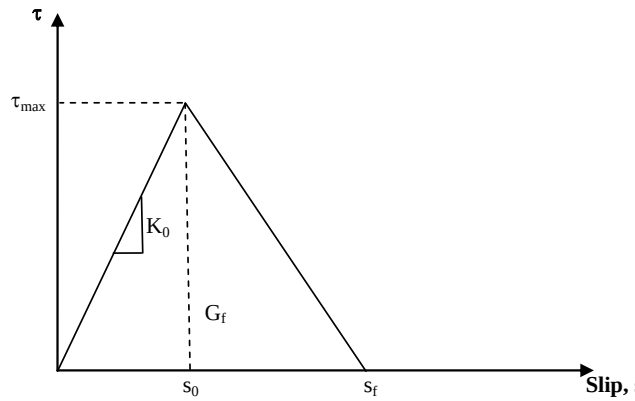

(a) Bilinear model.

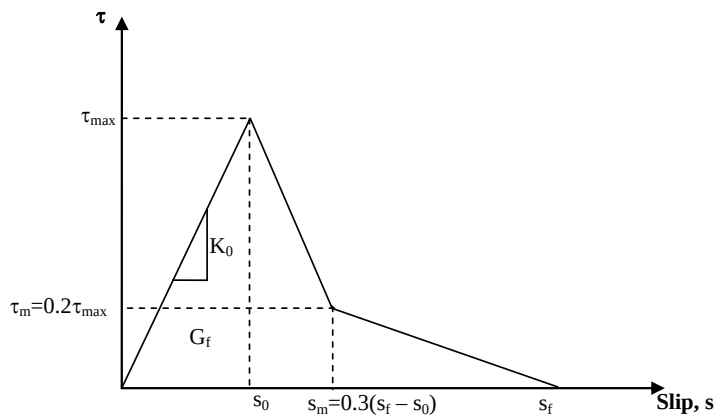

(b) Trilinear model.

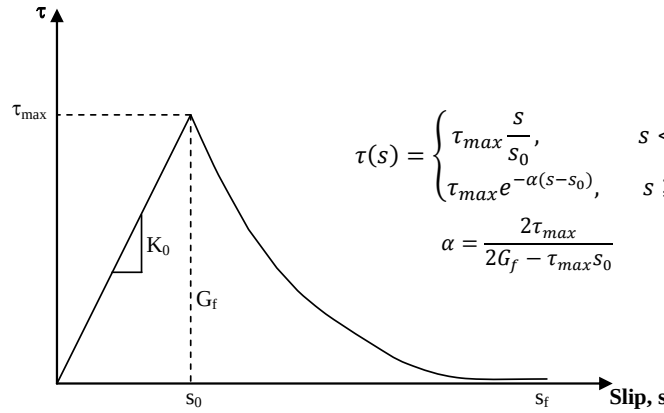

(c) Exponential model.

Fig. 3. Simplified bond-slip curves.

3. Experimental data

Experimental data was obtained from previous research projects by Woo and Lee (2010), Mazzotti et al. (2008), Bizindavyi and Neale (1999), Dai et al. (2005), Pan and Leung (2007), Ming and Ansari (2004), Chajes et al. (1996) and from a literature review by Sharma et al. (2006).

A total of eighteen prisms, strengthened with FRP, were selected for comparison with the numerical results. The prisms were connected to the machine through a steel frame with steel supports in order to prevent vertical and horizontal displacement, see Fig. 4. Strain gauges were mounted on the fibre reinforcement along the bonded length and load and corresponding strain along the FRP was measured. In most of the tests, the single lap pullout test method was used. In some specimens, Fig. 4b, the FRP was not bonded to the concrete close to the edge. This was to avoid early failure due to concrete splitting caused by high transversal tensile stresses. In Ming et al. (2004), the double lap pull out test was used as shown in Fig. 4d. Geometry data and material properties of the specimens are presented in Table 1 and Table 2.

Table 1. Geometry, type of FRP of specimens and maximum load.

Series Specimens	Concrete				FRP				Max. Load (kN)
	b_c (mm)	h (mm)	L_c (mm)	h_c (mm)	b_f (mm)	t_f (mm)	L_f (mm)	Type	
Series A, Woo and Lee (2010)									
A1	**200**	**200**	**500**	180	**50**	**1.4**	**250**	**CFRP**	**26**
Series B, Mazzotti et al. (2008)									
B1	**150**	**200**	**600**	**140**	**50**	**1.2**	**100**	**CFRP**	**22.3**
B2	**150**	**200**	**600**	**140**	**50**	**1.2**	**200**	**CFRP**	**19.8**
B3	**150**	**200**	**600**	**140**	**50**	**1.2**	**400**	**CFRP**	**23**
B4	**150**	**200**	**600**	**140**	**80**	**1.2**	**100**	**CFRP**	**30.5**
B5	**150**	**200**	**600**	**140**	**80**	**1.2**	**200**	**CFRP**	**33**
B6	**150**	**200**	**600**	**140**	**80**	**1.2**	**400**	**CFRP**	**37**
Series C, Bizindavyi and Neale (1999)									
C1	**150**	**150**	**400**	130	**25.4**	**1**	**180**	**GFRP**	**11.4**
C2	**150**	**150**	**400**	130	**25.4**	**0.33**	**160**	**CFRP**	**8**
Series D, Dai et al. (2005)									
D1	**400**	**200**	**400**	180	**100**	**0.11**	**330**	**CFRP**	**23.4**
Series E. Pan and Leung (2007)									
E1	**100**	**100**	**500**	80	**50**	**0.11**	**300**	**CFRP**	**11.7**
Series F, Ming and Ansari (2004)									
F1	**400**	**150**	**200**	130	**80**	**1**	**80**	**CFRP**	**18.59**
Series G, Chajes et al. (1996)									
G1	**228.6**	**152.4**	**152.4**	130	**25.4**	**1**	**50.8**	**CFRP**	**8**
G2	**152.4**	**152.4**	**228.6**	130	**25.4**	**1**	**152.4**	**CFRP**	**12**
G3	**152.4**	**152.4**	**228.6**	130	**25.4**	**1**	**203.2**	**CFRP**	**11.6**
Series H, Sharma et al. (2006)									
H1	**100**	**100**	**500**	80	**30**	**4**	**100**	**GFRP**	**11.75**

* The data not in bold was assumed.

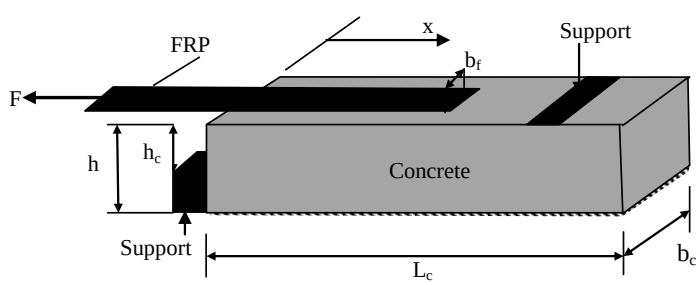

(a) Woo and Lee (2010).

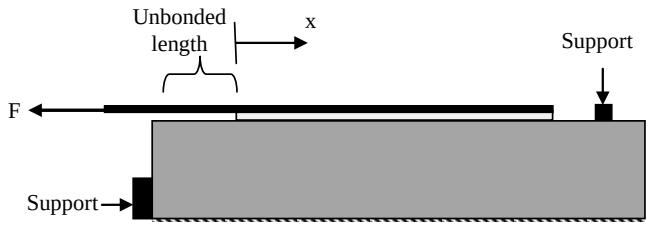

(b) Mazzotti et al. (2008), Bizindavyi and Neale (1999) and Pan and Leung (2007).

(c) Dai et al. (2005), Chajes et al. (1996) and Sharma et al. (2006).

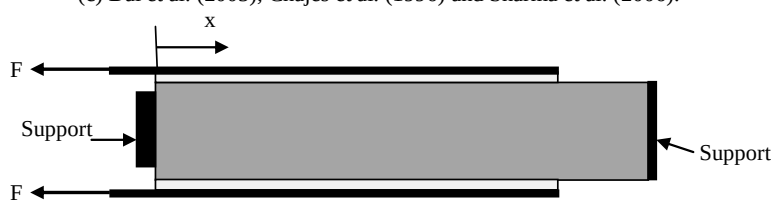

(d) Ming and Ansari (2004).

Fig. 4. Test setup.

Table 2. Mechanical properties of materials used.

Material		**Series A**	**Series B**	**Series C**	**Series D**	**Series E**	**Series F**	**Series G**	**Series H**
Concrete	Compressive strength, f'_c (MPa)	**30**	**52.6**	**42.5**	**35**	**44.7**	**38.8**	**36.43**	**35.82**
	Tensile strength, f_{ct} (MPa)	1.81	**3.81**	**3.5**	1.95	**3.26**	**3.73**	2	**3.08**
	Elastic modulus, E_c (GPa)	26	**30.7**	**33.5**	28	31.4	**33.73**	28	**35.3**
	Fracture energy, G_{cr} (J/m^2)	65	96	83	72	86	78	74	73
CFRP	Elastic modulus, E_f (GPa)	**152.2**	**195.2**	**75.7**	**230**	**235**	**73.1**	**108.45**	-
	Tensile strength, f_f (GPa)	**2.85**	-	**1.014**	**3.55**	-	**0.96**	-	-
GFRP	Elastic modulus, E_f (GPa)	-	-	**29.2**	-	-	-	-	**32.7**
	Tensile strength, f_f (GPa)	-	-	**4.72**	-	-	-	-	-
Adhesive	Elastic modulus, E_a (GPa)	**18**[1]	**12.84**	-	**2.45**	**3.3**	**2**	**1.584**	**18**[1]
	Tensile strength, f_a (MPa)	-	**30.2**	-	**48.1**	-	**30**	-	**17.8**
	Shear modulus, G_a (GPa)	6.52	4.65	**1.18**	0.89	1.2	0.72	0.57	6.52
	Poisson's ratio, ν_a	0.38[2]	0.38[2]	**0.4**	**0.38**	0.38[2]	0.38[2]	0.38[2]	0.38[2]
	Thickness, t_a (mm)	1	**1.5**	**1**	1	1	1	1	1

The values in bold are given in references. Values not in bold were calculated according to the equations in section 4.1. Poisson ratio for concrete and CFRP was assumed to be 0.2 and 0.3, respectively.

1 This value was obtained from the manufacturer based on data given in the references.

2 Assumed values.

4. Finite element analysis

Finite element failure analysis was performed to model the nonlinear behaviour of the specimens. The FEM package Abaqus/standard, Hibbitt et al. (2000), was used for the analysis.

4.1. Material properties and constitutive models

4.1.1 Concrete

A plastic-damage model was used in order to predict the constitutive behaviour of concrete. In this approach, it is assumed that compressive crushing and tensile cracking are the main failure mechanisms of concrete. When not given in the cited papers, the concrete tensile strength, f_{ct}, elastic modulus, E_c, and fracture energy, G_{cr}, were estimated from Eq. (1), Eq. (2), ACI 318-99, and Eq. (3), Beton (1993).

$$f_{ct} = 0.33\sqrt{f_c'} \tag{1}$$

$$E_c = 4700\sqrt{f_c'} \tag{2}$$

$$G_{cr} = G_{fo}\left(\frac{f_c'}{10}\right)^{0.7} \tag{3}$$

where f_c' is the concrete compressive strength given in MPa. G_{fo} is a constant value related to maximum aggregate size, Beton (1993). The maximum aggregate size was assumed to be 20 mm.

The concrete softening curve under uniaxial tension is shown in Fig. 5. The tensile damage is specified by an assumed linear relationship between a tension damage variable d_t and the crack opening δ. The damage variable can take values from zero, representing the undamaged material, to one, which represents total loss of strength.

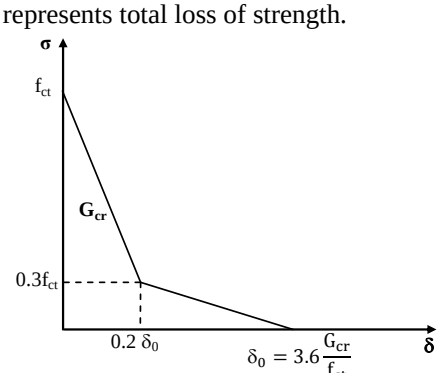

Fig. 5. Softening curve of concrete under uni-axial tension.

Under uni-axial compression the response is linear until the value of initial yield, σ_{c0}. In the plastic regime the response is typically characterized by stress hardening followed by

strain softening beyond the ultimate strain. The stress–strain relationship proposed by Saenz (1964) was used to construct the uni-axial compressive stress–strain curve for concrete:

$$\sigma_c = \frac{E_c \varepsilon_c}{1+(R+R_E-2)\left(\frac{\varepsilon_c}{\varepsilon_0}\right)-(2R-1)\left(\frac{\varepsilon_c}{\varepsilon_0}\right)^2+R\left(\frac{\varepsilon_c}{\varepsilon_0}\right)^3} \quad (4)$$

Where:

$R = \frac{R_E(R_\sigma-1)}{(R_\varepsilon-1)^2} - \frac{1}{R_\varepsilon}, \quad R_E = \frac{E_c}{E_0}, \quad E_0 = \frac{f_c'}{\varepsilon_0}$

and,

R_ε =4, R_σ = 4 as reported in Hu and Schnobrich (1989) and ε_0 = 0.0025.

4.1.2 FRP

The behaviour of the FRP plates is assumed linear elastic isotropic. The elastic modulus in the fibre direction of the unidirectional FRP material used in the numerical study was the values from the experimental studies, see Table 2. Since neither the tensile strength nor the strain were available for some experiments, the failure of FRP was not possible to consider in this study.

4.1.3. FRP – concrete interface

The interface was modelled using a cohesive zone model; see Obaidat et al. (2010). To investigate the influence of the shape of the local bond slip curve three models were used. Fig.3 shows the different traction-separation laws written in terms of the effective traction τ and slips.

The initiation of damage was assumed to occur when a quadratic traction function involving the nominal stress ratios reached the value one. This criterion can be represented by, Hibbitt et al. (2000):

$$\left\{\frac{\sigma_n}{\sigma_n^0}\right\}^2 + \left\{\frac{\tau_s}{\tau_s^0}\right\}^2 + \left\{\frac{\tau_t}{\tau_t^0}\right\}^2 = 1 \quad (5)$$

where σ_n is the cohesive tensile stress and τ_s and τ_t are the shear stresses of the interface. The values used for this study were $\sigma_n^0 = f_{ct}$, and $\tau_s^0 = \tau_t^0 = \tau_{max}$, Fig. 3.

4.2 Finite element mesh and computation procedure

8-node brick elements were used for the reinforced concrete and FRP in this model; see Fig. 6. 3-D 8-node cohesive elements were used to model the interface layer. The cohesive interface elements are composed of two surfaces separated by a thickness. The relative motion of the bottom and top parts of the cohesive element measured along the thickness direction represents opening or closing of the interface. The in-plane relative motion of these parts represents the transverse shear behaviour of the cohesive element.

In this study the total deflection applied was divided into a series of deflection increments. Newton method iterations provide convergence, within tolerance limits, at the end of each deflection increment. During the ultimate stage where a large number of cracks occur, the deflections are applied with gradually smaller increments. Automatic stabilization and small time increment were also used to avoid a diverged solution.

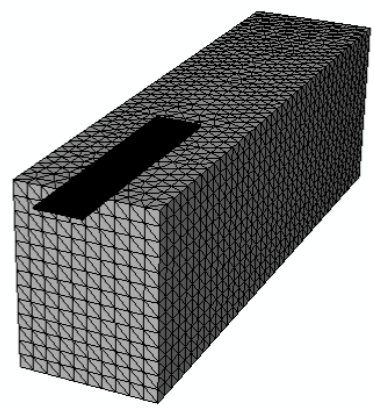

Fig. 6. Finite element mesh of specimen, B-B1.

5. Result

Simulations were performed and the results were compared with experimental results in order to find the curve shape and values of initial stiffness, K_0, shear strength, $\tau_{max,}$ and fracture energy, G_f, that give the best fit.

At low load the strain distribution in the FRP is mainly governed by the initial stiffness, K_0, of the interface. Because of this it is considered suitable to start with evaluating initial stiffness, and the experimental results for a load of 0.2 maximum load, F_{max}, were used for this purpose.

The shear strength, τ_{max}, and fracture energy, G_f, together determine the fracture behaviour. These were thus varied together to obtain the combination of τ_{max} and G_f that gives the best fit for maximum load and strain distribution at maximum load.

Preliminary results showed that the curve shape was of minor influence. This was verified by finally examining the results obtained using different curve shapes.

5.1 Interfacial initial stiffness

Experimental results for a load of 0.2 maximum load, F_{max}, were used for evaluating interfacial initial stiffness. At this stage the materials are essentially in an elastic state, but still in the numerical simulation, there may be some fracture initiation locally. Because of this the complete bond-slip behaviour of the interface needs to be defined. For this purpose the bilinear model was used to represent the bond behaviour. The maximum shear stress, τ_{max}, was at this stage obtained from Eq. (10), Lu et al. (2005), and the value of fracture energy, G_f, was obtained from Eq. (11), Lu et al. (2005).

5.1.1 Effect of interfacial initial stiffness

Fig. 7 shows the strain along the FRP plate for various values of K_0 at load corresponding to 0.2 F_{max} for three of the simulated specimens. At this load debonding has not been initiated and therefore the initial interfacial stiffness is believed to govern the strain distribution. A low value of interfacial stiffness results in a low rate of stress transfer to the concrete. This means that the stress transfer length will increase with a decrease in stiffness, which can be clearly seen in e.g. Fig. 7b. A high rate of stress transfer corresponds to high shear stress in the interface. This means that a high initial stiffness will cause a shear stress concentration in the interface, which will increase the risk of debonding.

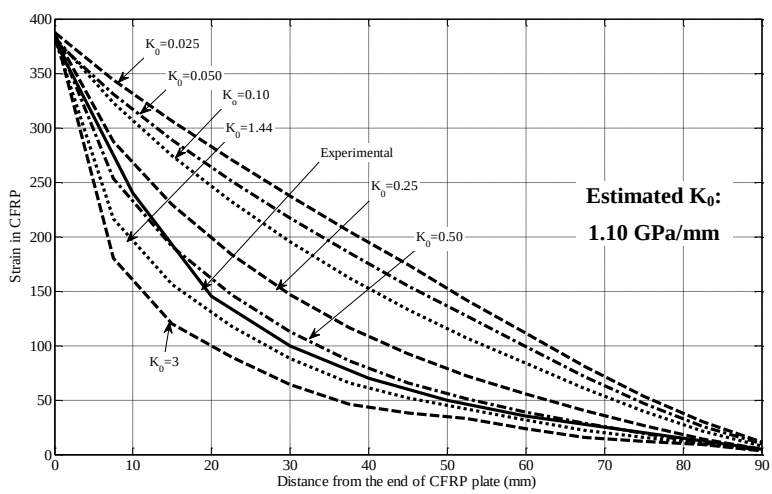

(a) Series B-B1.

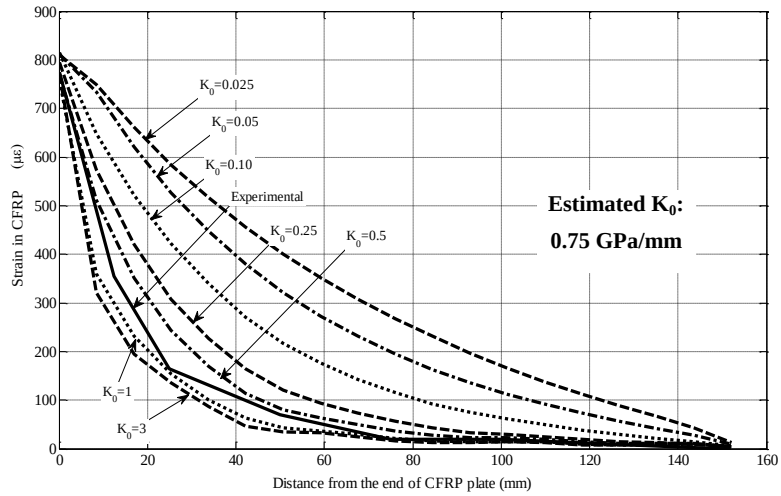

(b) Series G-G2.

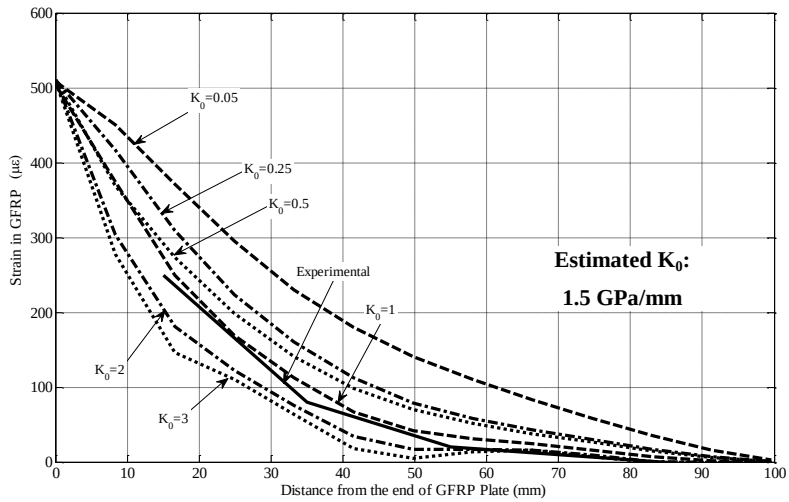

(c) Series H.

Fig. 7. Strain distribution in FRP reinforcement for various values of interfacial stiffness, K_0, at load $0.2F_{max}$.

5.1.2 Proposed model

The present work covers a wide range of adhesives in concrete FRP systems and aims at proposing an equation for K_0 that is related only to the properties of the adhesive. Essentially the shear stiffness of the bond should be related to G_a/t_a where G_a is the shear modulus of the bond material and t_a is the thickness of the bond layer.

Simulations were performed for different values of interfacial initial stiffness. The obtained strain distributions in the FRP for various values of K_0 were compared with strain

distributions from the cited studies, see Fig. 7. For each specimen, the K_0 corresponding best to the experimental result was estimated. The estimated value of K_0 is shown in bold in the diagrams.

The relationship between estimated values of K_0 and G_a/t_a for each specimen is shown in Fig. 8. This figure shows that the interfacial initial stiffness increases almost linearly with G_a/t_a. Based on this observation the relation

$$K_0 = 0.16\frac{G_a}{t_a} + 0.47 \tag{6}$$

is proposed, where t_a is adhesive thickness (mm) and G_a is shear modulus of adhesive (GPa).

A correlation coefficient, R^2, of 0.915 was obtained for this equation.

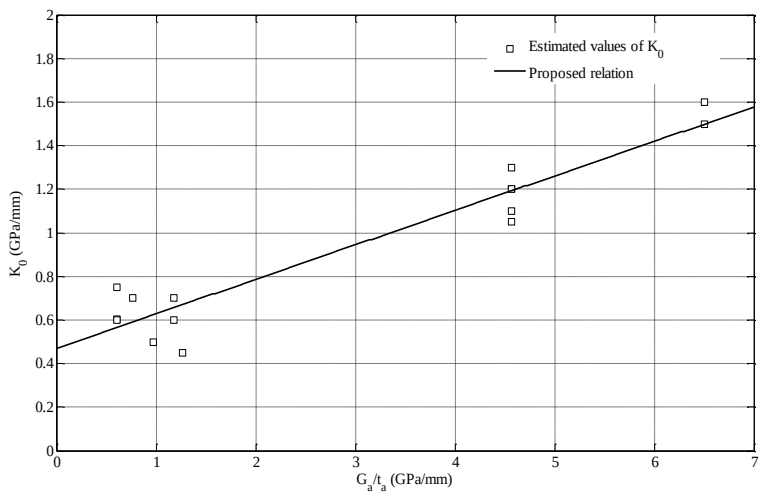

Fig. 8. Relation between estimated value of K_0 and G_a/t_a.

5.1.3 Comparison with Lu et al. Lu et al. (2005) model

Lu et al. (2005) proposed three different variants of a bond slip model. The "Precise model" is the more complicated model and has a shape similar to Fig 2 with a non-linear ascending shape. The initial stiffness was assumed to be related to the properties of the adhesive in contact with the concrete as well as the initial layer of the concrete substrate, see Eq. (7).

$$K_0 = \frac{1}{\frac{t_a}{G_a} + \frac{t_c}{G_c}} \tag{7}$$

where t_a is the adhesive thickness, t_c is a representative concrete thickness, and G_a and G_c are the shear modulus of adhesive and concrete respectively.

The "simplified model" is similar to the precise model, but the initial stiffness is approximated as infinity.

The "bilinear model" of Lu is a further simplification with a shape like the bilinear model in Fig. 3. That is, in this model, the stiffness is constant until τ_{max} is reached, like in the models proposed in this paper. The initial stiffness was assumed to be

$$K_0 = \frac{\tau_{max}}{s_0} = \frac{1.5\beta_w f_{ct}}{0.0195\beta_w f_{ct}} = 0.077 \text{ GPa/mm} \quad (8)$$

The stiffness is thus constant and not related to any material or geometrical parameters.

Lu et al. (2005) obtained good fit with experimental results by using their models. The results were also similar for the three models, even though the precise model performed slightly better. The results were also close for strain distribution at low load, even though the initial stiffnesses differ between the models.

From a principal point of view it is however not desirable to involve the properties of concrete in a constitutive model describing the initial stiffness of the bond, and the same applies to not involving the properties of the adhesive at all.

A comparison was made between the proposed model, Eq. (6), and the bilinear model of Lu et al. The bilinear model was chosen because it has a shape similar to the model used in this paper and it gave results close to the more complicated models of Lu et al. Strain distributions obtained by using K_0 according to Lu et al, Eq. (8), the proposed relation, Eq. (6) as well as simply G_a/t_a are shown in Fig. 9. A value of K_0 according to Eq. (6) gives a strain distribution with closer agreement with the experimental results than the other models. G_a/t_a seems to give too high stiffness value, especially for the experimental values with a relatively high interfacial stiffness, e.g. B1 and H. Eq. (8) gives a clearly low value of the stiffness, which is not surprising considering the low value of Eq.(8). The models by Lu et al. with decreasing stiffness in the ascending part of the curve would probably give a result slightly closer to the experimental even though they were shown to give almost the same strain distribution also at low load in Lu et al. (2005). Thus, the new model Eq. (6), which is related to the properties of the bond, performs better than the other models.

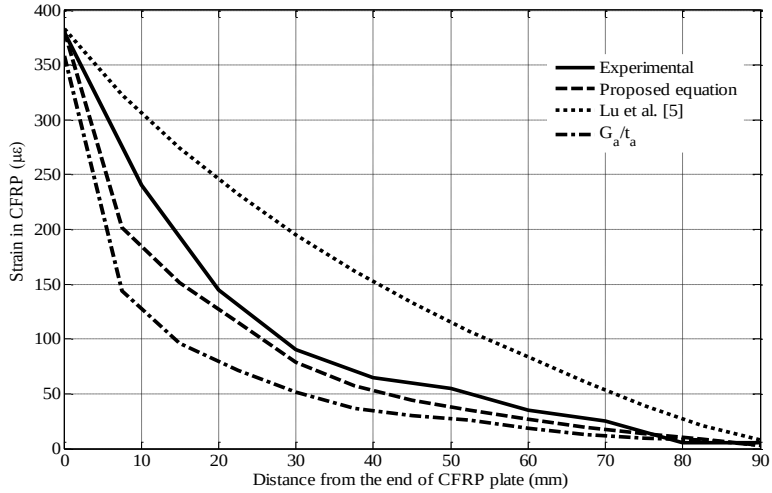

(a) Series B-B1.

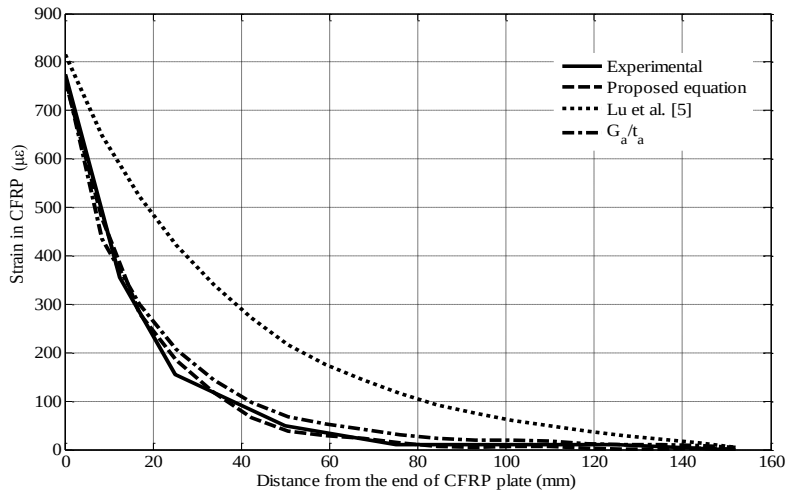

(b) Series G-G2.

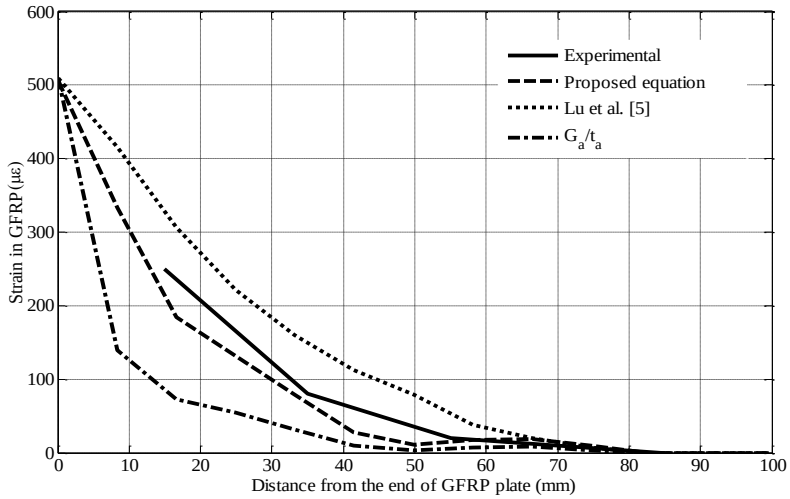

(c) Series H.

Fig. 9. Comparison between proposed equation and other equations.

5.2 Interfacial Fracture Energy and shear strength:

Simulations were also performed to evaluate the influence of fracture energy and shear strength since the effectiveness of a retrofitted structure is highly dependent on these parameters. Simulations were performed for different combinations of shear strength and fracture energy values, with interfacial initial stiffness calculated using Eq. (6). The value combinations used are shown in Fig. 10.

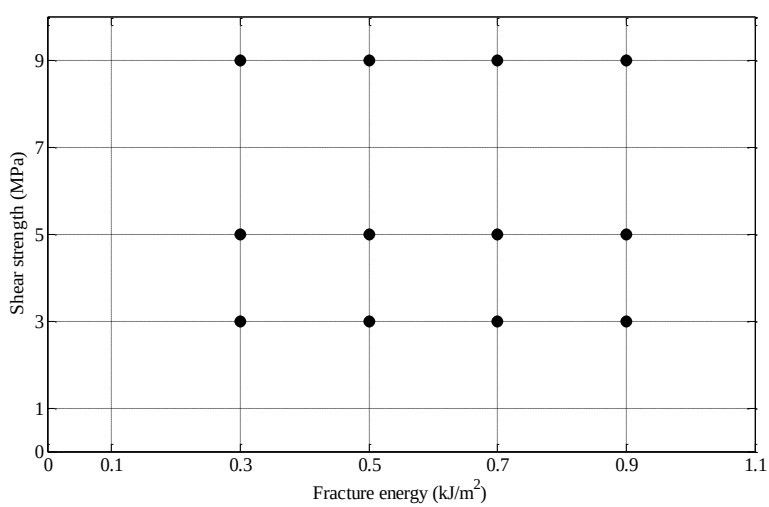

Fig. 10. Values for shear strength and fracture energy used in the parametric study. Dots indicate simulations.

5.2.1 Proposed model

It is desirable to involve the effect of adhesive properties in the model describing the bond between FRP and concrete. On the other hand, the local bond–slip relation should be independent of geometric conditions. Therefore the objective of this study is to find relations between G_f and τ_{max} and the properties of concrete and adhesive, without including any geometry parameters.

The obtained load versus slip relation and strain distribution in the FRP at maximum load for various combinations of fracture energy and shear strength was compared with experimental data from the cited studies; see Fig. 11 and Fig. 12. The experimental value of maximum load is indicated by a horizontal line. For each specimen, the fracture energy and shear strength combinations giving the closest fit with the experimental results for maximum load and strain distribution were chosen. The combinations chosen are shown in bold in the diagrams. In this step different combinations were found. Thereafter these combinations were drawn as shown in Fig.13 and the intersection was taken as the values that give fit with maximum load and strain distribution curves at the same time. In some specimens, e.g. B1, there were no intersections. In these cases, the average between the two closest values was taken.

Some remarks can be drawn concerning results in Fig. 12. For some specimens as in B1, FRP strains show the decay of curve starting near to the loaded section at x = 0, whereas they are almost constant close to loaded end, for other specimens. This is can be attributed to the fact of onset of debonding phenomenon. For the specimen B1, decay profile of strains along the anchorage is almost linear. These profiles indicate a more uniform distribution of shear stresses along the anchorage. This is probably due to the fact that the bond length of this specimen is less than the anchorage length. Since the debonding phenomenon depends on the length of FRP and these specimens have different length, it is expected to have different curve shape.

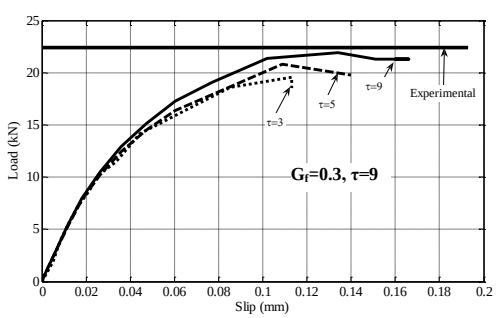

a) G_f= 0.3 kJ/m^2, K_0=0.97 GPa/mm.

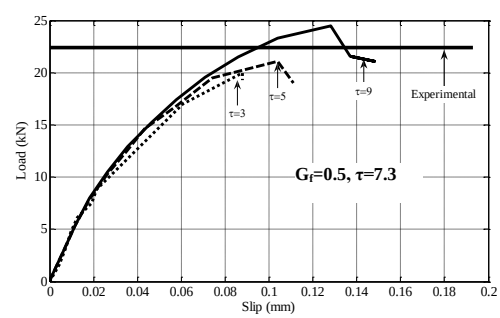

b) G_f= 0.5 kJ/m^2, K_0=0.97 GPa/mm.

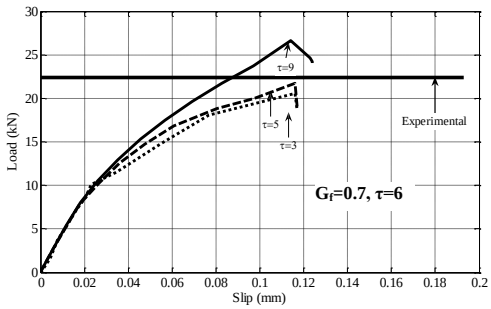

c) G_f= 0.7 kJ/m^2, K_0=0.97 GPa/mm.

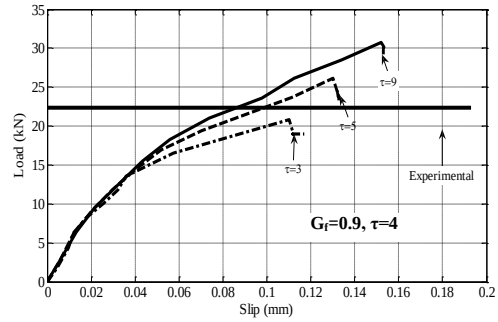

d) G_f= 0.9 kJ/m^2, K_0=0.97 GPa/mm.

(a) Series B-B1.

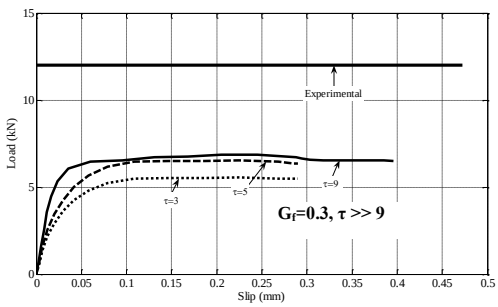

a) G_f= 0.3 kJ/m^2, K_0=0.57 GPa/mm.

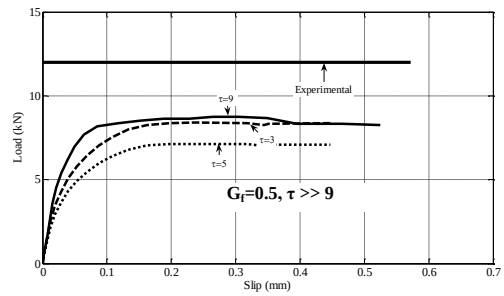

b) G_f= 0.5 kJ/m^2, K_0=0.57 GPa/mm.

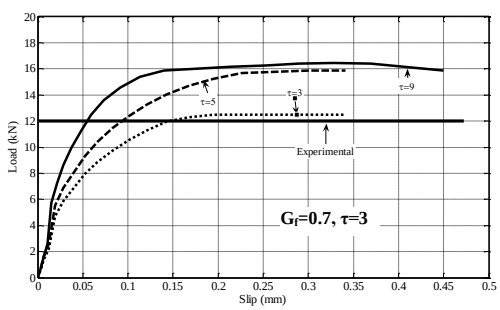

c) G_f= 0.7 kJ/m^2, K_0=0.57 GPa/mm.

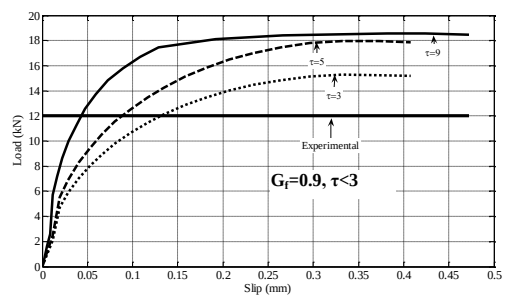

d) G_f= 0.9 kJ/m^2, K_0=0.57 GPa/mm.

(b) Series G-G2.

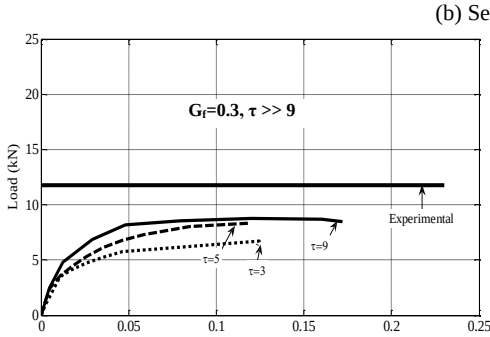

a) G_f= 0.3 kJ/m^2, K_0=1.5 GPa/mm.

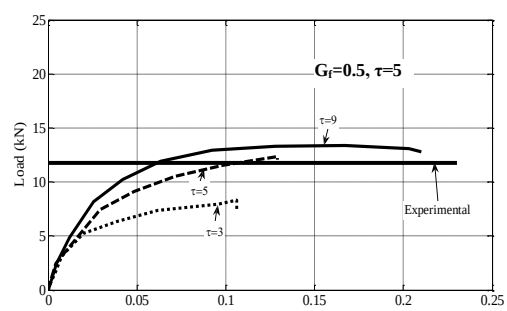

b) G_f= 0.5 kJ/m^2, K_o=1.5 GPa/mm.

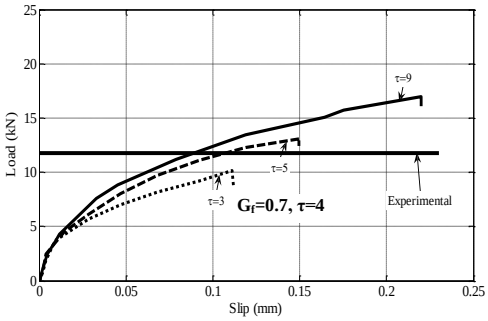

c) G_f= 0.7 kJ/m^2, K_0=1.5 GPa/mm.

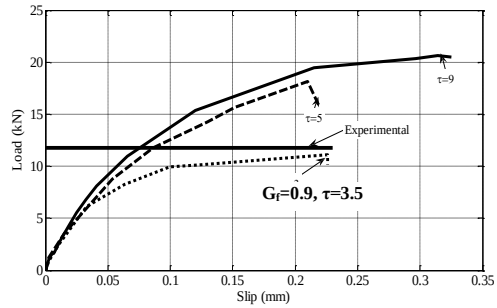

d) G_f= 0.9 kJ/m^2, K_0=1.5 GPa/mm.

(c) Series H.

Fig. 11. Load versus horizontal displacement in FRP for different values of fracture energy and shear strength.

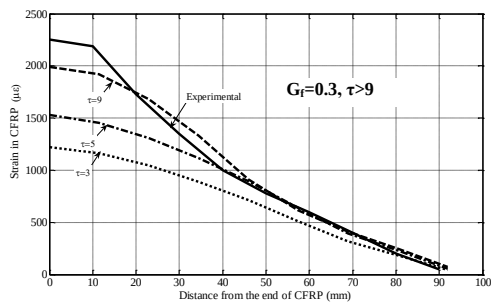

a) G_f= 0.3 kJ/m^2, K_0=0.97 GPa/mm.

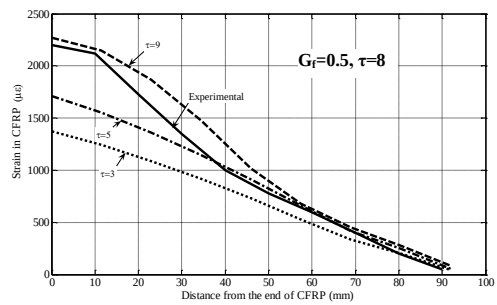

b) G_f= 0.5 kJ/m^2, K_0=0.97 GPa/mm.

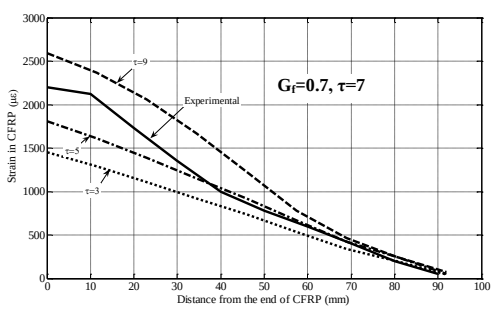

c) G_f= 0.7 kJ/m^2, K_0=0.97 GPa/mm.

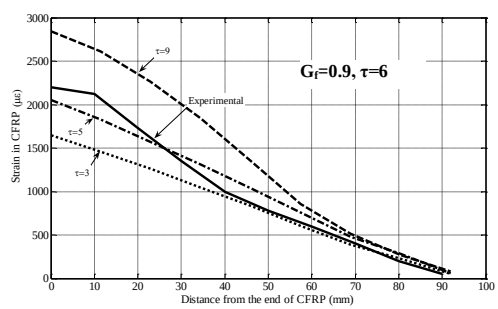

d) G_f= 0.9 kJ/m^2, K_0=0.97 GPa/mm.

(a) Series B-B1.

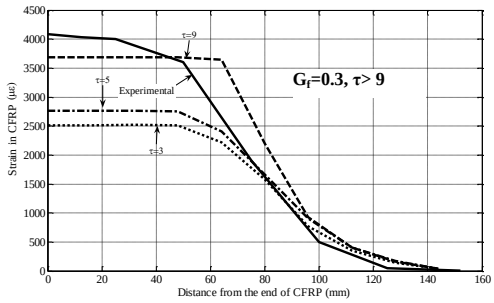

a) G_f= 0.3 kJ/m^2, K_0=0.57 GPa/mm.

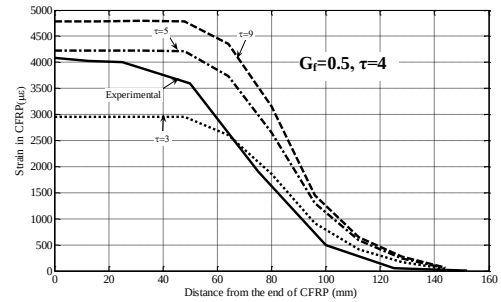

b) G_f= 0.5 kJ/m^2, K_0=0.57 GPa/mm.

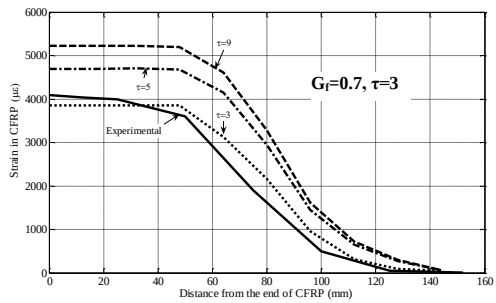

c) G_f= 0.7 kJ/m^2, K_0=0.57 GPa/mm.

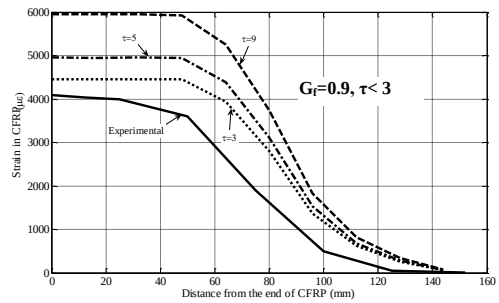

d) G_f= 0.9 kJ/m^2, K_0=0.57 GPa/mm.

(b) Series G-G2.

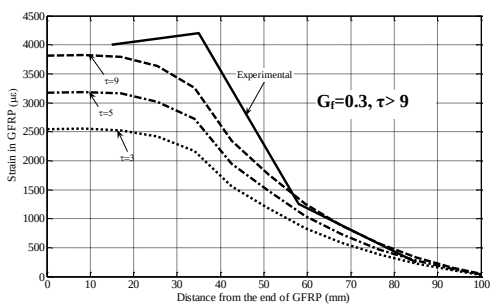

a) G_f= 0.3 kJ/m^2, K_0=1.5 GPa/mm.

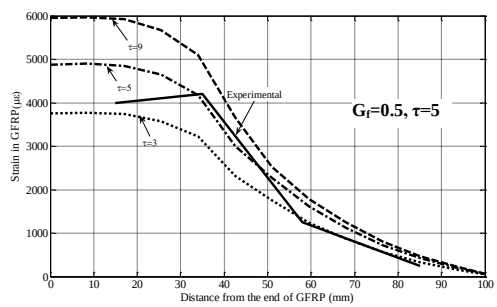

b) G_f= 0.5 kJ/m^2, K_0=1.5 GPa/mm.

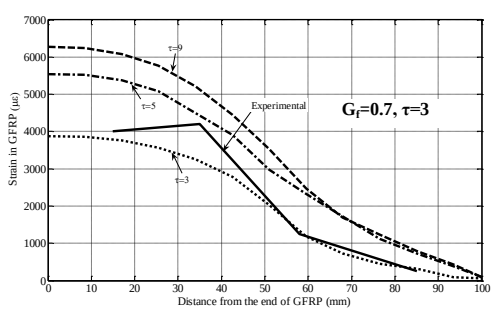

c) G_f= 0.7 kJ/m^2, K_0=1.5 GPa/mm.

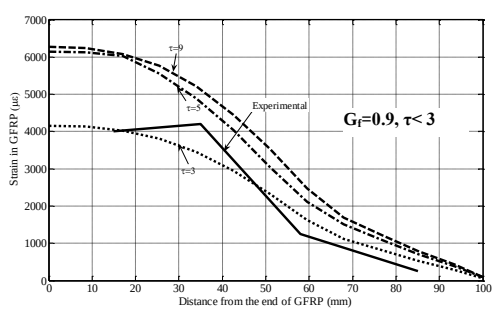

d) G_f= 0.9 kJ/m^2, K_0=1.5 GPa/mm.

(b) Series H.

Fig. 12. The strain distribution in FRP versus fracture energy and shear stress.

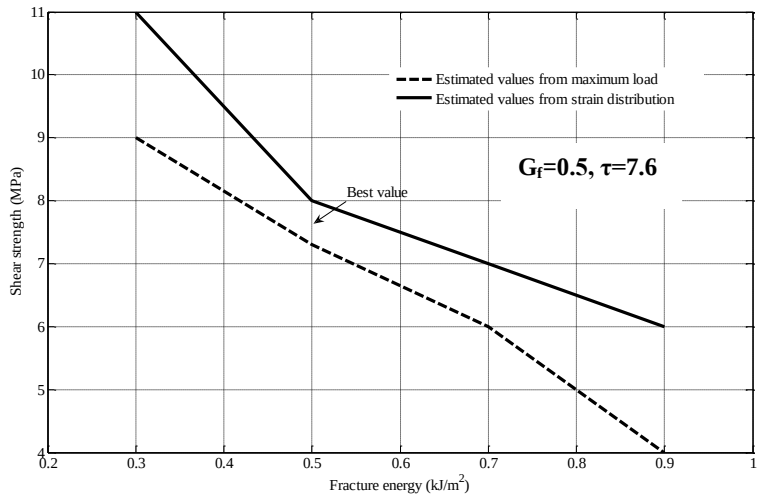

(a) Series B-B1.

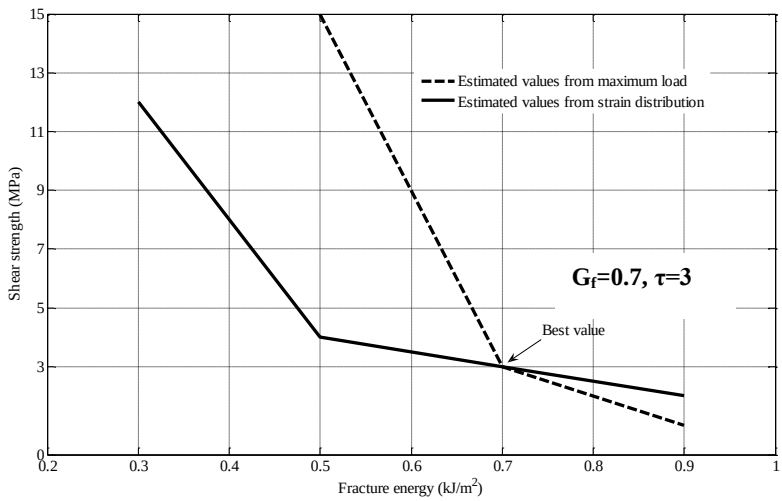

(b) Series G-G2.

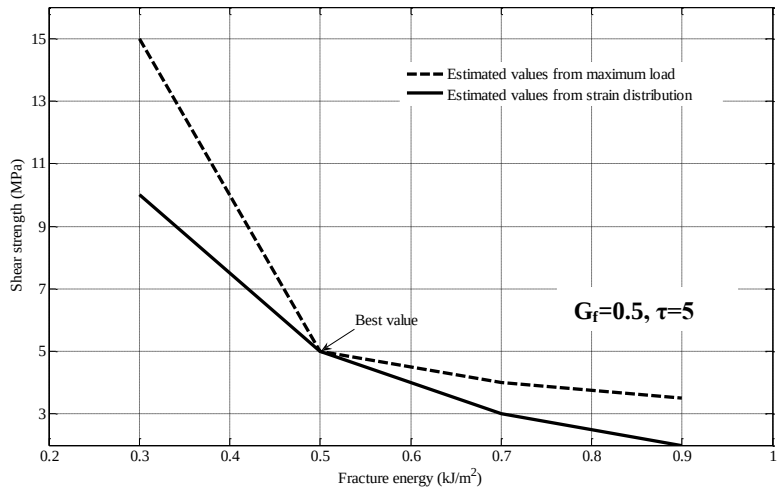

(c) Series H.

Fig. 13. The estimated values for shear strength and fracture energy.

The equations for fracture energy and maximum shear strength were proposed as follows:

$$G_f = a_1 {G_a}^{a_2} {f_{ct}}^{a_3} \tag{9}$$

$$\tau_{max} = b_1 {G_a}^{b_2} {f_{ct}}^{b_3} \tag{10}$$

where G_a is the shear modulus of the adhesive (GPa) and f_{ct} is the tensile strength of concrete (MPa).

To determine a_1- a_3, and b_1- b_3 in these equations multiple regression was used. To perform this, Eq (9) was rewritten in a linear form, as:

$$\ln G_f = \ln a_1 + a_2 \ln G_a + a_3 \ln f_{ct} \tag{11}$$

Then a relationship between fracture energy and shear modulus of adhesive and tensile strength of concrete was found by determining the coefficients a_1- a_3 which give the best fit to the data available. This yields the relation

$$G_f = 0.52 {f_{ct}}^{0.26} {G_a}^{-0.23} \tag{12}$$

The relationship between fracture energy and the quantity ${f_{ct}}^{0.26} {G_a}^{-0.23}$ is shown in Fig. 14. A correlation coefficient, R^2, of 0.939 was obtained for Eq. (12). The values of ${f_{ct}}^{0.26} {G_a}^{-0.23}$ for the different specimens are shown as squares.

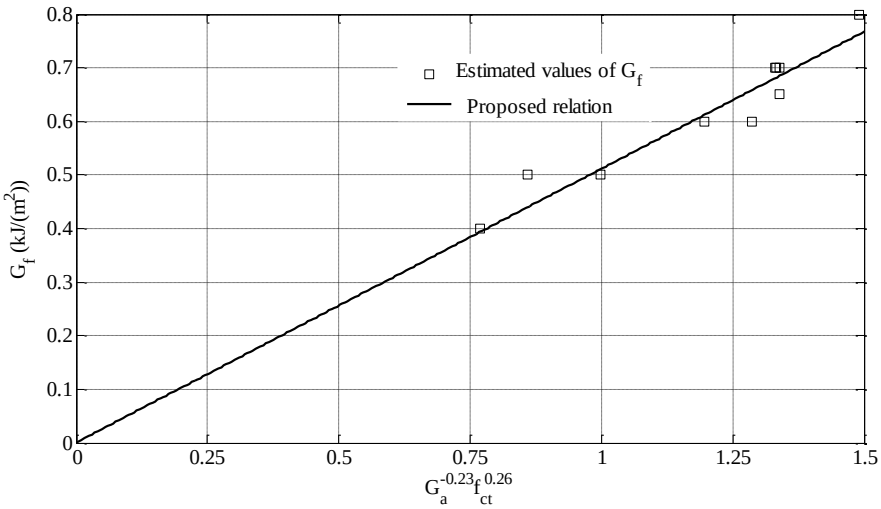

Fig. 14. Relation between estimated value of G_f and $G_a{}^{-0.23} f_{ct}{}^{0.26}$.

The relation between shear strength and shear modulus of adhesive and tensile strength of concrete was correspondingly found to be:

$$\tau_{max} = 1.46 G_a{}^{0.165} f_{ct}{}^{1.033} \tag{13}$$

Fig. 15 shows the relationship between estimated values of shear strength and the quantity $G_a{}^{0.165} f_{ct}{}^{1.033}$. A correlation coefficient, R^2, of 0.924 was obtained for Eq. (13).

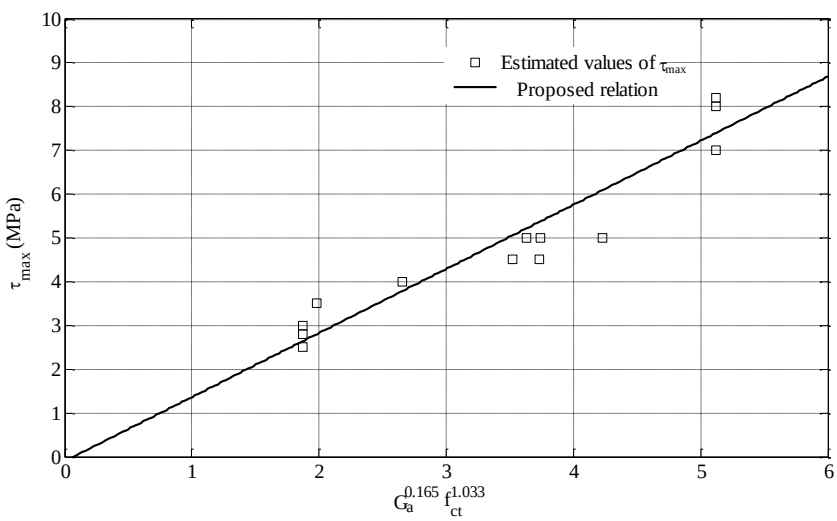

Fig. 15. Relation between estimated value of τ_{max} and $G_a{}^{0.165} f_{ct}{}^{1.033}$.

5.2.2 Comparison with Lu et al. (2005) model

Lu et al. (2005) related the shear strength and fracture energy to concrete properties and to FRP-to-concrete width ratio Eq. (14) and Eq. (15).

$$\tau_{max} = 1.5\,\beta_w f_{ct} \tag{14}$$

$$G_f = 0.308{\beta_w}^2\sqrt{f_{ct}} \tag{15}$$

where;

$$\beta_w = \sqrt{\left(2.25 - \frac{b_f}{b_c}\right)/\left(1.25 + \frac{b_f}{b_c}\right)} \tag{16}$$

β_w is a correction factor taking into account out-of-plane effects, which Lu et al. needed to include, since their model was based on plane stress simulations.

A comparison between results from the bilinear model of Lu et al. and the proposed equations, Eq. (6), Eq. (12) and Eq. (13), is shown in Fig. 16. The figure shows that the results from the proposed equations have good agreement with experimental work and is also close to Lu et al. The proposed model gives equally good results as the Lu et al. model, without including any geometry related correction factors. This means that the present model is applicable to more general geometries. Table 3 shows a comparison between maximum load values obtained from simulation by using either Lu et al. (2005) or proposed model.

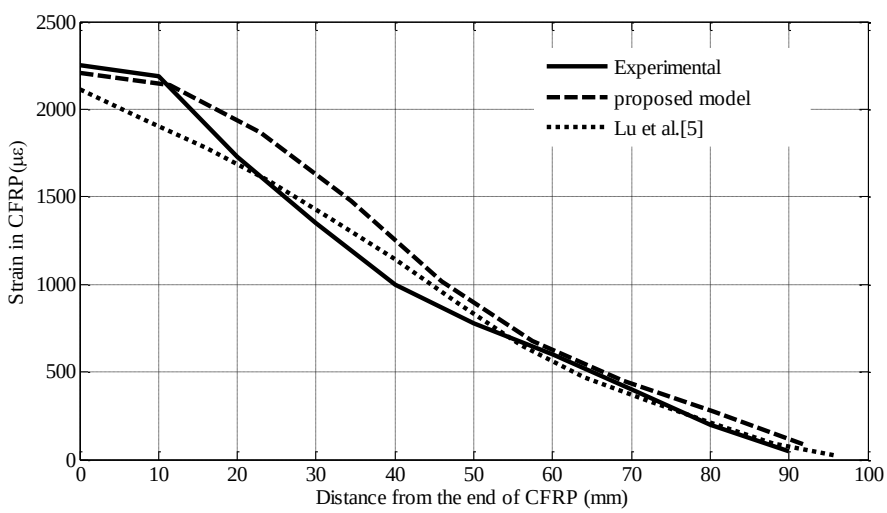

(a) Series B-B1.

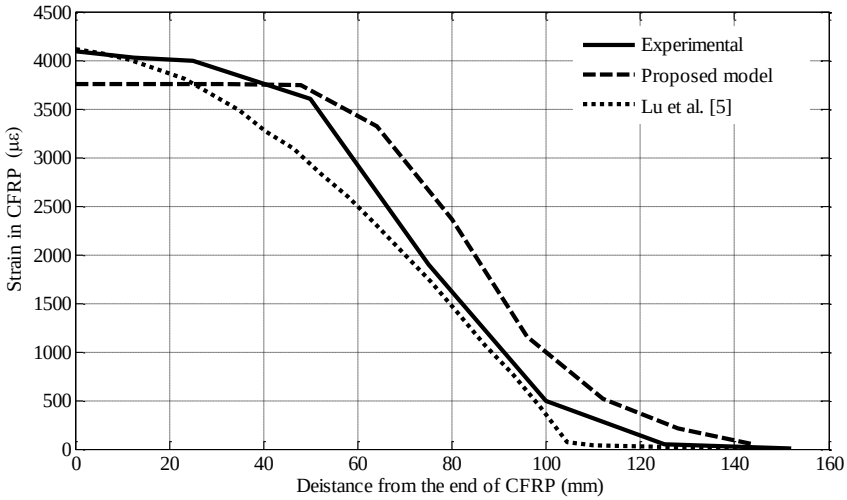

(b) Series G-G2.

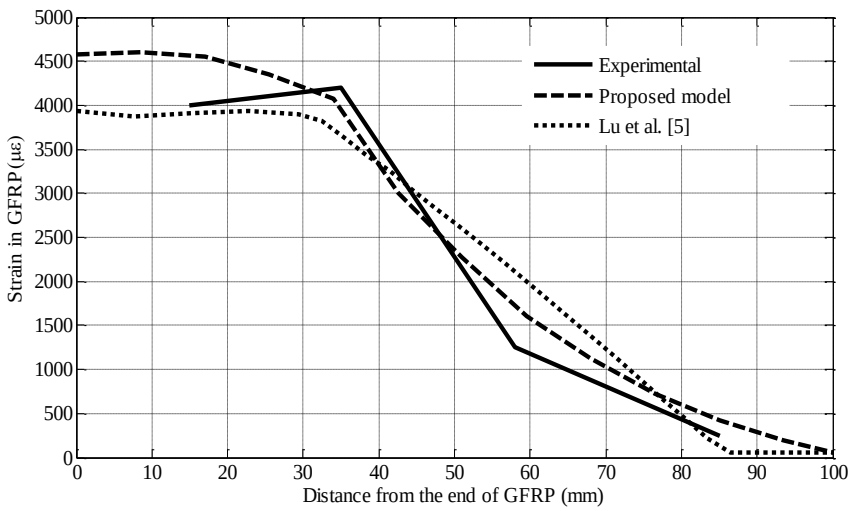

(c) Series H.

Fig. 16. Comparison between proposed model and Lu at el. (2005) model.

Table 3 Maximum load values obtained from simulation by using either Lu et al. (2005) or proposed model.

Specimens	**Experimental value (kN)**	**Proposed Model**	**Lu at el. (2005)**
B1	22.3	25.1	18.1
G2	12.0	11.3	14.3
H	11.7	11.5	10.3

5.3 Shape of bond-slip curve

The finite element results with bilinear bond-slip model, trilinear bond-slip model and exponential bond-slip model were compared with the test results, see Fig. 3. K_0, τ_{max} and G_f were calculated according to the models proposed in this paper.

Comparison of the load versus slip relations obtained from the finite element analysis and the experimental maximum load are shown in Fig. 17. The results obtained using the different curve shapes only show very little difference in load-slip relation and the maximum load is also close to the experimental.

The strain in the FRP was compared at three different load levels, 0.2/0.21, 0.6/0.64 and 1 times maximum loading, as shown in Fig. 18. It is shown that for all specimens, the finite element strain results are almost the same for bilinear, trilinear and exponential bond-slip models. For the load level 0.2/0.21 of maximum loading, before debonding occurs, there is no difference between the results from the models. For the maximum load levels, there is a deviation compared to the test results of the specimens, but the finite element strain results are still quite close to the test results. This means that after the debonding, a difference exists due to the different location of local cracks which does not affect the overall simulation. Nevertheless, it seems that the strain results obtained from models compared well with the test results especially at the lower load levels.

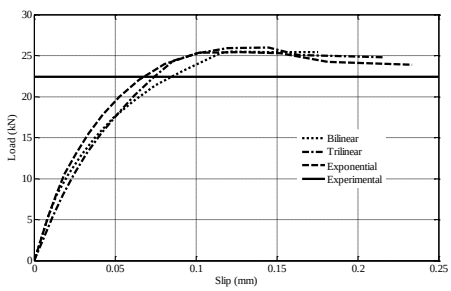

(a) Series B-B1.

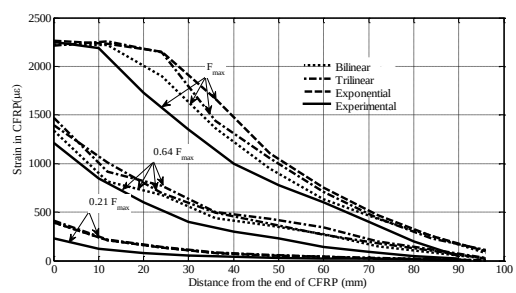

(a) Series B-B1.

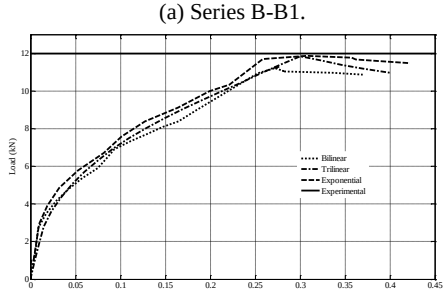

(b) Series G-G2.

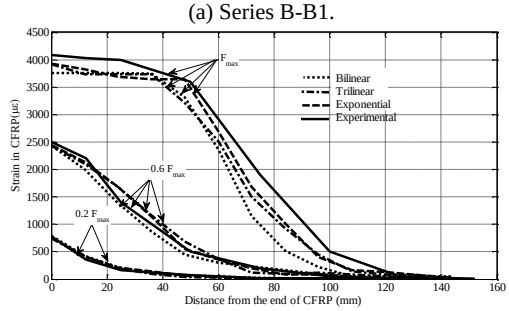

(b) Series G-G2.

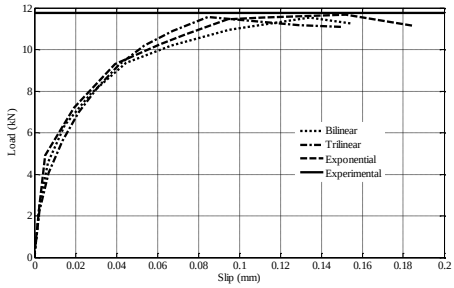

(c) Series H.

Fig. 17. Comparison of the load-slip relation for different bond-slip curve shapes.

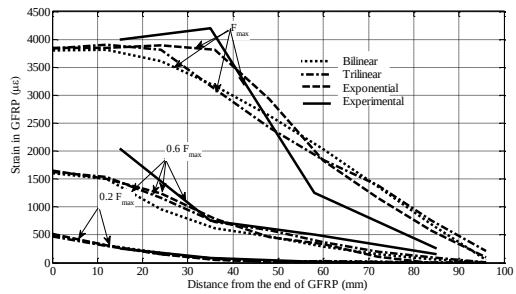

(c) Series H.

Fig. 18: Comparison of strain distribution in FRP for different bond-slip curve shapes.

As long as the interfacial properties K_0, τ_{max} and G_f are the same, the shape of the local bond stress-slip relationship does not have significant influence on the macro bond characteristics before debonding and on maximum load. Thus, it is proposed that the simplest curve shape, the bilinear one, is used.

6. Conclusion

A new model describing the behaviour of the FRP-concrete bond was developed by fitting simulation results to experimental results from literature. The investigated variables were initial interfacial stiffness, K_0, shear strength, τ_{max}, fracture energy, G_f and the shape of the bond-slip curve. The following relation for initial stiffness, K_0, as function of the adhesive properties, is proposed:

$$K_0 = 0.16\frac{G_a}{t_a} + 0.47 \tag{17}$$

This proposed relation was found to predict the strain distribution at low load better than the model by Lu et al. (2005). Shear strength and fracture energy were investigated through a parametric analysis. The proposed relations for those parameters are as follows:

$$\tau_{max} = 1.46{G_a}^{0.165}{f_{ct}}^{1.033} \tag{18}$$

$$G_f = 0.52{f_{ct}}^{0.26}{G_a}^{-0.23} \tag{19}$$

These relations were as good as the model by Lu et al. in predicting maximum load and strain distribution, without including an out-of-plane correction factor. This means that the model can be used for more general geometries.

Based on the results obtained, in term of load-slip relation and axial strain distribution of FRP, it is shown that the shape of the bond-slip curve has minor influence on the behaviour of the retrofitted members.

7. References

[1] Chajes, M. J., Finch, W. W., Januszka, T. F., and Thomson, T. A. (1996). "Bond and force transfer of composite material plates bonded to concrete". *ACI Structures Journal*, 93(2), 208-217.

[2] Sato, Y., Asano, Y., and Ueda, T. (2001). "Fundamental study on bond mechanism of carbon fibre sheet". *Concrete Library International, JSCE*, 97-115.

[3] Lorenzis, L. De., Miller, B., and Nanni, A. (2001). "Bond of fibre-reinforced polymer laminates to concrete". *ACI Materials Journal*, 98(3), 256-264.

[4] Yang, DS., Hong, SN., Park, SK. (2007). "Experimental observation on bond-slip behavior between concrete and CFRP plate". *International Journal of Concrete Structures and Material*, 1(1), 37-43.

[5] Lu, X.Z., Teng, J.G., Ye, L.P., Jiang, JJ. (2005). "Bond–slip models for FRP sheets/plates bonded to concrete". *Engineering Structures*, 27 (6), 920–37.

[6] Woo, S.K., Lee, Y. (2010). "Experimental Study on Interfacial Behavior of CFRP-Bonded concrete". *KSCE Journal of Civil Engineering*, 14(3), 385-393.

[7] Mazzotti, C., Savoia, M., Ferracuti, B. (2008). "An experimental study on delamination of FRP plates bonded to concrete". *Construction and Building Materials*, 22, 1409–1421.

[8] Bizindavyi, L. and Neale, K. W. (1999). "Transfer lengths and bond strengths for composites bonded to concrete". *ASCE Journal of Composites for Construction*, 3(4), 153–160.

[9] Dai J G, Ueda T, Sato Y. (2005). "Development of the non-linear bond stress-slip model of fiber reinforced plastic sheet-concrete interfaces with a simple method". *Journal of Composites for Construction*, ASCE; 3(1), 52−62.

[10] Pan, J.L. and Leung, C.K.Y. (2007). "Effect of concrete composition on FRP/concrete bond capacity". *Journal of Composites for Construction*, 11, 611-618.

[11] Ming, Z., Ansari, F. (2004). "Bond properties of FRP fabric and concrete joints". *In: Proc. of 13th world conferences on earthqauke engineering*, Paper 35.

[12] Chajes, M.J., Finch, W.W., Januszka, T.F., and Thomson, T.A. (1996). "Bond and Force Transfer of Composite-Material Plates Adhered to Concrete". *Structural Journal ACI*, 93(2), 208-217.

[13] Sharma, K., Mohamed Ali, M.S., Goldar, D., and Sikdar, P.K. (2006). "Plate–concrete interfacial bond strength of FRP and metallic plated concrete specimens". *Composites Part-B: Engineering*, 37 (1), 54–63.

[14] Hibbitt, Karlsson, Sorensen, & Inc. (2000). "ABAQUS Theory manual, User manual, Example Manual". *Version 6.7. Providence, RI.*

[15] ACI Comitte 318. (1999). "Building Code Requirements for Structural Concrete and Commentary (ACI 318-99)". *American Concrete Institute Detroit, MI*.

[16] Beton, C. E.-I. (1990). "CEB-FIP Model Code (CEB-FIP MC90)". *Bulletin D'Information* , No.215.

[17] Saenz, L. (1964). "Discussion equation for the stress - strain curve of concrete by Desayi P, Krishnan S". *ACI J*, 61, 1229–1264.

[18] Hu H.-T., Schnobrich W.C. (1989). "Constitutive modelling of concrete by using nonassociated plasticity". *J Mater Civil Eng (ASCE)*,1(4), 199–216.

[19] Obaidat,Y., Heyden, S., and Dahlblom, O. (2010). "The Effect of CFRP and CFRP/concrete interface models when modelling retrofitted RC beams with FEM". *Composite Structures*, 92, 1391–1398.

Paper F

Plate End Debonding: A Modified Approach to Predict Stress in FRP – Concrete Bond

F

Yasmeen Taleb Obaidat, Susanne Heyden and Ola Dahlblom

Submitted for publication

PLATE END DEBONDING: A MODIFIED APPROACH TO PREDICT STRESS IN FRP–CONCRETE BOND

Yasmeen Taleb Obaidat
PhD student
Structural Mechanics, Lund University
Box 118, 221 00 Lund, Sweden
*Yasmeen.Obaidat@construction.lth.se**

Susanne Heyden
Dr.
Structural Mechanics, Lund University
Box 118, 221 00 Lund, Sweden
Susanne.Heyden@construction.lth.se

Ola Dahlblom
Professor
Structural Mechanics, Lund University
Box 118, 221 00 Lund, Sweden
Ola.Dahlblom@construction.lth.se

Abstract

An important failure mode of RC beams retrofitted with FRP plates is plate end debonding. Design codes provide equations for estimating shear stress at the plate end, but none of these equations include the FRP to concrete width ratio. This paper suggests an improved equation for calculating shear stress that includes the width ratio. The new equation was obtained by fitting 3D nonlinear FEM results to a proposed relation and provided a clearly improved prediction of the shear stress. The simulations also showed that a large width ratio and an adhesive of low stiffness decrease the risk of debonding.

Keywords: Fibre Reinforced Plastic (FRP), Retrofitting, Debonding, Shear stress.

1. Introduction

There is a considerable number of existing reinforced concrete structures that do not fulfill design requirements due to upgrading of design standards, change in use, deterioration or accidents. Thus, these structures need to be retrofitted.

Retrofitting of flexural reinforced concrete elements is traditionally accomplished by externally bonding steel plates to concrete. Although this technique has proved to be effective in increasing strength and stiffness of reinforced concrete elements, it has the disadvantages of being vulnerable to corrosion and difficult to install. Most fibre reinforced polymer (FRP) materials are made of continuous aramid fibres, carbon fibres or glass fibres impregnated with a resin matrix. FRP has become an attractive alternative to steel plates in retrofitting because it has advantages such as their good corrosion resistance, ease of installation, high strength-to-weight and stiffness-to-weight ratios. The effectiveness of using FRP in increasing strength and stiffness of reinforced concrete flexural elements is evident from results of previous research work [1-6].

The main problem associated with FRP retrofitted RC beams is debonding of the plate from the existing structure. Debonding can take place in different ways; intermediate crack debonding is caused by a large flexural crack developing in the concrete. As this crack grows, tension is relieved in the concrete and transferred to the FRP plate. This causes high stresses

in the bond between the FRP plate and the concrete. As the load increases, these stresses become larger until debonding initiates and spreads towards the plate end. Plate end debonding, on the other hand, is caused by a stress concentration at the plate end and then spreads towards the maximum moment region.

Although the technique of externally bonded FRP is quite new, there are several codes and guidelines available for engineers. However, it has to be noted that in some respects the existing design rules are still under development.

The European group fib was one of the first publishing a guideline, fib Bulletin 14 [7], in the field of externally bonded reinforcement. This guideline noted that several failure modes need to be considered to prevent debonding of FRP; debonding initiated at flexural cracks, debonding at the end of the FRP plate and debonding initiated at shear cracks. The American concrete institute ACI 440.2R-08 guideline, [8], places a limitation on the strain level in the laminate to prevent debonding of FRP from the concrete substrate. In the United Kingdom, TR55 design guidance for strengthening concrete structures [9] has been published. To avoid debonding failure, TR55 sets limitations for the strain in the FRP and the shear stress. CNR [10] in Italy has a different procedure for calculation of the stress concentration at the end of the plate. However, CNR does not take into consideration all cases of debonding. Täljsten, [11], also controls the shear and normal stress at the end of the adhesive layer. fib Bulletin considers all the cases of debonding width different simple approaches compared to the other guidelines. Therefore, fib Bulletin was taken in this study.

fib Bulletin 14 predicts interfacial shear stress at the end of the plate using an equation by Roberts [12]. His analytical model was developed in three stages. During the first stage, stresses were determined assuming full composite action between the RC beam and an adhesive bonded steel plate. During the second and third stages, the analysis was modified to take into account the actual boundary condition at the ends of the steel plate. The complete solution was then obtained by superposition. Roberts found that the shear stress concentrations in the adhesive layer at the end of the steel plate depend significantly on e.g. the shear force, thickness of plate, shear stiffness of the adhesive, elastic modulus of the plate and the moment at the end of the plate. He simplified further and omitted terms of minor significance in his analytical model to obtain an acceptable level of complexity for predicting shear and normal stress concentration in the adhesive layer of a plated RC structure. Based on the above, the maximum shear stress at the end of the plate was calculated as the following

$$\tau_f = \left[V_{x=0} + \left(\frac{G_a}{E_f t_f t_a}\right)^{0.5} M_{x=0}\right] \frac{t_f(h-x_e)}{I} \quad (1)$$

where $V_{x=0}$ is the shear force at the end of the laminate plate, $M_{x=0}$ is the bending moment at the end of the laminate plate, t_f is the thickness of the laminate plate, t_a is the thickness of the adhesive layer, I is the second moment of area of fully composite transformed equivalent FRP plate, $h - x_e$ is the distance from neutral axis of the strengthened section to the plate, G_a is the shear modulus of the adhesive layer, and E_f is the elastic modulus of the laminate plate.

The shear force term in Eq. (1) corresponds to ordinary beam theory with full composite action, while the bending moment term is a correction due to the actual boundary condition at the end of the plate with assuming the plate to be bonded to the beam by an adhesive layer. This simplified equation may according to Roberts underestimate the magnitude of the stress concentration up to 30% [12], and he suggested that the moment should be taken at distance $(h+t_f)/2$ from the end of the FRP, where h is a concrete depth and t_f is plate depth. [7], however, uses this equation without taking the moment at a distance from the end of the FRP.

A problem with Roberts' equation is that it does not include the width ratio, $\frac{b_f}{b_c}$- where b_f is

FRP width and b_c is RC beam width- which is known to affect the plate end shear stress concentration, [13]. The aim of this study was to modify Roberts' equation of determining shear stress at the end of the plate used in fib Bulletin by including the width ratio. Therefore, simulations were performed and the results were compared with values from Eq. (1) in order to find the effect of the third dimension quantified by width ratio, $\frac{b_f}{b_c}$.

2. Beam analysis

Simply supported RC beams subjected to uniformly distributed load were studied using FEM, Fig. 1. The beams were required to carry a design load equal to 56.75 kN/m. The steel reinforcement was chosen so that the flexural strength requirement was not met, but the shear strength was sufficient. In order to enhance the flexural capacity of the beams they were strengthened with externally bonded FRP plates attached to the beam soffit.

fib Bulletin guidelines [7] were adopted to calculate the required area of FRP. Geometry data and material properties of the beams are presented in Table 1 and 2.

Two different beam geometries were chosen, to study how the stiffness of the beam affects the behaviour. Two characteristic compressive concrete strengths were also adopted to study their effect on the behaviour of a strengthened beam. In order to be able to observe possible out-of-plane effects different FRP widths were used, keeping the cross-section area constant. Two shear modulus values for the adhesive were also used. Adhesive types with low and high stiffness values were chosen.

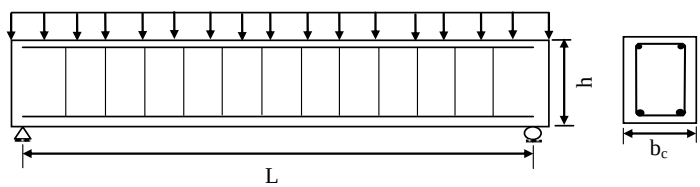

Figure 1. Geometry, arrangement of reinforcement and load of the beams.

Table 1. Geometry of specimens.

Beam	Concrete			Steel			FRP		
	L (mm)	b_c (mm)	h (mm)	Longitudinal tensile steel	Longitudinal compression steel	Shear steel (mm/mm)	Width (b_f), (mm)	Thickness (t_f), (mm)	Length (L_f) (mm)
A	1500	115	146	2ϕ10 mm	2ϕ10 mm	6/60	46.0	1.30	1480
							57.5	1.04	1480
							76.7	0.78	1480
							86.3	0.69	1480
							115.0	0.52	1480
B	2700	150	300	2ϕ10 mm	2ϕ10 mm	8/100	50.0	1.00	2680
							60.0	0.83	2680
							75.0	0.67	2680
							100.0	0.50	2680
							112.5	0.44	2680
							150.0	0.33	2680
C	1500	115	146	2ϕ10 mm	2ϕ10 mm	6/60	46.0	1.52	1480
							57.5	1.22	1480
							76.7	0.91	1480
							86.3	0.81	1480
							115.0	0.61	1480
D	2700	150	300	2ϕ10 mm	2ϕ10 mm	8/100	50.0	1.40	2680
							60.0	1.17	2680
							75.0	0.93	2680
							100.0	0.70	2680
							112.5	0.62	2680
							150.0	0.47	2680

Table 2. Mechanical properties of materials used.

Material		Beam A and B	Beam C and D
Concrete	Compressive strength, f_c' (MPa)	39.70	30.00
	Tensile strength, f_{ct} (MPa)	2.10	1.70
	Elastic modulus, E_c (GPa)	30.40	28.00
	Poisson's ratio, ν_c	0.20	0.20
Steel	Elastic modulus, E_s (GPa)	200	200
	Yield strength, f_y (MPa)	414	414
FRP	Elastic modulus, E_f (GPa)	200	200
	Tensile strength, f_f (GPa)	2.5	2.5
	Ultimate strain (%)	1.30	1.30
Adhesive	Shear modulus, G_a (GPa)	0.97	0.97
		4.00	4.00
	Poisson's ratio, ν_a	0.38	0.38
	Thickness, t_a (mm)	1.00	1.00

Finite element failure analysis was performed to model the nonlinear behaviour of the beams. The model used was validated by Obaidat et al. [14], and was shown to have good fit with experimental work. The FEM package Abaqus/standard [15] was used for the analysis. 4-node linear tetrahedral elements were used for the reinforced concrete, reinforcement and FRP. 8-node 3-D cohesive elements were used to model the interface layer between concrete and FRP. One quarter of the specimen was modelled by taking advantage of the double symmetry of the beam.

A plastic damage model was used to represent the concrete in compression and in tension. The FRP composite was assumed to be a linear elastic isotropic material and the steel was assumed to be elastic-plastic. In addition, perfect bond between the steel and the concrete was assumed. A bilinear cohesive model was used to represent the bond between the concrete and FRP. The parameters in this model are initial stiffness, K_0, shear strength, τ_{max}, and fracture energy, G_f. Those were determined according to [16]

$$K_0 = 0.16\frac{G_a}{t_a} + 0.47, \text{ GPa/mm} \quad (2)$$

$$\tau_{max} = 1.46\ {G_a}^{0.165}{f_{ct}}^{1.033}, \text{ MPa} \quad (3)$$

$$G_f = 0.52\ {f_{ct}}^{0.26}{G_a}^{-0.23}, \text{ kJ/m}^2 \quad (4)$$

where t_a is the adhesive thickness, mm, G_a is the shear modulus of the adhesive, GPa, and f_{ct} is the tensile strength of concrete, MPa. The total applied load was divided into a series of load increments. Since there is a possibility of unstable behaviour during the analysis, the modified Riks method [17] was used. During concrete cracking and the ultimate stage where a large number of cracks occur, small time increments were used to avoid a diverged solution.

3. Results

Different combinations of beam geometry, concrete compressive strength, concrete-FRP width ratio and type of adhesive were studied. Figure 2 shows load-deflection relationships for all specimens with G_a=0.97. In the cases marked with D there was plate end debonding failure.

The ultimate load increases with the width ratio. This because the smaller the width ratio, the smaller is the bond area available to take part in the transfer of shear force. This means that if the FRP width is large enough the shear stress concentration decreases and debonding failure may be avoided.

It should be noted that the disparity between the beams A-D in Fig. 2 is due to the different relative stiffness of FRP and concrete in the beam series. The concrete stiffness of series B and D is higher than the concrete stiffness of series A and C. Series C and D have about the

same stiffness value of FRP, series B has the lowest stiffness. In other words, the relative stiffness of FRP compared to concrete is higher in series A and C than in series B and D, respectively. This means that the probability of debonding is higher in series A and C than in series B and D, because the stress concentration decreases when the stiffness of FRP decreases compared to the beam stiffness.

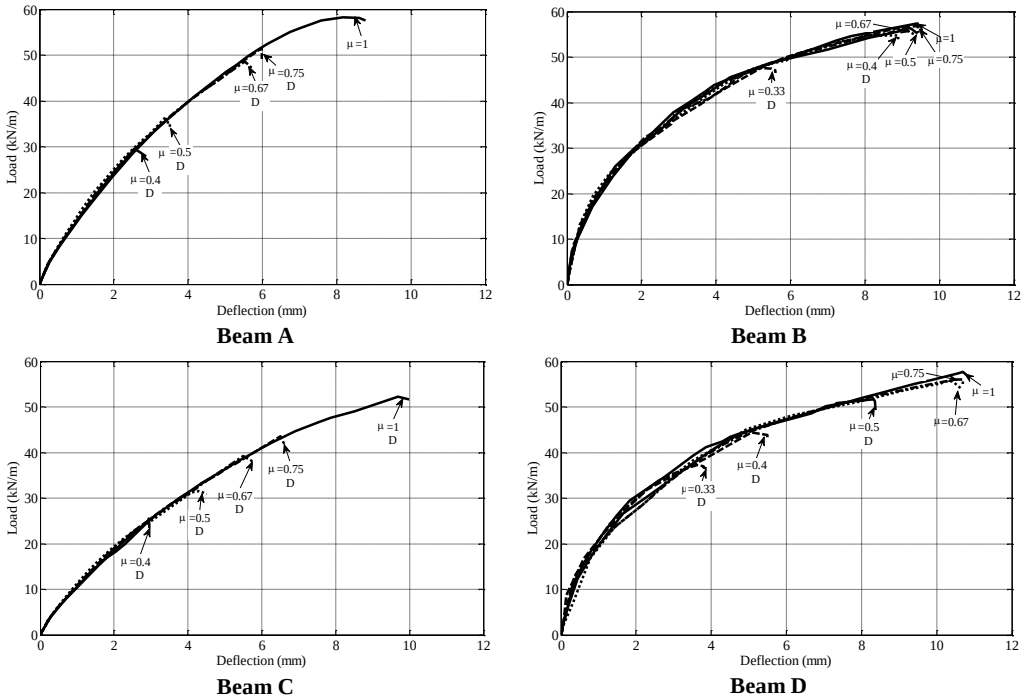

Figure 2. Load-deflection relationships for different width ratios, $\mu = \frac{b_f}{b_c}$, for specimens A-D, G_a=0.97.

Table 3 shows the debonding load for all specimens. Some of the beams failed due to plate end debonding and some failed due to steel yielding and concrete crushing. Since the intention was to study debonding, new simulations were performed for the cases where steel yielding occurred before debonding. In these simulations steel yielding and concrete crushing were suppressed. Steel yielding was prevented by increasing the steel yield stress to 1 GPa. In series A the concrete compressive strength was also increased to 50 MPa in the compression zone. Debonding then occurred also in those cases. The debonding load for those cases is presented using italic font in Table 3.

Table 3 shows the effect of the adhesive shear modulus. When a high shear modulus is used, debonding prevail with a decrease of the debonding load. This is due to the fact that a high shear modulus value of the adhesive increases the rate of stress transfer between FRP and concrete, which leads to stress concentrations in the interface, which will increase the risk of debonding.

Table 3. Debonding load from simulation and shear stress at debonding load from simulation, Eq. (1) and Eq. (6), respectively. The values in italic font represent the debonding load values from the simulations, where other fracture modes than debonding were suppressed.

Width Ratio	Debonding load obtained from simulation (kN/m)	Shear stress (MPa)			Simulation / Equation (1)	Simulation / Equation (6)
		Simulation	Equation (1)	Equation (6)		
Beam A						
G_a= 0.97 GPa, τ_{max}= 3.13 MPa						
0.4	26.51	3.05	2.03	2.98	1.50	1.03
0.5	33.12	3.01	2.12	2.97	1.42	1.01
0.67	43.67	2.95	2.22	2.93	1.33	1.01
0.75	48.30	2.92	2.25	2.91	1.29	1.00
1	*61.49*	2.95	2.30	2.81	1.28	1.05
G_a= 4 GPa, τ_{max}= 3.95 MPa						
0.4	24.77	3.93	2.64	3.87	1.49	1.02
0.5	30.27	3.91	2.75	3.85	1.42	1.02
0.67	40.26	3.94	2.98	3.94	1.32	1.00
0.75	44.96	3.91	3.08	3.98	1.27	0.98
1	*57.28*	3.91	3.23	3.94	1.21	0.99
Beam B						
G_a= 0.97 GPa, τ_{max}= 3.13 MPa						
0.33	43.80	3.07	2.02	3.07	1.52	1.00
0.4	52.80	3.10	2.09	3.06	1.48	1.01
0.5	*64.40*	3.05	2.15	3.01	1.42	1.01
0.67	*85.58*	3.09	2.28	3.01	1.36	1.03
0.75	*94.89*	2.98	2.33	3.01	1.28	0.99
1	*119.73*	3.09	2.46	3.00	1.25	1.03
G_a= 4 GPa, τ_{max}= 3.95 MPa						
0.33	38.43	3.92	2.51	3.81	1.56	1.03
0.4	46.25	3.92	2.65	3.88	1.48	1.01
0.5	*56.49*	3.93	2.78	3.89	1.41	1.01
0.67	*71.70*	3.91	2.89	3.82	1.35	1.02
0.75	*83.02*	3.92	3.11	4.02	1.26	0.98
1	*107.46*	3.91	3.15	3.84	1.24	1.02
Beam C						
G_a= 0.97 GPa, τ_{max}= 2.51 MPa						
0.4	20.52	2.47	1.69	2.48	1.46	0.99
0.5	25.50	2.49	1.75	2.45	1.42	1.02
0.67	35.17	2.49	1.92	2.54	1.30	0.98
0.75	38.57	2.49	1.93	2.49	1.29	0.99
1	49.80	2.49	1.99	2.43	1.25	1.03
G_a= 4 GPa, τ_{max}= 3.17 MPa						
0.4	18.63	3.10	2.11	3.09	1.47	1.00
0.5	22.03	2.97	2.12	2.97	1.40	0.99
0.67	30.15	3.09	2.36	3.12	1.31	0.99
0.75	33.59	3.11	2.43	3.14	1.28	0.99
1	41.40	2.98	2.46	3.00	1.21	0.99
Beam D						
G_a= 0.97 GPa, τ_{max}= 2.51 MPa						
0.33	30.62	2.47	1.64	2.49	1.50	0.99
0.4	36.70	2.46	1.67	2.45	1.47	1.01
0.5	44.90	2.45	1.71	2.39	1.43	1.02
0.67	*59.60*	2.46	1.82	2.41	1.35	1.02
0.75	*68.80*	2.46	1.92	2.48	1.28	0.99
1	*85.10*	2.47	2.00	2.44	1.23	1.01
G_a= 4 GPa, τ_{max}= 3.17 MPa						
0.33	26.10	2.95	1.92	2.92	1.53	1.01
0.4	31.20	3.01	1.99	2.92	1.51	1.03
0.5	37.68	2.91	2.07	2.90	1.41	1.00
0.67	51.43	3.10	2.30	3.04	1.34	1.02
0.75	*57.44*	3.01	2.38	3.08	1.27	0.98
1	*73.80*	3.10	2.54	3.10	1.22	1.00

When two beams which are equal, except that they have different compressive strength, are compared, e.g beams A and C, it can be seen that the beam with the higher compressive strength has higher debonding load. This has mainly two causes. A higher compressive strength leads to a smaller FRP area. A less stiff FRP will lead to a less pronounced stress

concentration. The shear strength and fracture energy of the cohesive zone is also related to the compressive strength. A higher compressive strength implies a higher tensile strength which leads to a higher shear strength, a higher fracture energy and higher debonding load.

Table 3 shows also the maximum shear stress at debonding load obtained from the simulations. The obtained values are the average of the values at the integration points for the elements at the end of the plate. It can be seen that the stress values obtained from the simulations are slightly smaller than the shear strength τ_{max}. This is because the normal stress is also included in the fracture criterion.

The obtained shear stress values at the end of the FRP at the debonding load for various values of the width ratio were compared with values according to Roberts, Eq. (1), Table 3. The shear stress from Eq. (1) was calculated at a load corresponding to the debonding load obtained from the simulation. It can be seen that Eq. (1) gives a smaller stress value compared to the simulation value. It can also be noticed that the ratio of stress from simulation and from Eq. (1) varies with the width ratio. Therefore it is reasonable to introduce a correction factor which depends on the width ratio for this equation. To take into account the width ratio the following is proposed:

$$\tau_f = a_1 \left(\frac{b_f}{b_c}\right)^{a_2} \left[V_{x=0} + \left(\frac{G_a}{E_f t_f t_a}\right)^{0.5} M_{x=0}\right] \frac{t_f(h-x_e)}{I} \quad (5)$$

To determine a_1 and a_2 in this equation the multiple regression method was used. a_2, which relates to the width ratio effect, was found to be -0.2. a_1, which represents the general underestimation of stress in Eq. (1), caused by other parameters not investigated in this study, was found to be 1.22. This yields the relation

$$\tau_f = 1.22 \left(\frac{b_f}{b_c}\right)^{-0.2} \left[V_{x=0} + \left(\frac{G_a}{E_f t_f t_a}\right)^{0.5} M_{x=0}\right] \frac{t_f(h-x_e)}{I} \quad (6)$$

The shear stress from Eq. (6), and the ratio of stress from simulations to stress from Eq. (6) is also shown in Table 3. This ratio is close to 1 which indicates that Eq. (6) gives a much better estimation than Eq. (1).

4. Conclusion

Plate end debonding load and shear stress in bond were obtained using 3D non-linear FEM. Beam dimensions, concrete compressive strength, adhesive stiffness and FRP to concrete width ratio were varied.

The debonding load was found to increase with decreased adhesive stiffness. Increased compressive strength gave higher debonding load, since the amount of FRP needed and the shear strength and the fracture energy of the bond are influenced by the compressive strength. A higher width ratio also gave a higher debonding load.

The method of calculating shear stress at the plate end in fib Bulletin 14 does not take the width ratio into account. A modified equation to predict shear stress at the plate end for simply supported RC beams bonded with FRP was proposed. The modified equation includes consideration of the effect of 3D by adopting the FRP concrete width ratio in the equation. Simulation results show that the proposed equation provides a clearly improved prediction of the interfacial shear stress in plated beams.

5. References

[1] AI-HUI, Z., WEI-LIANG, J., & GUI-BING, L., "Behaviour of preloaded RC beams strengthened with CFRP laminates", *Journal of Zhejiang University Science A*, 2006, pp. 436-444.

[2]. ASHOUR, AF, EL-REFAIE, SA, AND GARRITY, SW., "Flexural Strengthening of RC continuous beams using CFRP laminates", *Cement & Concrete Composites*, Vol. 26, 2004, pp. 765- 775.
[3]. ESFAHANI, M., KIANOUSH, M., & TAJARI, A., "Flexural behaviour of reinforced concrete beams strengthened by CFRP sheets", *Engineering Structures*, Vol. 29, 2007, pp. 2428-2444.
[4]. KHALIFA, A., TUMIALAN, G., NANNI, A. & BELARBI, A., "Shear Strengthening of Continuous RC Beams Using Externally Bonded CFRP Sheets", *American Concrete Institute, Proc., 4th International Symposium on FRP for Reinforcement of Concrete Structures (FRPRCS4), Baltimore, MD*, Nov. 1999, pp. 995-1008.
[5]. OBAIDAT,Y.,HEYDEN,S., DAHLBLOM, O., ABU-FARSAKH, G., & ABDEL-JAWAD, Y., "Retrofitting of reinforced concrete beams using composite laminates", *Construction and Building Materials*, Vol. 25, 2011, pp. 591–597.
[6]. SHAHAWY M. A., AROCKIASAMY T M., BEITELMANT T., AND SOWRIRAJAN R., "Reinforced concrete rectangular beams strengthened with CFRP laminates", *Composites*, Vol. 27, 1996, pp. 225-233.
[7]. fib Bulletin 14., "Externally bonded FRP reinforcement for RC structures", 2001.
[8]. ACI 440.2R-08, "Guide for the Design and Construction of Externally Bonded FRP Systems for Strengthening Concrete Structures", *ACI Committee 440, American Concrete Institute, Farmington Hills, Mich.*, 2008, pp. 1-76.
[9]. DARBY, A., IBELL, T., CLARKE, J., "TR55 Design guidance for strengthening concrete structures using fibre composite materials", *London: The Concrete Society*, 2004.
[10]. CNR-DT 200., "Guide for the design and construction of externally bonded FRP systems for strengthening existing structures", *Italian National Research Council*, 2004.
[11]. TÄLJSTEN, B., "FRP Strengthening of Existing Concrete Structures: Design Guidelines", *Division of Structural Engineering, Luleå University of Technology*, 2002, pp. 1-228.
[12]. ROBERTS, T.M., "Approximate analysis of shear and normal stress concentration in the adhesive layer of plated RC beams", *The Structural Engineer*, Vol. 67, No. (12/20), 1989, pp. 229-233.
[13]. OBAIDAT,Y., HEYDEN, S., & DAHLBLOM, O., "FEM study on the effect of CFRP stiffness and width on retrofitted reinforced concrete beam behaviour", *Submitted*, 2010.
[14]. OBAIDAT,Y., HEYDEN, S., & DAHLBLOM, O., "The Effect of CFRP and CFRP/concrete interface models when modelling retrofitted RC beams with FEM", *Composite Structures*, Vol. 92, 2010, pp. 1391–1398.
[15]. HIBBITT, KARLSSON, SORENSEN, & Inc., "ABAQUS Theory manual, User manual Example Manual", *Version 6.9. Providence, RI*, 2009.
[16]. OBAIDAT,Y., HEYDEN, S., & DAHLBLOM, O., "Bond action between FRP and concrete - A new model", *Submitted*, 2011.
[17]. BATHE, K.J., "Finite Element Procedures", *Prentice Hall*, 2006.

Paper G

Evaluation of Debonding Criteria in fib Bulletin 14 – A Case Study

G

Yasmeen Taleb Obaidat, Susanne Heyden and Ola Dahlblom

Submitted for publication

Evaluation of Debonding Criteria in fib Bulletin 14 – A Case Study

Yasmeen Taleb Obaidat*, Susanne Heyden and Ola Dahlblom
Division of Structural Mechanics, Lund University, Lund, Sweden

Abstract

In this case study, a defective beam in Om Katheer School in Jordan was studied. One aim was to propose a suitable method for strengthening the beam by application of fibre reinforced polymer. Another aim was to evaluate the design criteria in fib Bulletin 14 by comparing with FEM analysis results. Three CFRP widths and three different adhesives of different stiffness were evaluated. The results indicate that brittle failure can develop at a load much lower than expected when CFRP of too small width or length and too stiff adhesive are used. The results showed that modification of the criterion used for checking plate end debonding is needed. The suggested modification implies when calculation shear stress at the plate end considering the width ratio between concrete and CFRP.

Keywords: Fibre reinforced polymer; CFRP; Strengthening; Interfacial shear stress; Interfacial stiffness; Cohesive model; Fracture energy.

1. Introduction

Many reinforced concrete (RC) structures are in need for strengthening. The need for strengthening may arise when there is an increase in load requirements, a change in use, inadequate strength of materials or a corrosion problem.

In this case study a beam in Om Katheer School in Jordan is studied. This beam is not able to carry the required load due to inadequate strength of concrete.

One strengthening method is to glue external reinforcement consisting of steel or fibre-reinforced polymer (FRP) onto the structure. FRP materials do not, as steel, suffer from corrosion problems, and most of their mechanical and physical properties are much better than those of steel plates. Therefore, one potential solution to increase the load-carrying capacity of the studied beam is to strengthen the structure with FRP materials. The effectiveness of using FRP in increasing strength and stiffness of reinforced concrete flexural elements is evident from results of previous research work [1-6].

Several types of failure modes have been observed in strengthened RC structures. Concrete failure modes include compression failure before or after steel yielding and shear failure due to a shear crack that extends from the vicinity of the support. FRP rupture failure can also

* Corresponding author.
E-mail address: Yasmeen.Obaidat@construction.lth.se

occur, before and after steel yielding. The last failure type is debonding of the FRP plate due to the stress concentration at the end of the FRP plate or at the bottom of a flexural or shear/flexural crack in the concrete member.

All design guidelines available for RC structures retrofitted with FRP are based on limit state design principles. The design is in most design guidelines based on the required strength and then checked for serviceability criteria. In all codes the analysis follows the following assumptions: a plane section before bending remains plane after bending, and no relative slip occurs between external FRP and concrete. The design codes are different in the way of predicting debonding between FRP and concrete. The European task group fib in Bulletin 14, [7], noted that the following failure modes need to be considered to prevent debonding of FRP; debonding at flexural cracks, debonding at the end of the FRP plate, end shear failure and debonding at shear cracks. The ACI guideline, [8], places a limitation on the strain level in the laminate to prevent debonding of FRP from the concrete substrate. TR55, [9], recommends a limit on the strain in the FRP. CNR, [10], calculates the anchorage length and limit the stress in FRP. Täljsten, [11], also controls the shear and normal stress at the end of the adhesive layer. fib Bulletin 14 was used in this study because the treatment of debonding failure is more comprehensive than in the other codes.

The aim of this study was twofold. One aim was to propose a suitable strengthening method for the studied beam. The other aim was to evaluate the design criteria in fib Bulletin 14 by comparing with FEM analysis results. Three CFRP widths and three different adhesives of different stiffness were evaluated.

2. Description of the case study

When the housing and public work ministry requested the Royal Scientific Society (RSS) in Jordan to assess the school building in Swaileh-Jordan, the RSS sent a team of experts from the Building Research Centre (BRC) to document and study the cracks and defects observed on different parts of the structure in question.

The building lies in Swaileh-Jordan and was constructed about 40 years ago, see Fig.1. The building under study consists of two floors with a total area of 2000 m^2, used as classrooms, library, facilities services and health room. Two internal staircases serve the building to the roof. The building is surrounded by concrete, sand and tile yards.

The structural system of the building consists of reinforced concrete one way ribbed slabs with thickness 200 mm and frames of either drop beams or hidden beams and concrete columns and walls supported by continuous footings. There were no drawings or documents available related to this school, therefore architectural and structural drawings representing the reality as close as possible were prepared based on the field inspection.

Fig. 1. Om Katheer secondary school.

A BRC/RSS investigation team has visited the site many times performing the field part of the study. The scope of the field investigation included visual inspection, data collection, structural survey, measurements, sampling, and photographic documentation of the defective elements.

Based on the findings of this investigation, there is inadequate concrete strength in some structural elements; therefore the work teams have suggested enhancing the capacity for those elements. One of these elements was chosen for this study, see Fig. 2.

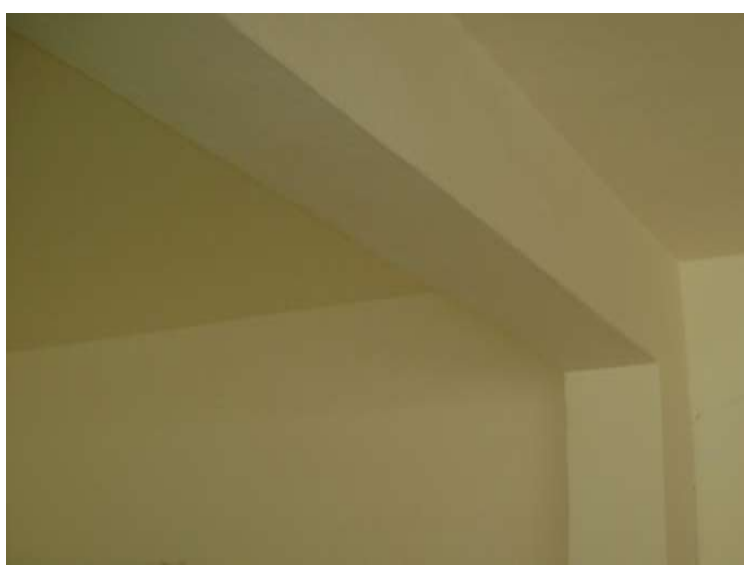

Fig. 2. A beam that has an inadequate strength.

The approach suggested in this study is based on utilizing adhesive bonded CFRP plates for strengthening the structural element. In this case, the CFRP plates should be bonded to the soffit of the beam to enhance its flexural capacity.

The beam selected for this study was a one span beam located in the first east floor of the school building. The beam has a width of 200 mm, 600 mm depth and a length of 6600 mm. The beam was reinforced with 6ϕ16 mm deformed longitudinal steel. The reinforcing bars were tied with ϕ8 steel bars, spaced at 200 mm centre to centre. The concrete cover from the centre of the steel bars was 40 mm. The beam geometry and reinforcement is shown in Fig. 3. The load on this beam is a uniformly distributed load, which has a value of 20 kN/m of dead load and 5 kN/m of live load.

Characteristic values for the material properties, which were found by inspection, are shown in Table 1.

CFRP plates in the Sika CFRP system Type S was used for this study. Three different CFRP widths were considered. In addition, three commercially available adhesive systems formulated for civil engineering applications, Fosoroc Nitofix, Sikadur-31 LP and Sikadur-30, were used. The properties of the selected CFRP and adhesives are shown in Table 1.

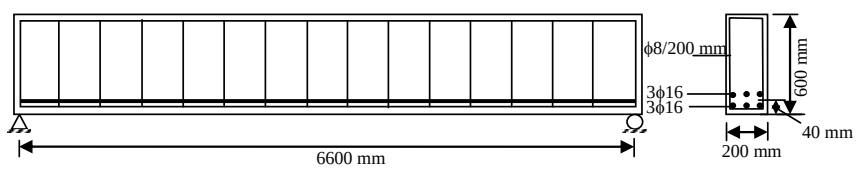

Fig. 3. Beam geometry and reinforcement.

Table 1. Mechanical properties of the materials.

Concrete	Cube compressive strength, f_{cuk} (MPa)		16.4
	Characteristic tensile strength, f_{ctk} (MPa)*		1.21
	Elastic modulus, E_c (GPa)*		18.0
Steel	Elastic modulus, E_s (GPa)		200
	Yield strength, f_y (MPa)		276
CFRP [12]	Elastic modulus, E_f (GPa)		165
	Ultimate strength, f_f (GPa)		2.80
	Ultimate strain (%)		1.7
Adhesive	**Fosoroc Nitofix [13]**	Elastic modulus, E_a (GPa)	2.00
		Shear modulus, G_a (GPa)	0.72
		Thickness, t_a (mm)	1.50
	Sikadur-31 LP [12]	Elastic modulus, E_a (GPa)	4.30
		Shear modulus, G_a (GPa)	1.50
		Thickness, t_a (mm)	1.50
	Sikadur-30 [12]	Elastic modulus, E_a (GPa)	12.8
		Shear modulus, G_a (GPa)	4.50
		Thickness, t_a (mm)	1.50

* These values were calculated according BS EN 1990:2002 [14] equations.

3. Design according to fib Bulletin 14

The beam was analysed according to fib Bulletin 14 guideline of practice for structures, [7]. The design procedure consists of determining the required CFRP cross-sectional area and control of several possible debonding failure modes. Notations are given in section 7.

3.1 Design load

To obtain the design load, the load was multiplied by partial safety factors of 1.15 and 1.5, for dead load and live load, respectively, according to BS EN 1990:2002 [14]. The design load was 30.5 kN/m, which gives a design moment of 166 kNm.

3.2 Material parameters

The design strength was obtained by dividing the characteristic strength by a material safety factor. The material safety factors are 1.5 and 1.15 for concrete and steel respectively. For CFRP, the material safety factor depends on the application type and for this case it was taken as 1.35. The ultimate strain and strength reduction of concrete used is 0.0035 and 0.85 respectively.

3.3 Required area of CFRP

The required CFRP cross-sectional area to achieve the desired resisting moment for the retrofitted flexural element can be determined, in accordance with fib Bulletin 14. This ensures that the beam would become fit for the intended use if debonding does not occur. From the general equation for the moment capacity of a strengthened concrete section, the required CFRP area was determined to be 252 mm^2. CFRP plates of width 90 mm, 135 mm and 180 mm with were chosen, resulting in width ratios, $\frac{b_f}{b_c}$, of 0.45, 0.675 and 0.90 respectively. Ductile failure in a retrofitted beam can occur through steel yielding followed by concrete compression crushing or steel yielding followed by CFRP rupture. The cross sectional analysis in this study indicated that the failure mode of the beam would be steel yielding and concrete crushing, if debonding does not dominate.

3.4 Composite action

Debonding is a critical problem in concrete retrofitted with CFRP observed in test results. This causes loss of composite action between concrete and CFRP. Debonding failure modes can be classified as debonding at flexural crack, debonding at uncracked anchorage zone,

debonding at shear crack and debonding at plate end due to a stress concentration or end shear failure. fib Bulletin 14 takes into consideration debonding as follows:

3.4.1 Ultimate limit state

fib Bulletin 14 proposes three different approaches to predict debonding at last crack and flexural cracks and two of these approaches were considered in this study, approaches 1 and 3.

Approach 1: Anchorage verification and FRP strain

To prevent plate end debonding at the last crack and flexural cracks the anchorage force existing at the last crack is checked. This approach also restricts the strain in the CFRP in the ultimate limit state to 0.0065-0.008. For this study the strain in the CFRP did not exceed this limitation in any case. To verify the end anchorage, fib Bulletin 14 uses Neubauer and Rostasy [15]. The maximum CFRP force which can be anchored can then be calculated according to

$$N_f = 0.64\alpha k_c k_b b_f \sqrt{E_f t_f f_{ctm}} \quad (1)$$

where

$$k_b = 1.06\sqrt{\frac{2-\frac{b_f}{b_c}}{1+\frac{b_f}{400}}} \leq 1 \quad (2)$$

The moment at the theoretical cut off point is then calculated using

$$M = \frac{N_f I}{\alpha_f A_f (h-x)} \quad (3)$$

Then the required anchorage length is calculated according to

$$l_b = \sqrt{\frac{E_f t_f}{2 f_{ctm}}} \quad (4)$$

The mean tensile strength of concrete, f_{ctm}, was calculated according to BS EN 1990:2002 [14] and was found to be 1.7 MPa. All units in Eqs. (1)-(4) should be in N, MPa and mm. Table 2 shows the anchorage force, anchorage length and total length calculated for each CFRP width. This means that debonding at last crack or at flexural cracks would not occur in any of the three cases, provided that the CFRP length is at least as given in Table 2.

Table 2. The anchorage force in FRP, anchorage length and total length for each CFRP width.

b_f (mm)	N_f (kN)	l_b (mm)	Cut off point from the support (mm)	Total length of CFRP (mm)
90	45.94	368	1210	4916
135	56.77	303	1438	4330
180	59.99	260	1520	4081

Approach 3: Verification of force transfer between FRP and concrete

The idea of this approach is to verify that flexural cracks would only produce stable micro-cracking at the CFRP-concrete interface and local debonding, which would not result in bond failure. This approach comprises two steps. The first involves verification of the end anchorage. The end anchorage has already been checked in approach 1. In the second step it should be verified that the shear stress at the CFRP-concrete interface, resulting from the change of tensile force along the CFRP, is less than the design bond strength. This is done by calculating the shear stress in a simplified way considering the case in which the steel bars are elastic or yield as following

$$\varepsilon_{s1} < \varepsilon_{yd}: \qquad \tau = \frac{V_d}{0.95 d b_f \left(1+\frac{A_S E_S}{A_f E_f}\right)} < f_{cbd} \tag{5}$$

$$\varepsilon_{s1} \geq \varepsilon_{yd}: \qquad \tau = \frac{V_d}{0.95 d b_f} < f_{cbd} \tag{6}$$

The shear stress from the two cases should be less than the design bond shear strength which according to fib Bulletin 14 is

$$f_{cbd} = 1.8 \frac{f_{ctk}}{\gamma_c} \tag{7}$$

where, f_{cbd} is this study was found to be 1.44 MPa for all cases and γ_c is the concrete material safety factor equal to 1.5.

Table 3 shows the result for the three dimensions of CFRP and three types of adhesive. From Table 3 it can be seen that for CFRP widths 135 and 180 debonding will not occur. For 90 mm CFRP width, however, there will be debonding after steel yielding. It should be noted that this debonding could not be prevented by increasing the CFRP length.

Table 3. The shear stress values at the CFRP- concrete interface.

b_f (mm)		**$\varepsilon_{s1} < \varepsilon_{yd}$**	**Status**	**$\varepsilon_{s1} \geq \varepsilon_{yd}$**	**Status**
90	Fosoroc Nitofix	0.23<1.44	No debonding	1.57>1.44	Debonding
	Sikadur-31 LP	0.23<1.44	No debonding	1.57>1.44	Debonding
	Sikadur-30	0.23<1.44	No debonding	1.57>1.44	Debonding
135	Fosoroc Nitofix	0.14<1.44	No debonding	0.9<1.44	No debonding
	Sikadur-31 LP	0.14<1.44	No debonding	0.9<1.44	No debonding
	Sikadur-30	0.14<1.44	No debonding	0.9<1.44	No debonding
180	Fosoroc Nitofix	0.096<1.44	No debonding	0.649<1.44	No debonding
	Sikadur-31 LP	0.096<1.44	No debonding	0.649<1.44	No debonding
	Sikadur-30	0.096<1.44	No debonding	0.649<1.44	No debonding

3.4.2 Debonding caused by shear crack

Shear cracks in concrete elements are inclined and may result in debonding. fib Bulletin 14 uses the following relation to check debonding caused by a shear crack

$$V_d \leq \tau_{rp} b_c d \tag{8}$$

where, V_d is design shear force equal to 100.6 kN in this case, and

$$\tau_{rp} b_c d = 256.0 \text{ kN} \tag{9}$$

$$\tau_{rp} = 0.38 + 151\rho_{eq} = 2.29 \text{ MPa} \tag{10}$$

$$\rho_{eq} = \frac{A_s + A_f \frac{E_f}{E_s}}{b_c d} = 0.0126 \tag{11}$$

Thus, $100.6 < 256.0$. This indicates that debonding at a shear crack would not occur for any of the CFRP dimensions used.

3.4.3 End shear failure

fib Bulletin 14 considers a simple criterion to predict end shear failure and concrete cover separation. This criterion does not depend on the material properties and geometry used in the retrofitting system. This approach employed the fictitious shear span concept, see Fig. 4.

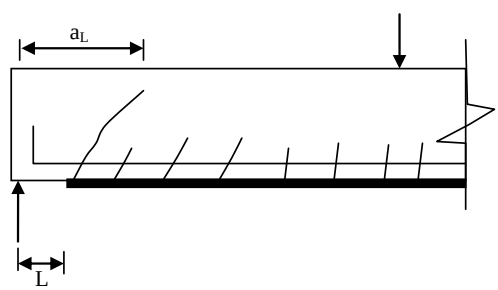

Fig. 4. Modelling analogy for the analysis of FRP end shear failure.

This criterion checks end shear failure as following:

$$V_{sd} \leq V_{Rd} = \tau_{Rd} bd \tag{12}$$

$$\tau_{Rd} = 0.15 \sqrt[3]{3\frac{d}{a_L}} \left(1 + \sqrt{\frac{200}{d}}\right) \sqrt[3]{100\rho_s f_{ck}} \tag{13}$$

$$a_L = \sqrt[4]{\frac{\left(1-\sqrt{\rho_s}\right)^2}{\rho_s} dL^3} \tag{14}$$

This gives a length of 6385 mm, equal for all cases since adhesive stiffness and CFRP to concrete width ratio is not included in the equations.

3.4.4 Serviceability limit state

Interfacial shear stress at plate end under service load is predicted according to an equation developed by Roberts, [16]. fib Bulletin 14 assumes the characteristic value of the concrete tensile strength, f_{ctk}, as a limit for interface shear stress.

$$\tau_f = \left[V_{x=0} + \left(\frac{G_a}{E_f t_f t_a}\right)^{0.5} M_{x=0}\right] \frac{t_f(h-x)}{I_c} \leq f_{ctk} \quad (15)$$

The length of CFRP needed to prevent debonding at the end of the plate could be calculated using Eq. (15) under service load. The length required for each case is shown in Table 4. With this length of CFRP, debonding would not occur due to the stress concentration at the end of the CFRP plate.

Table 4. Length of CFRP obtained from Eq. (15).

b_f (mm)	Type of adhesive	Length of CFRP, (mm)
90	Fosoroc Nitofix	6396
	Sikadur-31 LP	6466
	Sikadur-30	6524
135	Fosoroc Nitofix	6330
	Sikadur-31 LP	6416
	Sikadur-30	6496
180	Fosoroc Nitofix	6280
	Sikadur-31 LP	6380
	Sikadur-30	6450

4. FEM simulations

A three-dimensional finite element model was used to examine the structural behaviour of the beam of Om Katheer School in Jordan when applying CFRP laminates to enhance its capacity. The geometry, reinforcement and loading shown in section 2 were used.

By taking advantage of the symmetry of the beam, a quarter of the full beam was used for modelling. Concrete was modelled as a material capable of cracking and crushing by using a plastic damage model. The CFRP was modelled as a linear elastic isotropic material. Steel was modelled using an elastic-perfectly plastic model. A bilinear cohesive model was used to represent the bond between the concrete and CFRP, see Fig. 5. The parameters in this model are initial stiffness, K_0, shear strength, τ_{max}, and fracture energy, G_f. Those were determined according to [17],

$$K_0 = 0.16 \frac{G_a}{t_a} + 0.47 \quad (16)$$

$$\tau_{max} = 1.46\, {G_a}^{0.165} {f_{ctk}}^{1.033} \quad (17)$$

$$G_f = 0.52\, {f_{ctk}}^{0.26} {G_a}^{-0.23} \quad (18)$$

where t_a is the adhesive thickness, G_a is the shear modulus of adhesive (GPa), and f_{ctk} is the characteristic tensile strength of concrete, (MPa).

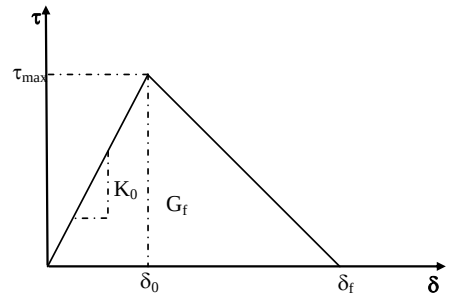

Fig. 5. Bilinear cohesive model.

Concrete, CFRP and steel were modelled using linear tetrahedral elements. 3-D 8-node cohesive elements were used to model the interface layer. The validity of this model was verified in Obaidat et al. [18].

The load was applied as a uniformly distributed pressure over the loaded area. The total applied load was divided into a series of load increments. Since there is a possibility of unstable behaviour during the analysis, the modified Riks method, [19], was used during the application of external loads. A stiff plate was added at the support. This provided a more even stress distribution over the support and prevented any stress localization or crushing of concrete near the supporting point. Moreover, a single line support was placed under the centreline of the steel plate to allow for rotation of the plate.

5. Result

5.1 Design according to ULS

In this section, FEM simulation results for the beams designed according to the ULS are presented. The CFRP length was determined by the end shear failure criterion which gave 6385 mm.

Fig. 6 shows load-deflection curves from the simulations and Table 5 summarises the type of failure modes obtained from fib Bulletin 14 and the simulations.

For 90 mm width, both fib Bulletin 14 and FEM predicts debonding at a crack. There is also agreement between fib Bulletin 14 and FEM on that the design load is not reached. Thus, a 90 mm wide CFRP plate is not a possible solution for retrofitting the beam.

For 180 mm width, both fib Bulletin 14 and FEM indicates that the design load is reached and failure will occur due to steel yielding and concrete crushing.

For the intermediate width, 135 mm, there is disagreement regarding the fracture mode, fib Bulletin 14 predicts steel yielding and concrete crushing while FEM predicts plate end interfacial debonding at a load lower than the design load. The following sections will be

focused on the 135 mm width, since this is where there is disagreement between the code and the simulation results.

Fig. 6 also shows the effect of adhesive modulus on the load-deflection curve. It can be seen that the stiffest adhesive always gives the lowest ultimate load value compared to those having lower values of shear modulus of adhesive, especially when plate end debonding is a limiting phenomenon, see Fig. 6b. That is, Fosoroc Nitofix adhesive has a higher ultimate load in all cases. Clearly, to minimize the stress concentration in the bond, an adhesive with small value of shear modulus is preferable. Fig. 6 shows the load-deflection curves for different width ratios. It can be seen that the plate with 180 mm width gives the highest ultimate load. This result is due to the fact that a small CFRP width increase the stress concentration at the end of CFRP plate, then debonding occurs at a small value of the load.

Table 5. Failure mode and maximum load of beams with CFRP length fulfilling ULS requirments.

b_f (mm)	Type of adhesive	CFRP length, (mm)	fib Bulletin 14 failure mode	FEM	
				Failure mode	Maximum load, (kN/m)
90	Fosoroc Nitofix	6385	DC	DC	28.1
	Sikadur-31 LP	6385	DC	DC	27.6
	Sikadur-30	6385	DC	DC	27.1
135	Fosoroc Nitofix	6385	SY/CC	PEID	30.8
	Sikadur-31 LP	6385	SY/CC	PEID	29.3
	Sikadur-30	6385	SY/CC	PEID	28.6
180	Fosoroc Nitofix	6385	SY/CC	SY/CC	32.8
	Sikadur-31 LP	6385	SY/CC	SY/CC	32.8
	Sikadur-30	6385	SY/CC	SY/CC	32.7

DC: Debonding due to a crack.

PEID: Plate end interfacial debonding.

SY/CC: Steel yielding and concrete crushing.

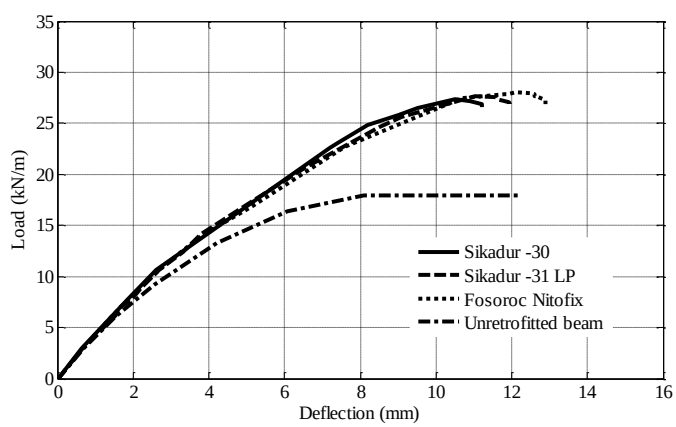

(a) Beam with 90 mm CFRP width.

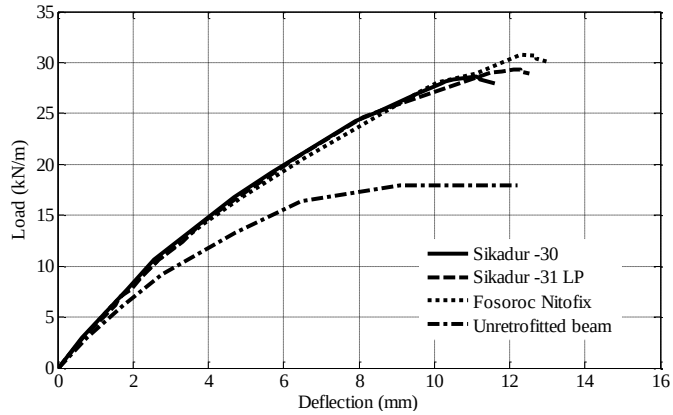

(b) Beam with 135 mm CFRP width.

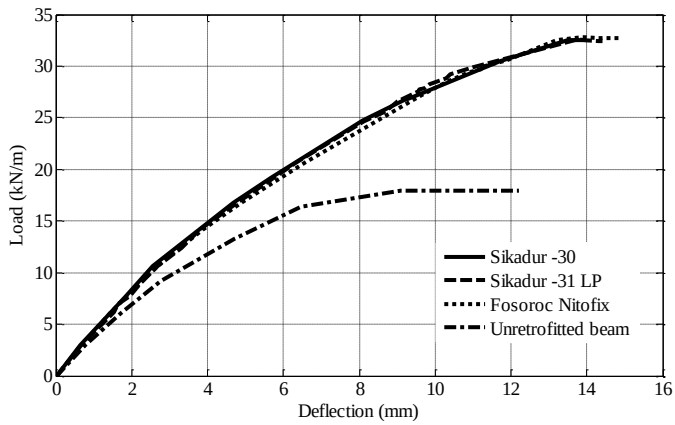

(c) Beam with 180 mm CFRP width.

Fig. 6. Load-deflection curves of beams with the length of CFRP calculated according to ULS requirements.

5.2 Design according ULS and SLS

In this section the analysed beams were designed to fulfil both the ULS and SLS requirements and only CFRP width 135 mm was considered. This means that the CFRP lengths were calculated according to Eq. (15), except for Fosroc Nitofix, where the length 6385 mm was needed to avoid end shear failure.

Fig. 7 shows load–deflection curves and Table 6 summarizes the failure types from fib Bulletin and the simulations.

It can be seen that according to FEM the design load is reached only for the soft adhesive, Fosoroc Nitofix. There is disagreement regarding the fracture mode for all three adhesives. This indicates that the procedure in fib Bulletin 14 for checking plate end debonding needs modification.

Table 6. Failure mode of beams with CFRP length fulfilling both ULS and SLS requirements.

Type of adhesive	CFRP length, (mm)	fib Bulletin 14 failure mode	FEM	
			Failure mode	Maximum load, (kN/m)
Fosoroc Nitofix	6385	SY/CC	PEID	30.8
Sikadur-31 LP	6416	SY/CC	PEID	29.4
Sikadur-30	6496	SY/CC	PEID	28.8

PEID: Plate end interfacial debonding.

SY/CC: Steel yielding and concrete crushing.

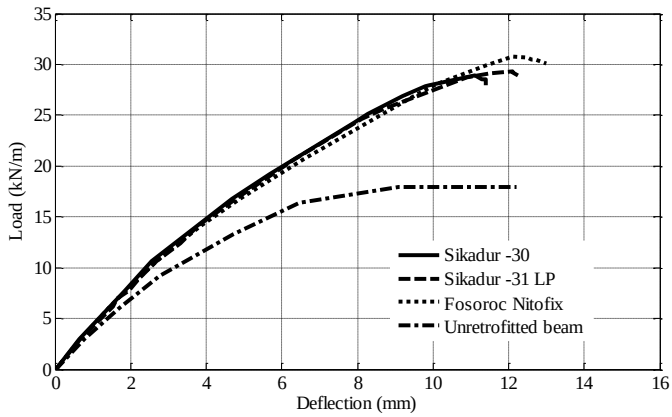

Fig. 7. Load-deflection curve of beam with the CFRP length fulfilling both ULS and SLS requirements.

One suggestion would be to predict interfacial shear stress at plate end using Eq. (15) in ULS. That would imply that the design load should be used instead of the service load when calculating the CFRP length required for satisfying Eq. (15). It seems quite logical to consider plate end debonding in the ULS, since it concerns a fracture phenomenon.

The lengths that this gives are shown in Table 7 and the corresponding load-deflection curves are shown in Fig. 8. This increases the ultimate load, but for the two stiffest glues the design load is still not reached. As can be seen from Table 7 debonding is still the limiting failure mode in all cases according to FEM and this disagrees with fib Bulletin 14 prediction. This means Eq. (15) is still in need for a modification.

Table 7. Length of CFRP from Eq. (15) under design load.

Type of adhesive	CFRP length, (mm)	fib Bulletin 14 failure mode	FEM	
			Failure mdoe	Maximum load, (kN/m)
Fosoroc Nitofix	6390	SY/CC	PEID	31.0
Sikadur-31 LP	6458	SY/CC	PEID	30.4
Sikadur-30	6518	SY/CC	PEID	30.1

PEID: Plate end interfacial debonding.

SY/CC: Steel yielding and concrete crushing.

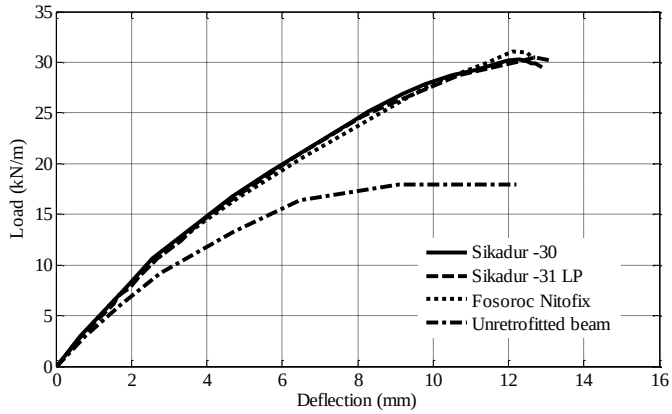

Fig. 8. Load-deflection curve of beam with CFRP length according to Eq. (15) with design load, 135 mm plate width.

It has been shown in Obaidat et al. [20] that the risk of debonding depends on the width ratio, a fact that is not considered in Eq. (15). To take the width ratio into account a correction factor for Eq. (15) was proposed in Obaidat et al. [20]. This gives

$$\tau_f = 1.22\left(\frac{b_f}{b_c}\right)^{-0.22}\left[V_{x=0} + \left(\frac{G_a}{E_f t_f t_a}\right)^{0.5} M_{x=0}\right]\frac{t_f(h-x)}{I_c} \qquad (19)$$

Using this equation, with design load, yields an even longer CFRP length, see Table 8.

Table 8. New length for 135 mm width of CFRP from Eq. (19) under design load.

Type of adhesive	CFRP length, (mm)	fib bulletin 14 failure mode	FEM	
			Failure mode	Maximum load, (kN/m)
Fosoroc Nitofix	6458	SY/CC	SY/CC	32.1
Sikadur-31 LP	6502	SY/CC	SY/CC	31.4
Sikadur-30	6544	SY/CC	PEID	30.8

PEID: Plate end interfacial debonding.

SY/CC: Steel yielding and concrete crushing.

Both fib Bulletin and FEM now predicts that debonding will not occur for Fosroc and Sikadur-31 LP. For 135 mm plate with Sikadur-30 there is still a disagreement in failure mode between fib Bulletin 14 and FEM. However, FEM indicates that the design load is reached in all cases, see Fig. 9. It is important to reach the maximum load regardless the type of failure mode. This means Eq. (19) with design load is sufficient to estimate the CFRP length needed to retrofit the beam in this case.

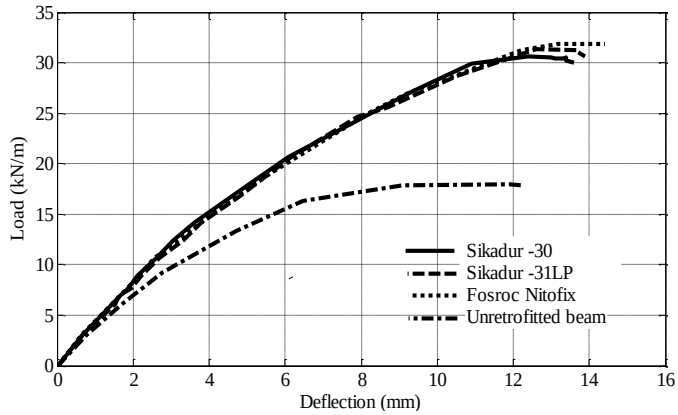

Fig. 9. Load-deflection curve of beam with new CFRP length, 135mm plate width.

It can be concluded from the above that plate end interfacial debonding due to stress concentration should be verified in the ULS, considering material properties and geometry. Eq. (19) with design load would be useful to estimate the length of CFRP.

6. Conclusion

6.1 Case study

After simulations were performed for different widths and adhesives and compared to design guideline results, a suitable width of CFRP and adhesive were chosen; the CFRP width and the adhesive which gave the highest ultimate load was found to be CFRP of 180 mm width with 1.4 mm thickness and 6400 mm length, bonded with Fosoroc Nitofix adhesive. This retrofit scheme resulted in ductile failure and increased the beam capacity to the required design load. Based on the obtained results it can be concluded that this retrofit system well fits its uses.

6.2 General

Several different phenomena can limit the load bearing capacity of a retrofitted beam. This study indicated that the design criteria for plate end interfacial debonding in fib Bulletin 14 is not satisfactory in all cases. The authors' suggestion is that plate end interfacial debonding should be considered in the ultimate limit state, and that a correction factor taking into account the effect of CFRP to concrete width ratio should be introduced, see Eq. (19).

Adhesive properties and width of CFRP was also investigated is this study. In general, a wide CFRP with suitable length and not too stiff adhesive is preferable in retrofitting and increase the utilization of CFRP in a retrofitted beam.

7. Notation

A_f	Cross sectional area of CFRP.
A_s	Cross sectional area of steel.
E_f	Elastic modulus of the CFRP.
E_s	Elastic modulus of steel.
G_a	Shear modulus of the adhesive layer.
I	Second moment of area of the cracked section.
I_c	Second moment of area of fully composite transformed equivalent FRP plate.
L	Distance of the CFRP end from the support.
L_f	Length of the CFRP plate.
M	Bending moment at the cut-off point.
$M_{x=0}$	Bending moment at the end of the laminate plate.
V_d	Design shear force.
V_{sd}	Shear force at plate end.
$V_{x=0}$	Shear force at the end of the laminate plate.
b_c	Width of beam.
d	Lever arms of internal forces for longitudinal steel.
f_{ck}	Characteristic value of the concrete compressive strength.
f_{ctk}	Characteristic value of the concrete tensile strength.
f_{ctm}	Mean tensile strength of concrete.
h	Depth from the extreme compression fibre to the externally bonded CFRP.
$h - x$	Distance from neutral axis of the strengthened section to the plate.
k_b	Geometry factor.
k_c	Factor accounting for the state of compacting of concrete and can generally be assumed to be equal to 1.
t_a	Thickness of the adhesive layer.
t_f	Thickness of the CFRP plate.
x	Depth from the extreme compression fibre to the neutral axis.
α	Reduction factor taken as 0.9.
α_f	Modular ratio for CFRP to concrete.
γ_c	Concrete material safety factor.
ε_{s1}	Strain of steel reinforcement.
ε_{yd}	Yield strain of steel reinforcement.
ρ_s	Longitudinal steel ratio.
τ_f	Interfacial shear stress at plate end.

8. References

1. Toutanji, H., Zhao, L., and Zhang, Y. Flexural behavior of reinforced concrete beams externally strengthened with CFRP sheets bonded with an inorganic matrix. Engineering Structures, 2006; 28: 557-566.

2. Ashour, AF, El-Refaie, SA, and Garrity, SW. Flexural strengthening of RC continuous beams using CFRP laminates. Cement & Concrete Composites, 2004; 26: 765- 775.

3. Esfahani, M., Kianoush, M., & Tajari, A. Flexural behaviour of reinforced concrete beams strengthened by CFRP sheets. Engineering Structures, 2007; 29: 2428-2444.

4. Khalifa, A., Tumialan, G., Nanni, A. and Belarbi, A., Shear strengthening of continuous RC beams using externally bonded CFRP sheets. American Concrete Institute, Proc., 4th International Symposium on FRP for Reinforcement of Concrete Structures (FRPRCS4), Baltimore, MD, Nov. 1999: 995-1008.

5. Obaidat,Y., Heyden,S., Dahlblom, O., Abu-Farsakh, G., and Abdel-Jawad, Y. Retrofitting of reinforced concrete beams using composite laminates. Construction and Building Materials, 2011; 25: 591–597.

6. Garden, H.N., and Hollaway, L.C. An Experimental study of the influence of plate end anchorage of carbon fibre composite plates used to strengthen reinforced concrete beams. Composite Structures, 1998; 42 (2): 175-88.

7. fib Bulletin 14. Externally bonded FRP reinforcement for RC structures. 2001.

8. ACI 440.2R-08. Guide for the design and construction of externally bonded FRP systems for strengthening concrete structures. ACI Committee 440, American Concrete Institute, Farmington Hills, Mich., 2008, 76p.

9. Darby, A., Ibell, T., Clarke, J. TR55 Design guidance for strengthening concrete structures using fibre composite materials. London: The Concrete Society, 2004.

10. CNR-DT 200: Guide for the design and construction of externally bonded FRP systems for strengthening existing structures, Italian National Research Council, 2004.

11. Täljsten, B. FRP Strengthening of existing concrete structures. Design guidelines. Division of Structural Engineering, Luleå University of Technology, Luleå 2002, 228 pp, ISBN 91-89580-03-6, 2002.

12. http://www.sika.ie [19.10.2011].

13. http://www.fosroc.com [19.10.2011].

14. BS EN 1990:2002, Basis of structural design.

15. Neubauer, U. and Rostasy, F. S. Design aspects of concrete structures strengthened with externally bonded CFRP plates, In: Proceedings of the 7th International Conference on Structural Faults and Repairs. Edinburgh, Scotland, ECS Publications. 1997; 2: 109–118.

16. Roberts, T.M. (1989). Approximate analysis of shear and normal stress concentration in the adhesive layer of plated RC beams. The Structural Engineer, 1989; 67 (12/20): 229-233.

17. Obaidat,Y., Heyden, S., and Dahlblom, O. Bond action between FRP and concrete - A new model. Submitted, 2011.

18. Obaidat,Y., Heyden, S., and Dahlblom, O. The effect of CFRP and CFRP/concrete interface models when modelling retrofitted RC beams with FEM. Composite Structures, 2010; 92: 1391–1398.

19. Bathe, K.J. Finite element procedures. Prentice Hall 2006.

20. Obaidat,Y., Heyden, S., and Dahlblom, O. Plate end debonding: A modified approach to predict stress in FRP–concrete bond. Submitted, 2011.